Analysis of *Trypanosoma brucei* motility

and the infection process

in the tsetse fly vector

Dissertation zur Erlangung des

naturwissenschaftlichen Doktorgrades

der Julius-Maximilians-Universität Würzburg

vorgelegt von

Sarah Schuster

geboren in Nürnberg

Würzburg, 2019

Eingereicht am:

Mitglieder der Promotionskommission:

Vorsitzender:

Gutachter:　　　Prof. Dr. Markus Engstler

Gutachter:　　　Prof. Dr. Klaus Brehm

Tag des Promotionskolloquiums:

Doktorurkunde ausgehändigt am:
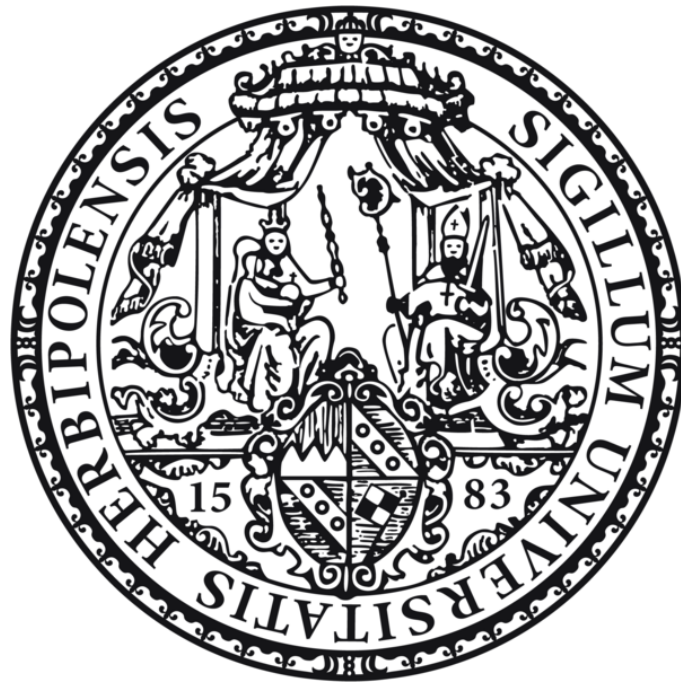
„*Believe you can and you´re halfway there.*"

Theodore Roosevelt

List of contents

1 Summary

1.1 Summary

African trypanosomes are protist pathogens that are infective for a wide spectrum of mammalian hosts. Motility has been shown to be essential for their survival and represents an important virulence factor. *Trypanosoma brucei* is transmitted by the bite of the bloodsucking tsetse fly, the only vector for these parasites. The voyage through the fly is complex and requires several migration, proliferation and differentiation steps, which take place in a defined order and in specific fly tissues.

The first part of this doctoral thesis deals with the establishment of the trypanosome-tsetse system as a new model for microswimmer analysis. There is an increasing interdisciplinary interest in microbial motility, but a lack of accessible model systems. Therefore, this work introduces the first enclosed *in vivo* host-parasite system that is suitable for analysis of diverse microswimmer types in specific microenvironments. Several methods were used and adapted to gain unprecedented insights into trypanosome motion, the fly´s interior architecture and the physical interaction between host and parasite. This work provides a detailed overview on trypanosome motile behavior as a function of development in diverse host surroundings. In additional, the potential use of artificial environments is shown. This can be used to partly abstract the complex fly architecture and analyze trypanosome motion in defined nature-inspired geometries.

In the second part of the thesis, the infection of the tsetse fly is under investigation. Two different trypanosome forms exist in the blood: proliferative slender cells and cell cycle-arrested stumpy cells. Previous literature states that stumpy cells are pre-adapted to survive inside the fly, whereas slender cells die shortly after ingestion. However, infection experiments in our laboratory showed that slender cells were also potentially infective. During this work, infections were set up so as to minimize the possibility of stumpy cells being ingested, corroborating the observation that slender cells are able to infect flies. Using live cell microscopy and fluorescent reporter cell lines, a comparative analysis of the early development following infection with either slender or stumpy cells was performed. The experiments showed, for the first time, the survival of slender trypanosomes and their direct differentiation to the procyclic midgut stage, contradicting the current view in the field of research. Therefore, we can shift perspectives in trypanosome biology by proposing a revised life cycle model of *T. brucei*, where both bloodstream stages are infective for the vector.

1.2 Zusammenfassung

Afrikanische Trypanosomen sind pathogene Protisten, die ein breites Spektrum von Säugetierwirten infizieren. Es wurde gezeigt, dass die Zellmotilität für das Überleben der Parasiten essenziell ist und einen wichtigen Virulenzfaktor darstellt. *Trypanosoma brucei* wird durch den Biss der blutsaugenden Tsetsefliege übertragen, dem einzigen Vektor für diese Parasiten. Der Entwicklungszyklus in der Fliege ist komplex und beinhaltet mehrere Migrations-, Proliferations- und Differenzierungsschritte, die in einer definierten Reihenfolge und in spezifischen Fliegenorganen stattfinden.

Der erste Teil dieser Doktorarbeit beschäftigt sich mit der Etablierung des Trypanosomen-Tsetse Systems als ein neues Modell für Motilitätsanalysen. Es besteht ein wachsendes interdisziplinäres Interesse an mikrobieller Motilität, aber es fehlen zugängliche Mikroschwimmersysteme. Deswegen stellt diese Arbeit das erste abgeschlossene *in vivo* Wirt-Parasit System vor, das für Analysen von verschiedenen Mikroschwimmertypen in spezifischen Umgebungen geeignet ist. Verschiedene Methoden wurden benutzt und adaptiert, um sowohl Einblicke in die Trypanosomenbewegung, die innere Fliegenarchitektur als auch die physikalischen Wechselwirkungen zwischen Wirt und Parasit zu erhalten. Diese Arbeit bietet einen detaillierten Überblick über das motile Verhalten von Trypanosomen als Funktion der Entwicklung in diversen Wirtsumgebungen. Zusätzlich ist die potenzielle Nutzung von artifiziellen Umgebungen gezeigt. Diese können benutzt werden, um die komplexe Architektur der Fliege teilweise zu abstrahieren und die Trypanosomenbewegung in definierten und von der Nature inspirierten Geometrien zu analysieren.

Im zweiten Teil dieser Arbeit wurde die Infektion der Fliege genauer betrachtet. Im Blut existieren zwei verschiedene Trypanosomenformen: proliferierende '*slender*' und Zellzyklus-arretierte '*stumpy*' Zellen. Bisherige Literatur besagt, dass *stumpy* Zellen präadaptiert sind, um in der Fliege zu überleben, wohingegen *slender* Zellen kurz nach der Aufnahme sterben. Dennoch konnten Infektionsexperimente in unserem Labor zeigen, dass auch *slender* Zellen potenziell infektiös sind. Während dieser Arbeit wurden weitere Infektionen so durchgeführt, dass die Möglichkeit für die Aufnahme von *stumpy* Zellen minimiert wurde und die Infektionskapazität der *slender* Zellen bestätigt werden konnte. Durch Lebendzell-Mikroskopie mit fluoreszenten Reporterzelllinien wurde eine vergleichende Analyse für die frühe Entwicklung von

slender und *stumpy* Parasiten nach der Infektion durchgeführt. Die Experimente zeigten zum ersten Mal das Überleben von *slender* Trypanosomen in der Tsetsefliege und ihre direkte Differenzierung in das prozyklische Mitteldarmstadium. Sie widersprechen demnach der aktuellen Auffassung im Forschungsbereich. Demzufolge können wir von einem Perspektivwechsel in der Trypanosomenbiologie sprechen und schlagen einen revidierten Lebenszyklus für *T. brucei* vor, in dem beide Blutstromformen für den Vektor infektiös sind.

2 Introduction

2.1 Trypanosomiasis and trypanosomes

2.1.1 African trypanosomes as causative agent for disease

Trypanosomes are unicellular eukaryotic parasites and the causative agents for many different diseases in various hosts. An important group of these parasites are African trypanosomes, containing the *brucei*-group (*Trypanosoma brucei brucei, Trypanosoma brucei rhodesiense* and *Trypanosoma brucei gambiense)*, which have a devastating socio-economic impact in endemic countries. These trypanosomes live extracellularly in the bloodstream of their host and are transmitted by the bite of the tsetse fly vector (*Glossina* spec.). Thus, the prevalence of these parasites is restricted to the distribution of these insects in Sub-Saharan Africa.

The connection between the bite of a tsetse fly and the disease nagana in cattle was made in 1857 by Livingstone during his exploratory travels in Africa (Livingstone, 1857). Nagana means 'loss of spirit' in the Zulu language and reflects the symptoms of affected animals. However, the identification of trypanosomes in the blood as the causative agent and the link to the tsetse fly was first described by Bruce in 1895 (Bruce, 1895). To honor his discoveries, *Trypanosoma brucei*, was named after him (Plimmer and Bradford, 1899). A few years later, trypanosomes and tsetse flies were also linked to sleeping sickness in humans, a prototypical neglected tropical disease (Dutton, 1902; Kleine 1909).

Today, we know that different trypanosome species are responsible for the animal disease, nagana, which is also called animal African trypanosomiasis (AAT). The most prevalent species are *Trypanosoma congolense*, *Trypanosoma vivax* and *Trypanosoma brucei brucei* (Rotureau and Van Den Abbeele, 2013). They do not just infect wildlife, but also livestock and domesticated animals, which has a severe impact on public health. Infected domesticated animals usually suffer from anemia, lethargy and emaciation, resulting in high mortality. Nagana causes massive economic losses, resulting from reduced agricultural productivity and cattle products, such as milk and meat (Simarro et al., 2008). In contrast, infected African wild game does not normally show disease symptoms: they serve as an important reservoir for trypanosomes, however (Anderson et al., 2011; Auty et al., 2012). They were able to co-evolve over millions of years and gained a kind of tolerance towards the parasites (Lambrecht, 1985).

Two subspecies*, T. brucei rhodesiense* and *T. brucei gambiense,* are responsible for human African trypanosomiasis (HAT), as they are the only trypanosomes able to survive in human blood. They are resistant to the human trypanolytic factor of the blood plasma, a combination of apoliprotein L1 and a haptoglobin-related protein, that is able to destroy all other trypanosome species (Pays et al., 2006; Wheeler, 2010). Both parasites are also able to infect livestock and wild game. These animals thus play an important epidemiological role as carriers or reservoirs from which tsetse flies can acquire HAT parasites (Brun and Balmer, 2006).

After the bite by an infected tsetse fly, the resulting infection is divided into two different phases. First, the parasites develop in blood, lymph and different tissues, with affected individuals showing non-specific symptoms such as fever, headache, shivering attacks and weakness. Early diagnosis of this haemolymphatic phase is very difficult to achieve and the disease is therefore often not detected in its first phase. The second phase, also called the meningo-encephalitic phase, is initiated when the parasites cross the blood-brain barrier and develop in the brain and central nervous system. Typical symptoms of this phase are disruptions of the sleep-wake cycle, muscular failure and neuro-psychiatric disorders. The name 'sleeping sickness' originates from one of the major symptoms, as patients show sleep disorders and ultimately fall into a coma and die (Brun et al., 2010; Kennedy, 2013). The two pathogens responsible for HAT, *T. b. rhodesiense* and *T. b. gambiense* cause different types of infections. *T. b. rhodesiense* causes an acute infection, lasting from a few weeks to several months, whereas *T. b. gambiense* causes a chronic form that can last several years, sometimes even without major symptoms in the beginning (Brun et al., 2010).

Both forms of HAT are fatal if untreated, however, with several epidemic outbreaks having been reported over the last century. In 2009, the number of reported cases dropped below 10,000 for the first time in 50 years, with just 1,447 new cases documented in 2017 due to sustained control efforts. However, sleeping sickness affects 36 Sub-Saharan countries with millions of people living at risk and many cases remaining undiagnosed (Franco et al., 2018; WHO, 2018). A lack of infrastructure makes it difficult to treat patients, as the disease primarily affects poor and isolated regions with little economic power. To date, there are only a few suitable treatments available, but drugs are expensive and some are highly toxic with severe

side effects for both humans and animals. There are also no vaccines against trypanosomes, the only prevention being a reduction in the frequency of tsetse fly bites.

In contrast to other vectors like mosquitos or sand flies, both male and female tsetse flies are obligate blood feeders and able to transmit trypanosomes. Since African trypanosomes are only transmitted by the *Glossina* species, a vector-orientated control is one of the major attempts against the disease. One approach is the sterile insect technique that is already conducted in parts of Africa, which takes advantage of the unusual reproductive cycle of flies (Vreysen, 2001). Female tsetse flies only need to mate once in their life, as they are able to store the male sperm in spermathecae and fertilize one egg every 9-10 days. Tsetse flies reproduce by adenotrophic viviparity, where females give birth to live offspring. The larva is nourished within the mother by a secretion from modified accessory glands. Pupation takes place a few hours after birth and a fly hatches after 30 days. For disease control, male tsetse flies are bred, sterilized and then released to the wild. If females mate with sterilized males, no larvae will develop during their lifetime, resulting in a decrease in the tsetse population over time. This technique was used successfully for the eradication of tsetse flies on Unguja Island in Zanzibar (Vreysen et al., 2000), but the high costs of this method restrict its use. This especially applies to areas with different tsetse fly species.

2.1.2 Cell architecture and cell cycle

Besides their relevance as a human pathogen, trypanosomes are established as a widely used model protist for molecular cell biology, genetics and parasitology. The best-studied species is *T. b. brucei*, of which two life cycle stages are cultured routinely. This species is of special interest due to its close relationship to human pathogenic trypanosomes. The fact that most organelles are present as a single copy and have a specific location within the cell body makes trypanosomes a well-suited model to study cell biological problems.
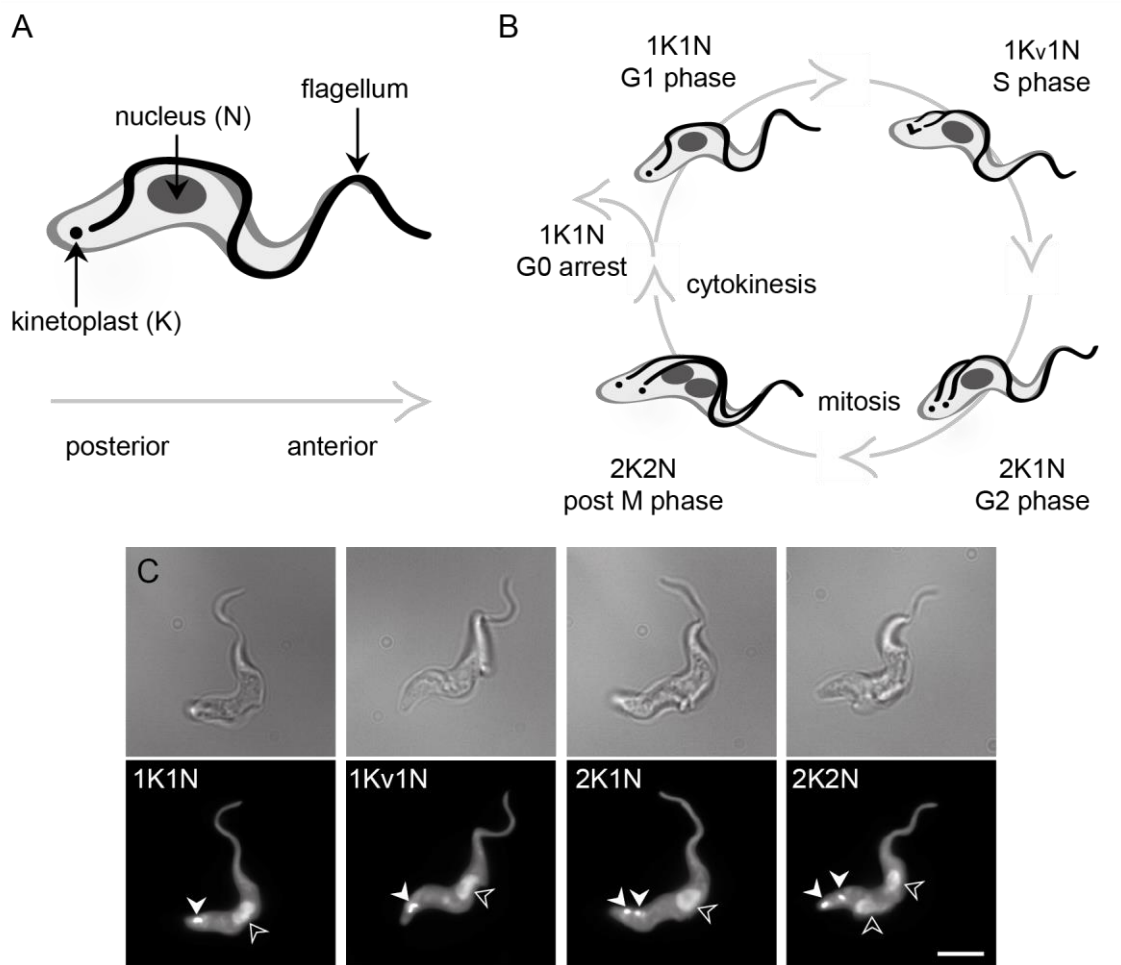
Figure 1: The trypanosome cell and binary cell division. (A) Schematic diagram of a trypomastigote trypanosome slender bloodstream form cell. Shown are the localization of the kinetoplast (K), nucleus (N), the flagellum and the posterior and anterior poles of the cell. The gray arrow indicates the swimming direction. (B) Schematic representation of binary fission with G1, S, G2, post M and G0 phases shown. Duplication of organelles occurs in a defined timeline. In G1 phase cells possess a single copy of each organelle, termed 1K1N. In S phase, the kinetoplast has a V-shaped form and starts dividing, and the new flagellum is visible (1Kv1N). When segregation of the kinetoplasts is completed the cells are termed 2K1N. Nuclear DNA is replicated by mitosis, resulting in a 2K2N cell in post M phase. Binary division occurs by cytokinesis, resulting in two 1K1N cells. From here cells have two options: either re-enter the cell division process, or enter the cell cycle-arrested G0 phase. (C) Chemically-fixed parasites in different phases of cell cycle. The upper row shows transmission images and the lower row shows the cells stained with DAPI (DNA) and AMCA-sulfo-NHS (cell surface). Kinetoplasts (filled) and nuclei (unfilled) are marked with arrowheads. The scale bar represents 5 μm.

Trypanosomes are members of the order Kinetoplastida. This group is defined by the presence of the kinetoplast, the condensed circular DNA of the single mitochondrion (Vickerman and Preston, 1976). The mitochondrion spans the whole cell, whereas the kinetoplast is localized to the posterior end. It is physically connected to the origin of the flagellum, the basal body. The basal body is a key cytoplasmic organizer and plays a central role in controlling cell division (Robinson and Gull, 1991). Cell types of

kinetoplastid protists are defined by the relative positions of the nucleus, kinetoplast, and flagellum. If the kinetoplast is positioned posterior of the nucleus, the cell is defined as a trypomastigote form (e.g. figure 1 A), while a kinetoplast anterior to the nucleus defines the epimastigote stages (Hoare and Wallace, 1966).

Trypanosomes possess a single flagellum that emerges from the flagellar pocket near the posterior pole of the cell. It is attached via the flagellum attachment zone (FAZ) along the cell body and extends beyond to the anterior end of the cell, to produce the free anterior part of the flagellum (Taylor and Godfrey, 1968). Although the different trypanosome life cycle stages have highly variable flagella lengths, they all swim with the flagellum leading at the anterior end. The flagellar pocket is an invagination of the plasma membrane and the only place where endo- and exocytosis can take place (Grünfelder et al., 2003; Engstler et al., 2004; Overath and Engstler, 2004; Field and Carrington, 2009). Underneath the plasma membrane, trypanosomes have a cytoskeleton corset of parallel, regularly-spaced microtubules, which determine the shape of the cell (Hemphill et al., 1991). The cell division process is characterized by microtubule extension at the posterior end and occurs without breakdown of the microtubule corset (Robinson et al., 1995; Rotureau et al., 2011).

In the G1 phase prior to cell division, a trypanosome cell possesses one nucleus (N) and one kinetoplast (K) (1K1N) (figure 1 B-C). The binary fission is organized in a highly accurate and precisely timed manner, beginning with the duplication of the basal body (figure 1 B-C) (Sherwin and Gull, 1989). The new basal body allows the emergence of the new flagellum (Lacomble et al., 2010), with the new flagellum located in a more posterior position (Sherwin and Gull, 1989). The replication of the mitochondrial DNA starts shortly before nuclear S phase (Woodward and Gull, 1990). As soon as the cell enters S phase, the segregation of mitochondrial DNA and the flagellar pocket occurs. In this stage, an elongated V-shaped kinetoplast is visible and the cell starts to replicate the nuclear DNA (1Kv1N). When cells enter G2 phase, the segregation of the kinetoplast is complete, and the cells possess two kinetoplasts and one nucleus (2K1N). After nuclear S phase, the nucleus divides in a closed mitosis without disassembly of the nuclear envelope. The cell then enters post M phase, with two kinetoplasts and two nuclei (2K2N) (Ogdadoyi et al., 2000). As soon as all organelles are replicated, cytokinesis is initiated at the anterior end of

the cell body by a cleavage furrow that proceeds along the longitudinal axis, resulting in two identical daughter cells. It was shown that flagellar motility is necessary for the cell division process (Branche et al., 2006; Broadhead et al., 2006; Ralston et al., 2006). After cell division, cells can re-enter the cell division process or enter the cell cycle-arrested G0 phase.

2.2 *Trypanosoma brucei* life cycle

African trypanosomes possess a complex life cycle. They shuttle between a mammalian host and the tsetse fly vector, having developed various strategies to survive in these different environments (MacGregor et al., 2012; Rotureau and Van Den Abbeele 2013). Besides adaptations in metabolism and surface protein composition, they have also developed multifunctional morphological modifications. For *T. brucei,* at least two different life cycle stages in the mammalian host, as well as various vector-specific stages, have been described. The process of transition from one stage to the other is called differentiation. So far, the best-characterized parasite stages are those that can be grown in culture, namely the slender and stumpy bloodstream forms, and the procyclic tsetse fly form which colonizes the insect midgut *in vivo*. Knowledge of the other developmental stages in the fly is mostly limited to basic morphological characteristics and a few known surface proteins (Sharma et al., 2009). Cultivation and differentiation requirements for the other fly-specific forms have not been established yet. For that reason, working with these forms is limited to the availability of infected tsetse flies. However, the small number of trypanosomes that can be recovered from flies and the difficulty of removing contaminating fly tissue and bacteria makes working with these cells challenging.

2.2.1 Development and survival within the mammalian host

When an infected tsetse fly bites a mammal, infective metacyclic forms are injected into the skin with the saliva. In the host, the G0-arrested metacyclic cells re-enter the cell cycle and differentiate to the long slender bloodstream form stage, but reside in the region of the insect bite during the first days of infection (Dwinger et al., 1988; Caljon et al., 2016). This can cause the typical trypanosome chancre, a swelling at the bite site in humans and animals (Barry and Emery, 1984). Later, parasites enter

the lymphatic system and the bloodstream and are now able to disseminate throughout the host body. Living extracellularly in the blood is both advantageous and challenging. On the one hand, nutrition in the form of glucose is always available, but on the other hand, parasites are continuously exposed to the host immune system. To cope with this situation, trypanosomes have developed various strategies to survive under these harsh conditions and evade the host´s defense mechanisms.

One important survival strategy of the bloodstream form involves the parasite's specialized protein surface coat, consisting of a monolayer of approximately 10^7 identical copies of the variant surface glycoprotein (VSG) (Jackson et al., 1985). VSGs are homodimers, which can freely diffuse on the plasma membrane and make up around 10% of the total protein amount present in bloodstream forms. This dense VSG coat is believed to shield the parasite from the environment and to prevent host antibodies from binding to other proteins than VSGs (Schwede et al., 2011). However, the VSG itself is highly immunogenic and provokes a fast response from the host´s immune system with the production of IgM and IgG antibodies.

At low antibody titers, cells can actively remove antibodies that are bound to the VSGs, a process called antibody clearance. Efficient forward movement creates a hydrodynamic drag that pushes VSGs and antibodies to the posterior end of the cells, where they are endocytosed in the flagellar pocket (Engstler et al., 2007). Antibodies are degraded in the lysosome whereas the VSGs are transported back to the surface. With this combination of endo- and exocytosis the cells are able to clean and recycle their whole surface within 12 minutes (Engstler et al., 2004).

Alongside this first line of defense, the parasites successfully use a strategy that is often found in parasites, namely antigenic variation (Cross, 1977; Deitsch et al., 2009). All trypanosomes express a single copy of the VSG on their surface at any given time, out of a repertoire of more than 2,000 VSG genes and pseudogenes that are encoded in the genome (Cross et al., 2014). They are able to switch to another VSG due to a stochastic switch in expression, which can occur by different mechanisms (Taylor and Rudenko, 2006). The new VSG is immunologically unknown to the host´s immune system and therefore trypanosomes are able to survive and proliferate until antibodies to the new VSG develop and the cycle begins anew. This phenomenon causes the typical waves of parasitemia in infected individuals (Deitsch

et al., 2009). Antigenic variation is the major cause for the absence of a vaccine against sleeping sickness.

There are two different types of cells in the bloodstream, the long and proliferative slender form and the short and non-proliferative stumpy form. Stumpy cells are pre-adapted to survive the conditions in the fly intestine. They possess for example, a higher tolerance for changes in pH and proteolytic stress (Nolan et al., 2000; Engstler and Boshart, 2004; Dean et al., 2009; Matthews et al., 2015). In contrast to the slender forms, they have a limited life span of 2-3 days in the mammalian host (Turner et al., 1995; MacGregor et al., 2011), as they cannot undergo antigenic variation (Amiguet-Vercher et al., 2004). Instead, short stumpy cells fully depend on antibody clearance, which they can do at an even higher rate than long slender forms (Engstler et al., 2007).

Besides the slender and stumpy bloodstream stages discussed above, several other trypanosome life cycle stages have been described in the mammalian host, however, the exact classification is not yet fully established. The literature describes an intermediate form, which morphologically represents a cell during transformation from the slender to stumpy stage (Robertson, 1912; Vickerman, 1965; MacGregor et al., 2012). Other data suggests that trypanosomes of remarkably elongated shape found in the brain might represent a distinct developmental form of the parasite (Mogk et al., 2014 a and b; Mogk et al., 2017). New findings also show that the skin of the host acts as a reservoir for the parasites. Even in the absence of detectable parasitemia in the blood, substantial quantities of trypanosomes are detectable in the skin. These skin-dwelling populations are able to infect tsetse flies and complete the life cycle (Capewell et al., 2016). There is evidence that trypanosomes in extravascular adipose tissue represent an independent developmental form with a distinct transcriptional profile. Different genes are upregulated, suggesting that these forms are able to use fatty acids as an external carbon source (Trindade et al., 2016).

2.2.2 Differentiation of bloodstream forms and transmission to the tsetse fly

While parasites evolved optimal strategies to maximize survival and growth, a successful parasite also needs a strategy to prevent uncontrolled growth as this can

damage the host - a delicate balancing act (Frank, 1996; Seed and Wenck, 2003). In the case of trypanosomes, low parasitemia in the host might additionally result in a reduced transmission potential to the tsetse fly. Therefore, *T. brucei* has evolved a mechanism that limits the parasite burden and at the same time guarantees the maintenance of the infection.

As described in the previous chapter, there are at least two different developmental forms in the bloodstream: proliferative long slender parasites and cell cycle-arrested short stumpy parasites. The differentiation of long slender to short stumpy cells is induced at high parasite densities inside the host by a quorum sensing mechanism (figure 2). The involvement of such a mechanism was first indicated by the observation that trypanosomes stopped proliferating after treatment with plasma of infected animals that showed high levels of parasitemia (Seed and Sechelski, 1989). Reuner and colleagues were able show that the parasites themselves secrete this signal, as differentiation could be induced *in vitro* at high cell densities (Reuner et al., 1997). The signal accumulates over time until a specific threshold is reached that induces stumpy formation: it is therefore termed the stumpy inducing factor (SIF) (Vassella et al., 1997). SIF acts as an external trigger that is transduced into an intracellular signaling cascade (Tyler at al., 2001). If a certain threshold of SIF is reached, most slender forms differentiate to the G0/G1 cell cycle-arrested stumpy stage, with only a small percentage of the population remaining slender (MacGregor et al., 2011). The exact SIF detection mechanism and identification of this factor (or factors) still remains elusive. However, a recent study suggests a mechanism for both SIF production and reception. The authors were able to prove that oligopeptidases released by the parasite generate the paracrine quorum sensing signal and accelerate stumpy differentiation *in vivo* (Rojas et al., 2019). The cell density-triggered differentiation to stumpy cells helps the parasites to control their population size and thus survival of the host is prolonged. If stumpy cells are not taken up by a tsetse fly they will die after 2-3 days (Turner et al., 1995; MacGregor et al., 2011). Recently, a SIF-independent path for stumpy formation was found, which is exclusively controlled by the transcriptional status of the expression site (Zimmermann et al., 2017). Depending on the degree of expression site attenuation, an unsuccessful VSG switch does not automatically result in the death of the parasite; rather, it allows a synchronous differentiation to stumpy cells at low cell densities.
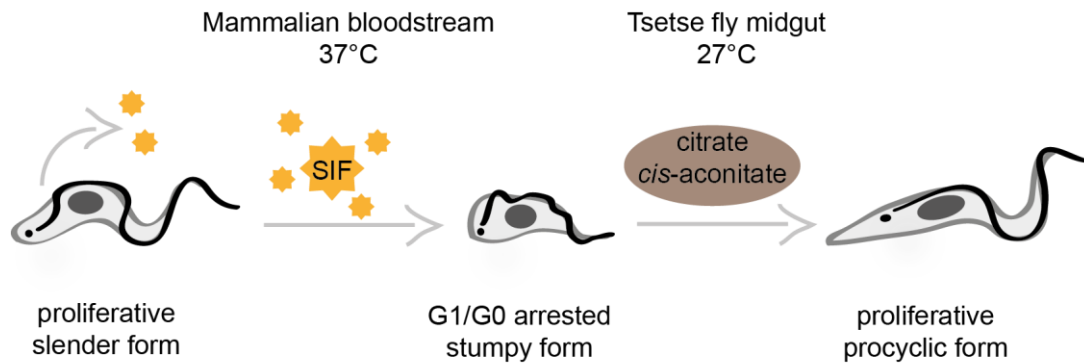
Figure 2: Differentiation from the slender to stumpy bloodstream form and further differentiation to the procyclic insect form. Proliferative long slender cells constitutively secrete the stumpy inducing factor (SIF) inside the mammalian host. If SIF levels reach a specific threshold, differentiation to the G1/G0 cell cycle-arrested short stumpy form is induced. The stumpy form is taken up by the tsetse fly and exposed to a temperature drop and citrate/*cis*-aconiate in the tsetse fly midgut. These changes trigger the further differentiation to the proliferative procyclic form, which is able to colonize the fly gut.

The 'proteins associated with differentiation' (PAD) 1 and 2 are carboxylate-transporters localized on the trypanosome cell surface (Dean et al., 2009). They enable the stumpy parasites to respond to the environmental changes they face during transmission from the bloodstream to the insect midgut. The expression of PAD1 mRNA is initiated and the transcripts accumulate during the early differentiation from slender to stumpy, when slender cells exit the cell cycle (MacGregor and Matthews, 2012). These cells are termed 'committed slender' and are still able to produce SIF. The committed slender cells divide another 2-4 times before exiting the cell cycle and develop further into the so-called intermediate form. In this intermediate stage, the morphological transformation to the short stumpy form starts and SIF is no longer released. The PAD1 mRNA level now reaches a maximum and cells develop further to the stumpy form (MacGregor et al., 2011, 2012). The PAD1 protein is only expressed after the morphological transformation to the stumpy form is almost completed and is distributed over the entire plasma membrane. In contrast, the distribution of the thermo-regulated transporter protein PAD2 is restricted to the flagellar pocket (Dean et al., 2009). The drop in temperature that naturally occurs during the transmission from the bloodstream to the insect from induces a higher protein expression of PAD2 and a relocalization from the flagellar pocket membrane to the whole cell surface, allowing a higher influx of citrate/*cis*-aconitate (Dean et al., 2009). Citrate/*cis*-aconitate are important differentiation triggers naturally found at micromolar concentrations in the midgut of the fly (Hunt et al., 1994). The differentiation of stumpy to procyclic cells can also be

triggered *in vitro* by a combination of temperature drop from 37 °C to 27 °C and the addition of citrate/*cis*-aconitate to the medium (Brun and Schönenberger, 1981; Czichos et al., 1986; Ziegelbauer et al., 1990; Engstler and Boshart, 2004).

The cell cycle arrest of the stumpy form is thought to be important for a synchronous differentiation to the procyclic form in the insect midgut (figure 2). This process includes a rapid change of the surface coat, where GPI-anchored procyclin proteins replace the VSG proteins (Overath et al., 1983; Roditi et al., 1989). The metabolism adapts to the environment in the fly gut where amino acids serve as the main nutritional source, instead of the blood glucose (Overath et al., 1986; Priest and Hajduk, 1994). The temperature drop alone is sufficient to induce the expression of the GPI-anchored procyclin proteins in both stumpy and slender cells, but procyclin localization to the cell surface is restricted to the stumpy stage (Engstler and Boshart, 2004). Experiments have shown that trypanosomes with a deficiency in procyclin proteins on their surface are still able to fulfill the parasite life cycle under laboratory conditions, but with lower efficiency (Vassella et al., 2009).

Morphologically, differentiation from the short stumpy to the procyclic stage involves the elongation of the posterior microtubule corset and repositioning of the kinetoplast midway between the posterior end and the nucleus (Matthews et al., 1995). Finally, cells exit the cell cycle arrest and proliferate as procyclics (Pays et al., 1993; Matthews and Gull, 1994).

For this work, the pleomorphic strain *T. b. brucei* AnTat 1.1 (*Antwerp Trypanozoon antigen type*) was used (Le Ray et al., 1977). Pleomorphic cells exhibit cell density-dependent growth regulation and differentiation and are comparable to wild-type strains found in natural infections. In contrast, monomorphic bloodstream strains only exist as slender forms. It is assumed that these cells have lost the ability to complete the life cycle and are no longer responsive to SIF due to serial passages and cell culture adaptations. Therefore, there is no development to the stumpy stage, no density-dependent check on population numbers, and infected animals are killed quickly by parasite growth. It has been shown that monomorphic cells still secrete SIF, but they appear to be 'signal-blind' and therefore unable to differentiate in response to the presence of SIF, resulting in their hypervirulent phenotype (Reuner et al., 1997; Breidbach et al., 2002). It is nonetheless possible to force cultured monomorphic cells to differentiate directly to the procyclic stage by using chemical

triggers. An increase in cyclic adenosine monophosphate (cAMP) concentration was measured at peak parasitemia and is thought to play a role as a second messenger in the slender/stumpy transition (Manchini and Patton, 1981; Laxman et al., 2006). Treatment with membrane permeable cAMP analogues causes transformation of monomorphic cells to a cell cycle-arrested stumpy-like stage and these cells can undergo synchronized differentiation to the procyclic form in the presence of *cis*-aconitate (MacGregor and Matthews, 2012). However, monomorphic strains remain unable to complete the full life cycle in the tsetse fly vector (Herder et al., 2007; Peacock et al., 2008).

2.2.3 Development inside the tsetse fly vector

The parasite *T. brucei* is exclusively transmitted by the bite of the blood-sucking tsetse fly and the parasite develops in the vector 20-30 days to reach maturation (Vickerman 1985; Rotureau and Van Den Abbeele 2013). By taking up a blood meal from an infected host, tsetse flies ingest proliferative slender and non-dividing stumpy cells, which are transported to the posterior midgut by muscular contractions called peristalsis. Rapid adaptations of the parasites are needed to survive the temperature drop, the change of food resources, digestive enzymes in the gut and immune molecules of the fly. A schematic of the life cycle is shown in figure 3.

The slender cells are unable to survive, whereas the pre-adapted stumpy cells are able to transform into proliferative procyclic forms within 24 hours in the midgut lumen (Fenn and Matthews, 2007). The protein coat of the cell surface changes quickly from VSGs to procyclin proteins (Roditi et al., 1987). There are two different types of procyclins that are characterized by their internal dipeptide (EP, glu-pro) or pentapeptide (GPEET, gly-pro-glu-glu-thr) repeats (Mowatt and Clayton 1987; Roditi et al., 1989; Roditi and Clayton, 1999). Within the first days, procyclic forms express predominantly GPEET proteins, a marker for the early procyclic form (Knüsel and Roditi, 2013). Later, GPEET expression is repressed and only EP expression is maintained, which coincides with the next level of infection (Vassella et al., 2000; Acosta-Serrano et al., 2001). Nevertheless, many of the ingested trypanosomes are eliminated by the fly´s innate immune system within the first days and in some cases the fly is able to eliminate all of the parasites (Maudlin et al., 1998).
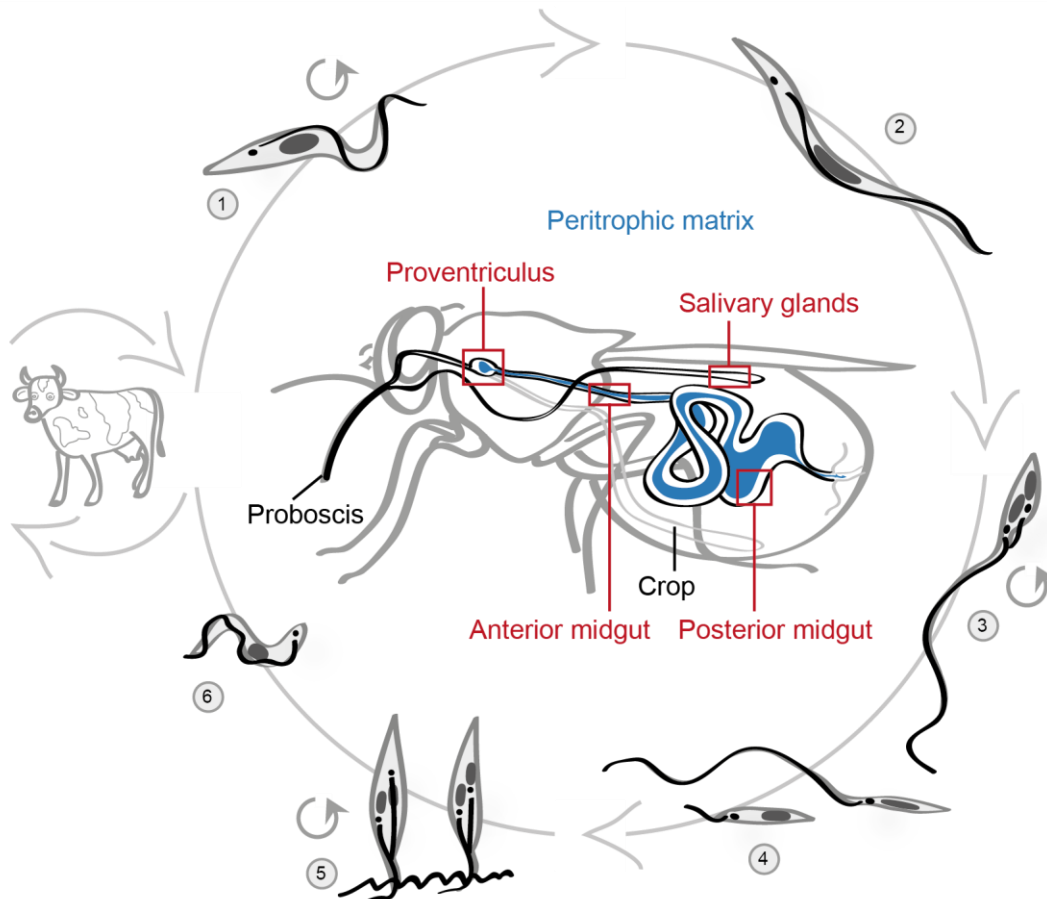
Figure 3: Schematic of the *T. brucei* life cycle inside the tsetse fly vector. Circular arrows indicate proliferative forms. When taken up during the blood meal from an infected mammal (represented here by a cow), trypanosomes are transported with the blood meal to the posterior midgut of the fly where they differentiate rapidly into the procyclic form (1). Procyclic cells cross the peritrophic matrix (blue), a protective sleeve lining the midgut and colonize the ectoperitrophic space between the matrix and the midgut epithelium. Here, they differentiate further to the cell cycle-arrested mesocyclic stage (2). Cells of this stage move towards the anterior end of the midgut, until they reach the proventriculus and differentiate further to the dividing epimastigote stage (3). This stage has an epimastigote configuration and moves from the proventriculus to the salivary glands. It divides asymmetrically, resulting in a short and long epimastigote cell (4). The long cell is thought to die, whereas the short one attaches to the salivary gland epithelium. This attached form is proliferative and two different types of division can occur (5). A symmetric division produces two identical gland-attached epimastigote daughter cells that can further colonize the gland. An asymmetric division produces one epimastigote and one trypomastigote daughter cell. The trypomastigote cell differentiates to the free-swimming infective metacyclic stage (6) that can be transmitted to a mammalian host via the saliva.

Procyclic cells that survive this first attack by the immune system are able to cross the peritrophic matrix within the first days of infection and hide from the fly´s immune system inside the ectoperitrophic space (Gibson and Bailey, 2003; Oberle et al., 2010). The peritrophic matrix is a semi-permeable, non-cellular, continuous and concentric structure inside the fly midgut (figure 3, blue). It consists of three layers, each differing in thickness and composition, but all formed by mixtures of glycosaminoglycans, glycoproteins and chitin (Lehane et al., 1996). Tsetse flies

secrete their peritrophic matrix continuously using a specialized group of cells that are present in the proventriculus (type II formation), regardless of the presence or absence of food (Moloo et al., 1970). One of its functions is to act as a physical barrier against infections with pathogens and abrasive food particles that are ingested with the blood meal (Lehane, 1997; Hegedus et al. 2009). The passage from the endoperitrophic space (the midgut lumen, containing the blood meal) to the ectoperitrophic space (the space between the peritrophic matrix and the midgut epithelium) represents an important bottleneck during the infection process. It is still unknown how exactly trypanosomes are able to cross this border and reach the ectoperitrophic space, but different suggestions have been made (Sharma et al., 2009; Dyer et al., 2013). An unproven, but widely-assumed path is a direct transmigration through of the peritrophic matrix by the parasites (Ellis and Evans, 1977; Evans and Ellis, 1978; Evans and Ellis, 1983; Gibson and Bailey, 2003). Conversely, a recent study proposed that the newly-secreted matrix in the proventriculus represents the entry for trypanosomes to invade the ectoperitrophic space, which also explains the frequent observation of trypanosomes trapped between the three layers of the matrix (Rose et al., 2019). Another study proposed that the flagellar phosphodiesterase PDEB1 is required to actively traverse the peritrophic matrix, and without this, parasites stay trapped in the endoperitrophic space (Shaw et al., 2019). It was also shown that when cells shed their VSG coat shortly after ingestion, the VSG molecules released from the parasites cause a compromised production of the peritrophic matrix by the proventriculus, which enhances the tsetse vector competence for infection (Aksoy et al., 2016).

To maintain the infection, some procyclic parasites stay at the posterior end of the midgut and continuously divide to provide a fresh supply of new parasites (figure 3, 1). Other cells transform into long mesocyclic cells and migrate anteriorly inside the midgut (figure 3, 2). These cells are cell cycle-arrested in G2 phase, where the elongated nucleus has undergone S phase but not mitosis (Van Den Abbeele et al., 1999; Sharma et al., 2008). They also have almost no free flagellum at their anterior end and move inside the ectoperitrophic space until they reach the proventriculus (Gibson and Bailey, 2003).

In the proventriculus another transition takes place and mesocyclic cells, which possess a trypomastigote configuration, differentiate into epimastigote cells. The cells become thinner and the nucleus migrates from the middle of the cell body to the

posterior end (Sharma et al., 2008). Kinetoplast segregation and nuclear mitosis are then initiated, resulting in a dividing epimastigote cell (figure 3, 3). This division occurs asymmetrically and produces a long and a short daughter cell, both possessing an epimastigote configuration (figure 3, 4) (Van Den Abbeele et al., 1999; Sharma et al., 2008). In contrast to other divisions in the parasites life cycle, this particular division involves nearly no increase in cell volume or length, only an extensive remodeling of the cytoskeleton (Rotureau et al., 2011). The cells are somehow able to re-enter the gut lumen and swim through the foregut and the salivary duct to the salivary glands. It is thought that the long cell might act as a transporter for the short cell, which is believed to be a less effective swimmer. When they reach the salivary glands the short epimastigote colonizes the glands and the long epimastigote is assumed to die (Van Den Abbeele et al., 1999; Sharma et al., 2008). This process seems to be another major bottleneck during the infection process as many flies can suffer a heavy midgut infection that does not proceed to a salivary gland infection (Oberle et al., 2010).

Short epimastigote cells attach to the epithelium of the salivary gland with an arborization of the flagellum membrane and colonize the gland by frequent divisions (figure 3, 5) (Tetley and Vickerman, 1985; Vickerman, 1985; Sharma et al., 2008). Cells in the salivary gland use two different types of divisions. The first produces two identical epimastigote daughter cells, which stay attached to the gland and continue to proliferate. This division type is favored during the early stage of salivary gland colonization to sustain the infection. The second division type is asymmetrical and produces an epimastigote and a trypomastigote cell (Rotureau et al., 2012). It is not clear how trypanosomes sense the amount of cells in the gland and what determines whether a symmetric or asymmetric division is used in any given cell cycle. However, it is hypothesized this could be triggered by physical contact or a local quorum sensing pathway.

The resulting trypomastigote cell is called a pre-metacyclic, which is still attached to the epithelium, and finally transforms into the infective metacyclic, a free-swimming cell in the salivary gland lumen (figure 3, 6). The attached parasite population can produce hundreds of metacyclic cells per day and flies stay infected during their entire life span of 3-4 months (Otieno and Darji, 1979). Cells of the metacyclic stage are, once again, cell cycle-arrested, and are the only cells able to establish an infection in a mammalian host. If the fly takes a blood meal, it is able to transmit the

metacyclic trypanosomes via the highly viscous saliva to the mammalian host (Patel et al., 1981). Metacyclic trypanosomes express a small set of metacyclic VSG (M-VSG) genes that prepares them for transmission to a host, where the life cycle begins anew (Barry et al., 1998).

Besides being the final production site of infective metacyclic parasites, the salivary glands are also the only known place where sexual exchange and reproduction of trypanosomes takes place: parasites can undergo meiosis and produce haploid gametes (Peacock et al., 2011; Peacock et al., 2014).

In some endemic countries, the percentage of wild flies that are infected with trypanosomes from the *brucei*-group is quite low (Aksoy et al., 2003; Brun et al., 2010; Kagbadouno et al., 2012; Simo et al., 2015). To ensure their frequent transmission to a host, trypanosomes are able to influence the feeding behavior of the fly during infection. By manipulating the composition of the fly's saliva proteins, trypanosomes cause a severe reduction of major anti-hemostatic activities, resulting in a hampered blood feeding process that forces the fly to feed more often, favoring the transmission of parasites and ensuring frequent vector/host contact (Van Den Abbeele et al., 2010).

Even though the basic route of the parasites through the fly and some critical checkpoints - for example the establishment of a midgut infection and the colonization of the salivary glands - are now established, there are still many open questions concerning the infection process. Most fly-specific forms cannot be cultivated *in vitro* and environmental triggers that influence parasite differentiation within the fly, as well as details on how the parasites interact with its environment, are mostly unknown.

2.3 Motility in the microscopic world

For a long time, it remained unclear exactly how microorganisms move and experience their environment. The Dutch draper van Leeuwenhoek was the first to observe small free-swimming organisms such as protists and bacteria with self-made microscopes in the 17th century (Leeuwenhoek, 1685; Dobell, 1932). He was also the first to discover and describe swimming spermatozoa of animals and humans and their possible role in reproduction (Leeuwenhoek, 1685). Since then, many technical advances have helped us understand the motility of microbial cells and the

mechanisms that are involved. However, there are still many unsolved questions. For example, it is still not fully understood how spermatozoa find their way through the genital tract to reach the egg (Suarez, 2016). Molecular as well as physical interactions play an important role and influence the swimming responses of cells. However, we are only beginning to understand the complex interplay of microswimmers with their natural environments, not least because there is a lack of suitable model systems for the direct analysis of their motility *in vivo*.

2.3.1 Swimming at low Reynolds number

Microorganisms live in a world of low Reynolds numbers, where physical forces affect them differently (Purcell, 1977). The Reynolds number represents the ratio of inertial forces to viscous forces, but at small scales, inertia is virtually irrelevant as the viscous force is many orders of magnitude stronger. This means that mechanisms of swimming that operates at the macro-scale simply do not work in the same way. The drag force of a flagellum immediately converts into active movement, and a stop of beating means an immediate halt for the microswimmer. As a consequence, a simple reversal of movement will bring the organisms back to the initial point. This phenomenon is called the scallop theorem, because a scallop, at a small Reynolds number regime, would move back and forth repeatedly using this reciprocal motion. To move forward, microorganisms must perform a non-reciprocal motion to break the time-reversal symmetry (Purcell, 1977; Lauga and Powers, 2009). Rotating helices (Turner et al., 2000) and cilia with flexible oar-like beats (Brokaw, 1965) exemplify this principle.

The influence of motility on biological interactions in this microscopic world was almost completely neglected for many years, despite its relevance for the overwhelming majority of organisms living on this planet. Besides trypanosomes, various biological model organisms such as the bacterium *Escherichia coli*, the green algae *Chlamydomonas reinhardtii* and spermatozoa all live in the world of small Reynolds numbers. In recent years, physicists and biologists have become more and more interested in these microswimmers and how exactly they have adapted to their environment.

2.3.2 Motility and parasites

Motility is a widespread formula for success amongst parasites to effectively colonize a host and survive in different habitats (Krüger and Engstler, 2015; Schwarz, 2015). Parasites can exploit various microhabitats within individual hosts or during vector transmission. A major group of motile eukaryotic parasites in animals and humans are the flagellates, which use one or more flagella for motion and possess a tremendous morphological variety.

The parasite *Trichomonas vaginalis,* for example, exists in different cellular forms. Its habitat ranges from the urogenital tract and oral cavity to the respiratory and digestive tracts, and it causes the most prevalent sexually transmitted infection in humans, the disease trichomoniasis (Poole and McClelland, 2013; Maritz et al., 2014). The free-swimming trophozoite stage possesses four free-beating flagella in combination with a fifth flagellum attached to the cell body, which forms an undulating membrane between flagellum and cell body (Brugerolle, 1991; de Andrade Rosa et al., 2013). This swimming stage is also known to form large cell aggregates, called swarms, which could represent a form of defensive reaction to the host immune response (Honigberg, 1990; Hirt, 2013). As soon as the parasite comes into contact with the vaginal epithelium, the free-swimming parasite transforms quickly into an amoeboid cell stage to increase surface contact. The parasite keeps its flagellar apparatus in order to rapidly detach and change its location within the vaginal mucosa, however (Kusdian and Gould, 2015).

Another important flagellated parasite is represented by the genus *Leishmania.* Transmitted by blood-sucking female sand flies, they are the causative agent of different leishmaniases (Bates, 2008). The motile stage in the vector is called a promastigote and swims extracellularly with one free anterior flagellum by producing planar waves (Gadelha et al., 2007). There are several different promastigote stages with distinct swimming capabilities. Motility is required to move within the vector´s midgut, and to ensure a favorable localization at the anterior of the midgut for transmission via the next insect bite (Sunter and Gull, 2017). Besides its obvious role in motility, the flagellum is also utilized for attachment mechanisms in the sand fly (Bates, 2007; Bates, 2008). In the human host, parasites invade phagocytotic cells and differentiate into the almost immotile and intracellular amastigote form. This cell

invasion process is also active and highly dependent on the polarized morphology and motility of the infective promastigote form (Forestier et al., 2011).

The examples described above highlight the importance of flagellated motility and the versatile role for different types of parasites. Motility must be adapted dynamically to varying physical environments and different parasite needs during the infection process (Krüger and Engstler, 2015; Schwarz, 2015). Most studies in parasite research, however, focus on general biology, biochemical or immunological processes. Physical challenges that the parasites face within the host environment - for example when crossing barriers or moving in flow forces, and the corresponding adaptations of the parasites - have been somehow neglected. Therefore, in most cases it is not entirely clear what constrains the shape and motion of a parasite. The profound impact of the microenvironment is however moving more and more into the focus of contemporary research (Muthinja et al., 2018). The detailed analysis of parasite motility allows insights into the role of different morphotypes and provides quantitative data on the physical forces that are involved in host parasite interactions, for example during host invasion. The interest in motility-associated virulence is increasing, but the required experiments often remain methodically demanding and appropriate model systems are rare (Elgeti et al., 2015; Schwarz, 2015; Muthinja et al., 2018).

2.3.3 Trypanosomes as a model microswimmer

African trypanosomes are true professionals when it comes to infecting a wide range of hosts and have developed various strategies to survive in their hosts. Due to their extracellular 'lifestyle', they were amongst the first parasites to be observed swimming around and "…, wriggling about like tiny eels and swimming from corpuscle to corpuscle,…" (Bruce, 1895). Motility of these parasites is tailored to a variety of habitats and biological niches, representing an important virulence factor. Most work on flagellated parasite motility has been conducted on the model organism *Trypanosoma brucei*.

As briefly mentioned in chapter 2.2.1, trypanosomes are able to remove VSG-bound antibodies from their cell surface (figure 4 A). During directional swimming, the resulting hydrodynamic force of the surrounding fluid is able to specifically

redistribute VSG-antibody complexes to the flagellar pocket (Engstler et al., 2007). This was the first description of a protein sorting mechanism due to pure physical forces and catalyzed interest in trypanosome motility. A swimming speed above a certain threshold is required to generate enough hydrodynamic force, but, surprisingly, the swimming velocities measured in cell culture conditions proved to be too low for sufficient antibody clearance. This raised the question of how the swimming mechanism of trypanosomes works and in particular, in what way swimming behaviors differ between cultured trypanosomes and trypanosomes in their natural environment.

One major characteristic of trypanosomes is the continuously beating flagellum that is attached to the parasite, describing a 180° turn around the cell body (figure 4 A). Due to the chiral, helical path of the flagellum, trypanosomes rotate during directional swimming along their longitudinal axis (Heddergott et al., 2012; Alizadehrad et al., 2015). They swim by producing travelling waves along the cell body, thereby producing a forward propulsion force. This means that the force direction and propagation of waves is opposite to the propulsive velocity of the swimmer. This mechanism was first quantitatively analyzed in sea urchin spermatozoa and is described by the resistive force theory (Gray and Hancock, 1955; Gray, 1955, Lauga and Powers, 2009). The flagellar waves are non-reciprocal, which is consistent with requirements for swimming at low Reynolds numbers (see chapter 2.3.1) (Purcell, 1977). This pattern of motion is also consistent with the swimming mechanisms used by mammalian sperm cells, the classic model flagellar microswimmers (Lindemann and Lesich, 2016).

A unique feature of trypanosomes is the fact that they are able to simultaneously produce flagellar waves from both ends. During forward motion they generate waves from the anterior tip of the cell, which travel along the body to the base of the flagellum at the posterior end of the cell (tip-to-base beat). This also works in the reverse, and parasites can go in the opposite direction simply by producing waves from the base of the flagellum that travel to the flagellar tip (base-to-tip beat). In addition, it is possible for the parasites to produce a forward and reverse wave at the same time (Heddergott et al., 2012). This seems unique for trypanosomes, as in other trypanosomatids a reversal of beat direction can only be initiated after the previous wave is completed (Gadelha et al., 2007).
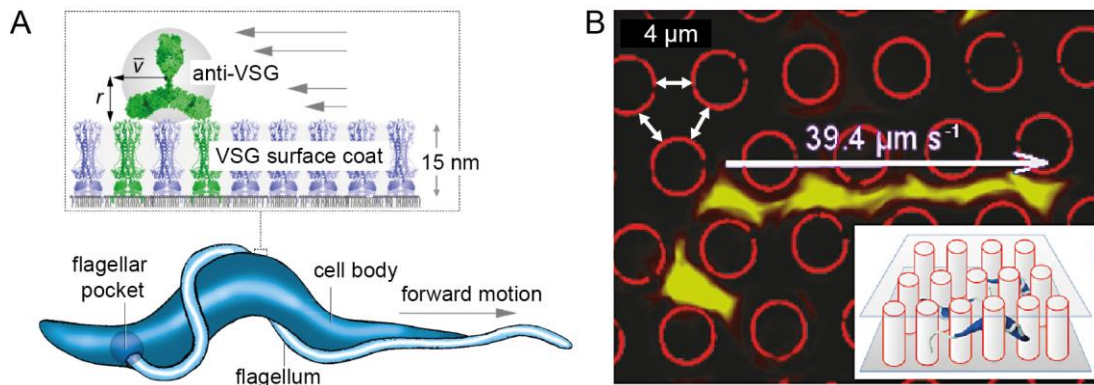
Figure 4: Bloodstream form trypanosomes use motility as a survival strategy. (A) Trypanosomes have a dense coat of VSG proteins. If antibodies bind to the parasite´s surface, the VSG-bound antibodies are redistributed via hydrodynamic flow to the flagellar pocket at the posterior end of the cell. Antibodies and VSGs are endocytosed, but the VSG proteins are recycled and transported back to the cell surface while antibodies are degraded. This process requires efficient forward motion of the parasite. Figure adapted from Krüger and Engstler, 2017. (B) Trypanosomes exposed to artificial pillar arrays (here 4 μm spacing) with diameters corresponding to the size of red blood cells swim more persistently and at higher velocities than when exposed to low-viscosity media or environments without obstacles. The motion is perfectly adapted to the crowded environment in the mammalian bloodstream. Figure adapted from Heddergott et al., 2012.

In low-viscosity fluids, trypanosomes tend to frequently tumble (i.e. undergo unproductive motility) and the beat reversal occurs randomly. In bloodstream trypanosomes, it was shown that this tumbling motion is produced by the frequent interruption of tip-to-base waves by single reverse waves that cause changes in swimming direction. The extent of tumbling is highly influenced by mechanical confinement and the viscosity of the environment (Heddergott et al., 2012; Bargul et al., 2016). Experiments with artificial pillar arrays revealed that the presence of obstacles resembling erythrocytes in the blood circulation in size, shape and spacing, enables slender bloodstream trypanosomes to reach their maximum forward velocity (figure 4 B) (Heddergott et al., 2012). In contrast, if the density of these artificial erythrocytes is increased, parasites reverse their flagella beats and swim backwards. In the host this behavior might prevent the parasites from getting trapped in tissue spaces or collagen networks. In the absence of obstacles, for example in commonly used liquid cell culture medium, parasites have irregular waveforms and tumble. Thus, the motion of trypanosomes is perfectly adapted to survive in the crowded environment of the mammalian bloodstream.

Their highly flexible swimming modes allow the parasites to respond to various cues in their environment and play an important role in colonizing the host tissues. The ability to manoeuver between different compartments of the host is essential for parasite survival and an endless supply of glucose in the blood allows incessant

motility. Although all African trypanosomes live in the bloodstream, Bargul and colleagues found that the morphotype and motile behavior of different species are correlated to the distinct niches they colonize inside their different hosts. These features can be described by the 'cellular waveform' of swimming parasites (Bargul et al., 2016). The cellular waveform is defined as the product of the chirality and the oscillation of the flagellum as well as the elastic modulus of the cell body. All these parameters can be combined to describe the unique and dynamic pleomorphism of individual trypanosomes in one model. For example, the waveform of *T. vivax* seems to be perfectly adapted for the topology of the bloodstream and enables the parasite to reach high swimming velocities. In contrast, *T. congolense* reveals a reduced and stiff waveform, which makes it a comparably weak swimmer, evolved for low flow areas of the blood circulation.

Flagellar attachment to the cell body, morphology and flexibility of the cell body affect motile behavior (Heddergott et al., 2012; Alizadehrad et al., 2015). High-speed microscopy data has enabled physicists to produce computer simulations of swimming parasites using multi-particle collision dynamics (Babu and Stark, 2012; Alizadehrad et al., 2015). This approach allowed the *in silico* prediction of adaptive values of morphology and the generation of hypothetical swimmer types. Such model data can be directly compared to *in vivo* data and used to explain morphological constraints and advantages of cell design in natural swimmers.

Some *in vitro* studies with early procyclic trypanosomes showed a form of collective behavior, called 'social motility'. When plated on semi-solid agar plates, parasites proliferate and move on the surface, producing radiating patterns outwards from the original colony (Oberholzer et al., 2010). This behavior occurs in the early procyclic stage and might mimic the early colonization of the fly´s midgut (Imhof et al., 2014). Apart from these social motility studies with procyclic cells, trypanosome motility has exclusively been analyzed for the bloodstream forms either in cell culture or for different species isolated from selected hosts (Heddergott et al., 2012; Bargul et al., 2016).

In fact, the tsetse fly itself and the developing, migrating trypanosomes infesting it, represent an untapped model system for trypanosome motion, despite the fact that motility plays a key role for a successful infection of the vector. The small size of the fly provides a tractable space for direct observations on different scales, from whole

infested organs to single trypanosomes. Many studies have investigated the morphological changes and distribution of the parasites inside the vector, but next to nothing is known about the parasite´s swimming behavior in its natural environment. It is known that motility is necessary to complete the life cycle (Rotureau et al., 2013), yet no quantitative motility data on the various tsetse fly forms are available. The direct interplay of these trypanosomes and their vector might give potential insight into the infection process and evolution of the host-parasite relationship. Therefore, this system might provide insights into relevant biological processes on the one hand, and represent an attractive model for microswimmer research on the other.

2.4 Aims of the thesis

Trypanosomes undergo a complex life cycle. Consecutive morphological changes ensure the parasite's adaptation to the various different environments they face within the mammalian host and tsetse fly vector. Tsetse flies are sensitive organisms and in fact, the maintenance of a colony is time-consuming and difficult. This is one of the reasons why only a few laboratories in the world work with tsetse flies and most scientists work with culture forms of procyclic trypanosomes *in vitro*. However, as shown for bloodstream trypanosomes, the behavior *in vitro* can be significantly different from natural conditions *in vivo* (Heddergott et al., 2012). Slender bloodstream trypanosomes are perfectly adapted to the crowded environment of the mammalian blood circulation, because cell morphology and motility correlate to allow fast and effective movement in the host environment (Heddergott et al., 2012; Bargul et al., 2016).

Due to these observations, one aim of this work was to correlate the parasite´s motility with both their cell morphology and the microenvironments within the vector. Therefore, at the beginning of this thesis, a stable tsetse fly colony was established in the laboratory. This allowed unlimited access to the parasite-infected vector. The goal was the establishment of the trypanosome-tsetse system as a new model for motility studies, containing diverse microswimmer types in their natural habitats. By using state-of-the-art microscopy techniques, the complex swimming behavior of fly-specific trypanosomes as well as topological constrains inside the fly were analyzed and characterized. In addition, nature-inspired artificial environments were

designed and tested. Controllable and defined geometries allow analysis of trypanosome motility that can be directly compared to the *in vivo* system.

Another part of this thesis focused on the infection process of the tsetse fly. Using the trypanosome-tsetse system, it was possible to revisit some key points of trypanosome biology. Previous data from the laboratory suggested that stumpy trypanosomes might not be the only infective stage for the tsetse fly, which contradicts the current literature (Robertson, 1912; Vickerman, 1965; MacGregor et al., 2012). Instead, experiments with pleomorphic stumpy and slender trypanosomes showed similar infection rates, both resulting in mature salivary gland infections. This suggested that slender trypanosomes might also be an infective form, which was further investigated during this work. For this purpose, additional fly infections were performed where the likelihood of stumpy trypanosomes being ingested was minimized. In addition, the early developmental processes of slender and stumpy populations inside the tsetse fly were under investigation. Due to low parasite numbers *in vivo*, live cell microscopy, cell cycle analysis and fluorescent reporter cell lines were used to detail the parasite´s development directly in the vector.

3 Results

3.1 Establishment of the trypanosome-tsetse model system for microswimmer analysis

3.1.1 Characterization of the trypanosome microenvironments in the tsetse fly vector

In order to make the trypanosome-tsetse system accessible as an experimental model system, it was first necessary to analyze the *in situ* environments that the fly body offers the parasites. The relatively small size of the fly as well as the translucence of its organs proved beneficial for microscopic analysis. The infection of the various tsetse organs by the trypanosomes is well known, but the three-dimensional architecture of the tissue and the physical parameters influencing the parasites have been largely neglected so far. Therefore, different microscopic approaches were adapted to gain an overview with sufficient resolution to map the fly´s internal topology and physical constraints.

3.1.1.1 Microarchitecture of fly tissue

Multicolor light sheet fluorescence microscopy (LSFM) was adapted for the tsetse system to detail the three-dimensional structure of infected organs. This technique allows the generation of high-resolution optical stacks of intact transparent tissue by imaging autofluorescent or fluorescently-labeled structures and simultaneously allows the mapping of the distribution of fluorescent trypanosomes contained therein.

At first, complete tsetse flies were analyzed to understand the inner organization and organ localization in 3D. For this purpose, the specimen preparation protocol for LSFM required adaptations due to the complex optical properties and the size of a complete fly (figure 5 A). Different conditions were tested, to allow an adequate fixation of the tissue. The best results were achieved after the head, legs and wings were removed. In addition, holes were cut into the cuticle, to achieve a better fixation of inner organs. An extensive bleaching step was necessary to eliminate the dark pigmentation of the insect´s cuticle. Different bleaching conditions (15%, 20%, 25% and 30% H_2O_2) and incubation times (3, 6, 7, 9 days) were tested. A clearing procedure using 30% H_2O_2 for 7-9 days was determined to be optimal (figure 5 B).

After several dehydration steps, flies turned translucent in a benzyl alcohol/benzyl benzoate (BABB) clearing solution (figure 5 C).
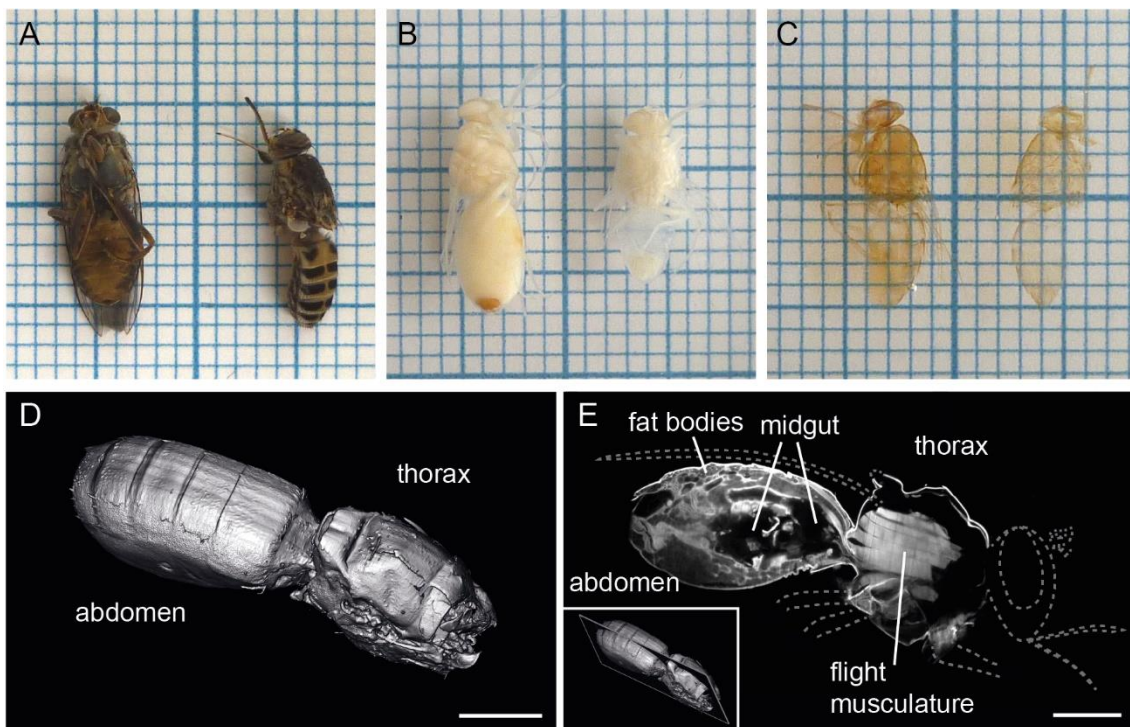
Figure 5: Tsetse fly tissue exhibits a strong autofluorescence signal, which can be recorded by light sheet fluorescence microscopy. Tsetse flies (A) were fixed, bleached (B), dehydrated and further cleared (C) in clearing solution (BABB). Images were taken on a millimeter paper background, to visualize the size and tissue transparency after the last protocol step. (D) Surface rendering model of a non-fertilized female tsetse fly, visualized by light sheet fluorescence microscopy. Head and extremities were removed and some holes cut into the cuticle, to allow better fixation of the tissue. (E) Cross-section of the three-dimensional image stack, visualizing internal anatomical details. Dotted lines indicate positions and approximate sizes of removed body parts. The cuticle, fat bodies and the flight musculature revealed a strong autofluorescence signal, whereas the autofluorescence of the abdominal midgut was comparably weak. The inset depicts the position in the image stack. Scale bars represent 1 mm. Image (D) and (E) and video 1 adapted from Schuster et al., 2017.

In total, 10 individual tsetse flies were analyzed by LSFM. Image stacks of the complete abdomen and thorax were recorded and analyzed using the Amira software package. The outline of a fly is shown in figure 5 D, using a surface rendered model of the strongly autofluorescent cuticle, recorded in the green fluorescence channel. A single slice from the original stack is shown in figure 5 E, visualizing details in the intestinal lumen and its typical structures (video 1). This example shows a mature non-fertilized female fly. Flight musculature in the thorax and fat bodies in the abdomen exhibited strong autofluorescence. The location of the abdominal midgut was visible as a black area, due to negligible autofluorescence compared to the surrounding abdominal tissue. The narrow midgut channel leading to the anterior part

in the thorax was clearly visible at the junction between abdomen and thorax. Due to the harsh bleaching procedure with 30% H_2O_2, for these specimens it was not possible to detect any fluorescence signals from beads, trypanosomes, or peritrophic matrix labeling.

To achieve higher resolution, complete digestive tracts were surgically removed from the flies. The midgut epithelium showed an adequate autofluorescence signal in the green emission wavelength, enabling visualization of all details. As the isolated midgut is almost transparent, no bleaching was needed in these preparations. Flies were fed with rhodamine-labeled wheat germ agglutinin (WGA) to specifically label the peritrophic matrix inside the midgut. WGA is a lectin and binds to the sugar N-acetyl-D-glucosamine, a main component of the peritrophic matrix. This highly specific binding was accomplished during the feeding process, and produced a strong red fluorescent signal labeling the peritrophic matrix, clearly separable from the green autofluorescent surrounding tissue. In total, 25 different dissected midguts were analyzed by LSFM.

Parts of the intact midgut were recorded in different fluorescence channels and three-dimensionally reconstructed. Figure 6 shows a representative section from the anterior (A) and posterior midgut (B) of an uninfected fly (video 2). In the top panel the epithelium and associated fat bodies are shown as a surface model (gray), enclosing the peritrophic matrix (cyan). The surface model of the peritrophic matrix itself is shown in the mid panel. The bottom panel shows a single slice from the corresponding original stack, revealing a significant degree of convolution. The peritrophic matrix in the anterior part of the gut had a smaller diameter and less surface area compared to the posterior part. In the unfed fly, the matrix was tightly packed and folded along the complete midgut. The significant available surface area of matrix towards the posterior end of the gut allows the massive swelling of the abdomen during blood uptake by of the fly without rupturing the protective sheath.

The results confirmed that LSFM is a powerful tool to obtain detailed information about the tsetse inner topology and *in vivo* boundary conditions.
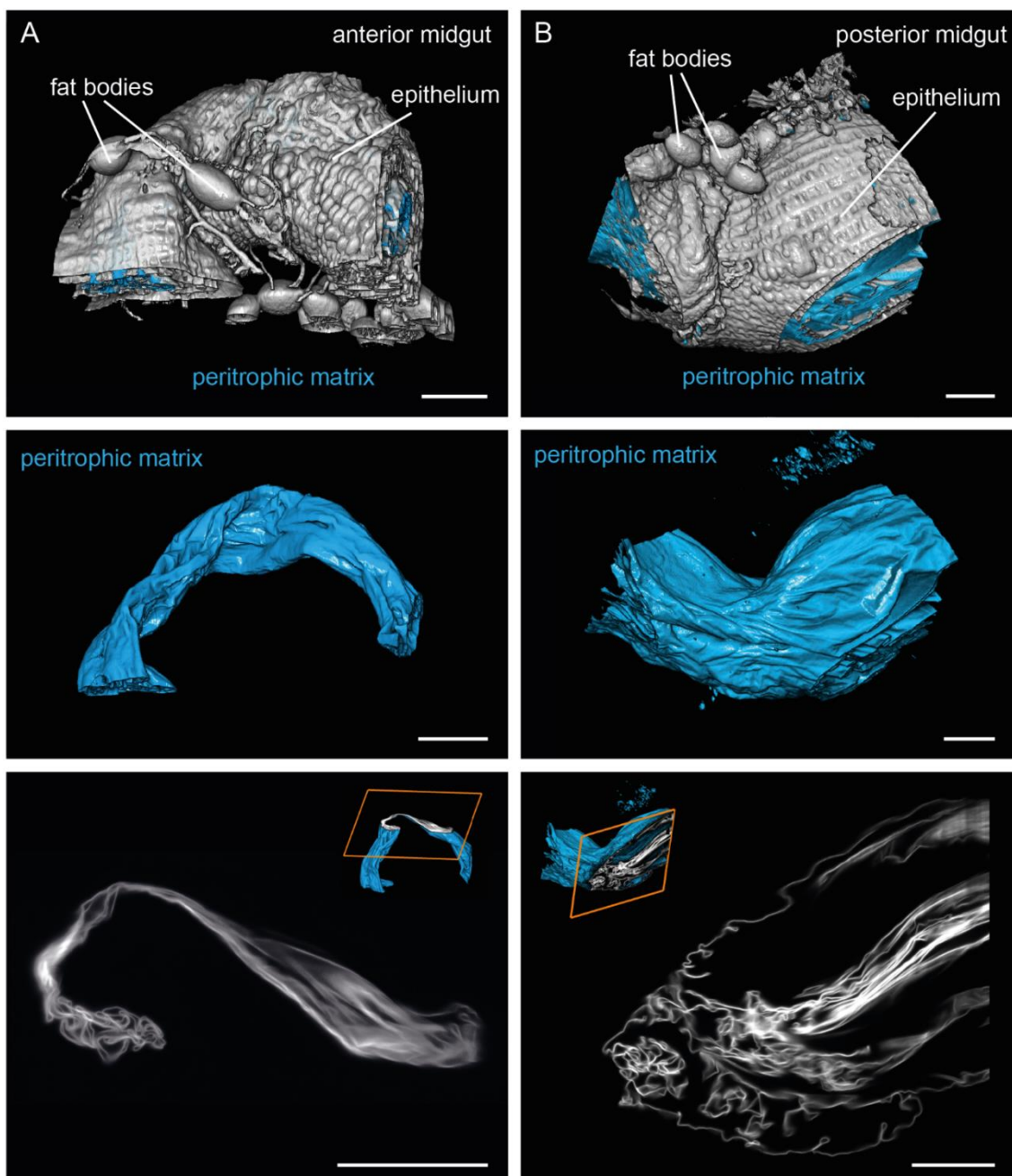
Figure 6: The peritrophic matrix inside the tsetse fly midgut shows a high degree of convolution. Fly tissue exhibits a strong autofluorescence signal, whereas the peritrophic matrix needed to be stained with rhodamine-labeled wheat germ agglutinin. Midguts were surgically removed 1-2 days after the last blood meal, immediately fixed and further prepared for multicolor light sheet fluorescence microscopy. The upper panel shows three-dimensional reconstructions of specific areas from the midgut of a tsetse fly, showing epithelial surrounding (gray) and peritrophic matrix (cyan). The middle panel only shows the surface of the peritrophic matrix. The bottom panel shows a single slice (orange box) from the corresponding original stack. (A) Representative part of the anterior midgut region with attached fat bodies on the epithelia surface. (B) Representative part of the posterior midgut region with attached fat bodies on the epithelia surface. Scale bars represent 100 µm. Video 2 shows animated versions of the models and the original stack (step size in z-projection 2 µm). Figure and video adapted from Schuster et al., 2017.

3.1.1.2 Visualization and localization of trypanosomes in the tsetse environment

After clarifying the uninfected fly´s interior architecture using LSFM, the next step was to visualize parasites inside the tissues. For this purpose, flies were infected with trypanosomes expressing various fluorescent proteins and recorded in different cell compartments. All fluorescent proteins were found to be expressed throughout the life cycle in all developmental stages.

In order to label trypanosome nuclei, a green fluorescent protein (GFP) was expressed as a fusion protein with a nuclear localization signal (NLS) peptide. Parasites expressing NLS:GFP showed a strong green fluorescence nuclear signal, easily detectable inside the fly tissue. Single cell nuclei could be resolved, allowing the accurate localization of single parasites. Depending on the position of the cell in the focal plane, the exact shape of the cell nucleus was recordable. The NLS:GFP cell line was additionally transfected with a construct encoding a N-terminal EGFP-tag (enhanced green fluorescent protein) fused to PFRA, one of the main extra-axonemal proteins of the paraflagellar rod (PFR). In cells expressing PFRA:EGFP and NLS:GFP, no flagellar fluorescent signal could be detected in the LSFM images, and only the nuclear signal was visible. In an attempt to improve signal intensities, the fluorescent protein mNeonGreen was used, which has a brighter fluorescence signal than GFP or EGFP (Shaner et al., 2013; Hostettler et al., 2017). Cells expressing mNeonGreen in the cytoplasm were visible inside the tissue, but in areas crowded with parasites it was difficult to distinguish individual cells. In some parts of the tissue, the autofluorescence did not allow a sharp separation of parasites and tissue. In order to circumvent this problem, a cell line expressing the high intensity red fluorescent protein, tdTomato (tandem dimer Tomato) in the cytoplasm was tested (Shaner et al., 2004, 2005). However, inside the tissue the red signal was weak and parasites could barely be identified in LSFM recordings.

Due to the intensity and stability of the NLS:GFP signal in the LSFM recordings, the NLS:GFP cell line was preferentially used to analyze trypanosomes inside the tsetse´s interior. Flies were analyzed at different time points after initial infection with procyclic trypanosomes. Figure 7 (video 3) shows representative examples of single trypanosome localizations inside the tsetse midgut, visualized in three-dimensional reconstructions. Flies were fed with rhodamine-labeled WGA to specifically label the

peritrophic matrix inside the midgut and fixed afterwards. For some samples, an additional staining with propidium iodide was performed after fixation, in order to label the surrounding epithelial cells simultaneously with the peritrophic matrix (figure 7 B). In the top panel the epithelium is shown as a surface model (gray), enclosing the peritrophic matrix (cyan) and trypanosome cell nuclei (yellow). The surface model of peritrophic matrix and cell nuclei is shown in the mid panel. The bottom panel shows a single slice from the corresponding original stack, with cell nuclei highlighted in yellow. Figure 7 A shows an area of the posterior midgut of a fly at the early stage of infection (2 days post infection with procyclic trypanosomes). Parasites are visible only in the endoperitrophic space, evenly distributed in the lumen and in some cavities of the peritrophic matrix. No parasites are located on the outer surface of the matrix, namely in the ectoperitrophic space between the matrix and the epithelium. In contrast, figure 7 B shows a posterior midgut at a later point of infection (>8 days post infection with procyclic trypanosomes). At this point, trypanosomes are thought to have crossed the peritrophic matrix and will have started colonizing the whole alimentary tract (Gibson and Bailey, 2003; Sharma et al., 2009). The model shows a cross section through an intact gut. No parasites are detected in the lumen, but cell nuclei are visible between the matrix and the epithelium. In the mid panel, the matrix is illustrated semi-transparently, allowing a visualization of trypanosomes underneath the matrix inside the ectoperitrophic space.

Due to its huge surface, the peritrophic matrix is extremely convoluted and fills in broad spaces in the midgut. In all samples analyzed, most trypanosomes were in close contact to the peritrophic matrix and various parasites were located inside the peritrophic matrix folds. Parasites were tightly packed in groups or as single parasites in large cavities or were even encased completely by the peritrophic matrix folds.

In summary, LSFM was sufficient to analyze parasite populations inside the tissue and determine the exact position of parasites inside the complex environment.

Besides the midgut and the complexity of the peritrophic matrix, there are other structurally interesting regions with biological relevance for the infection process. Therefore, the bacteriome and the proventriculus were analyzed as distinct regions and the parasite distribution determined.
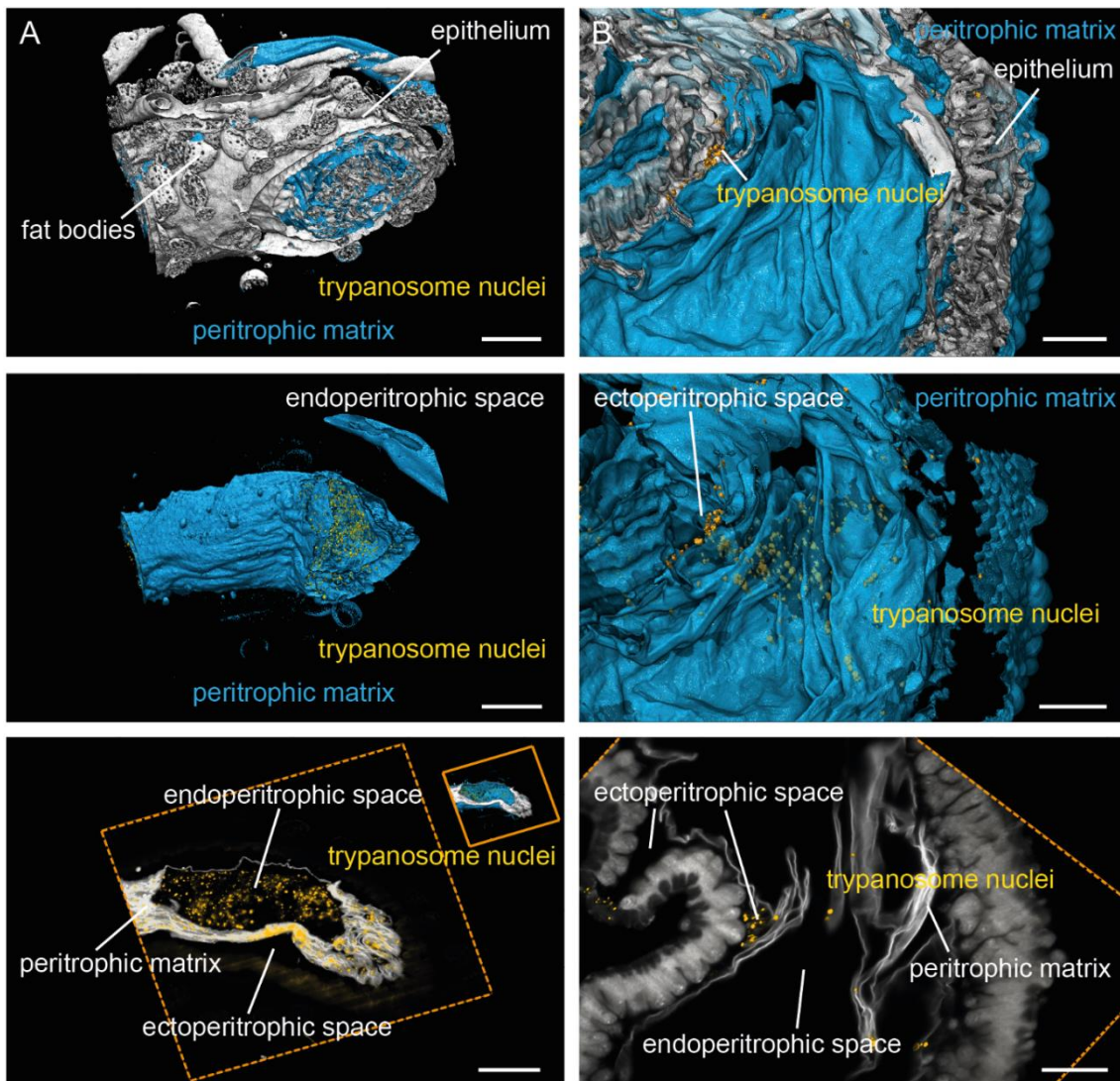
Figure 7: Trypanosome nuclei can be visualized within the complex folding of the peritrophic matrix on a single cell level at different time points after infection. Flies were infected with procyclic trypanosomes expressing GFP in the cell nucleus. Fly tissue exhibits a strong autofluorescence signal, whereas the peritrophic matrix was additionally stained with rhodamine-labeled wheat germ agglutinin (A and B). For (B) an additional staining with propidium iodide was performed, to label the epithelia cells. Midguts were surgically removed and immediately fixed and further prepared for multicolor light sheet fluorescence microscopy. The upper panel shows three-dimensional reconstructions of the posterior midgut of a tsetse fly whereas the middle panel only shows the cyan surface of the peritrophic matrix (A) and peritrophic matrix and epithelial surrounding (B). Trypanosome nuclei are depicted in yellow. The bottom panel shows a single slice (orange box) from the corresponding original stack. (A) Dissected posterior part of the midgut 2 days post-infection. Trypanosomes are exclusively localized in the endoperitrophic space inside the midgut lumen. (B) Dissected posterior midgut >8 days post-infection. The top panel showing the midgut lumen allows a view into the empty endoperitrophic space. The mid panel is displayed semi-transparently, to visualize trypanosomes in the ectoperitrophic space between the matrix and the epithelia cells. Scale bars represent 100 µm (A) and 50 µm (B). Video 3 shows animated versions of the models and the original stack (step size in z-projection 2 µm). Figure and video adapted from Schuster et al., 2017.

The bacteriome is an area in the anterior midgut of the fly, harboring essential bacterial symbionts, particularly *Wigglesworthia*. These endosymbiotic bacteria

reside intracellularly in the cytosol of specialized epithelial cells, the bacteriocytes (Aksoy, 1995; Wang et al., 2013). The bacteriocytes together form the horseshoe-shaped bacteriome. This area is metabolically highly active and therefore many trachea are attached to the surrounding epithelium. As shown in figure 8, trypanosomes were evenly distributed around the bacteriocytes (video 4). Figure 8 shows a surface model with the epithelium (gray) and trypanosome nuclei (yellow) (figure 8 A) as well as images of single slices from different bacteriome stacks to visualize the distribution around the bacteriocytes (figure 8 B, C, D). In all samples analyzed, accumulations of trypanosomes were in close contact to the bacteriome cells and the peritrophic matrix. The examples shown were taken from late-stage infections and parasites were located in the ectoperitrophic space.

Another structurally distinct region is the proventriculus, which represents an important bottleneck for the infection process (Oberle et al., 2010). The proventriculus is the connection between the anterior midgut, the crop and the oesophagus and is localized in the thorax of the fly. Trypanosomes have to migrate from the ectoperitrophic space back to the lumen and eventually reach the salivary duct, but how exactly trypanosomes cross this barrier is still unknown. The peritrophic matrix is continuously produced in the proventriculus and secreted by a specialized group of cells, which form a ring-like structure named the annular pad (Wigglesworth, 1929; Rose et al., 2019). In this organ, the foregut cells become confluent with the midgut cells. Figure 9 (video 5) shows examples of an infected proventriculus as a 3D model (A) and single slices from different original stacks generated by LSFM (B, C, D), in which the first image (B) represents the stack from the surface model (A). The surface model visualizes the proventriculus (gray) with its connections and trypanosome nuclei (yellow). Flies were infected with procyclic trypanosomes expressing GFP in the cell nucleus (A, B) or mNeonGreen in the cytoplasm (C, D). Flies were dissected at a later stage of infections, showing heavy infections and high parasite infection densities. The three-dimensional analysis showed that trypanosomes experience varying confinement conditions inside the proventriculus. The organ contains open regions as well as tissue invaginations, with limited space. Trypanosomes were massively concentrated around this toroid region, namely the annular pad, in all analyzed specimens (figure 9 A, B, C).
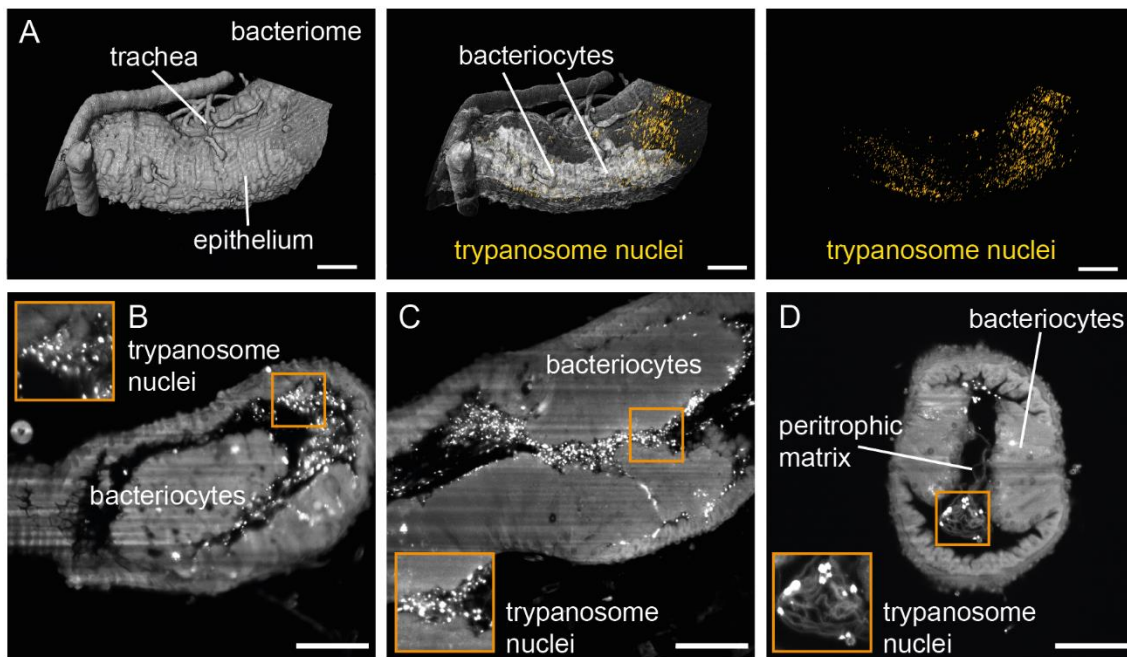
Figure 8: Multicolor light sheet fluorescence microscopy reveals the distribution pattern of trypanosomes around the bacteriome. Tsetse flies were infected with procyclic trypanosomes expressing GFP in the cell nucleus. Midguts were surgically removed and immediately fixed and further prepared for multicolor light sheet fluorescence microscopy. (A) A three-dimensional reconstruction of the bacteriome in the anterior midgut region. The first image shows the epithelial surrounding (gray) rendered using the autofluorescence. The middle image shows the 3D localization of trypanosome cell nuclei (yellow) within the semi-transparent organ model (gray). Cell nuclei were pinpointed using the strong GFP signal. (B, C, D) Single slices from original stacks show the extracellular distribution of trypanosomes around the bacteriocytes. Each inset (orange) represents an enlargement of trypanosome nuclei, whereas the position is indicated in the main image. Image (B) represents the stack corresponding to the surface model shown in (A). Trypanosomes were visible between the folds of the peritrophic matrix (D). Image (D) shows a transverse cut through the bacteriome. Scale bars represent 100 µm. Figure 8 A adapted from Schuster et al., 2017. Video 4 shows the original stacks (step size in z-projection 2 µm).

In summary, LSFM was shown to be a valuable microscopy technique for the analysis of the three-dimensional constraints parasites face in their natural environment. The usage of different fluorescent cell lines and specific tissue labeling allowed an accurate visualization of trypanosome distribution in their natural habitat at different infection time points and varying cell concentrations with single cell accuracy. It was possible to provide high-resolution maps of the *in vivo* topology that trypanosomes experience during their journey through the fly. It was shown that trypanosomes are exposed to varying boundary conditions and surface topologies. Parasites were often seen in close contact with the extensively folded peritrophic matrix and accumulating in areas such as the annular pad in the proventriculus. This information can be further used to understand the parasite-vector relation concerning

tissue architecture and trypanosome motility under natural conditions (see chapter 3.1.3).
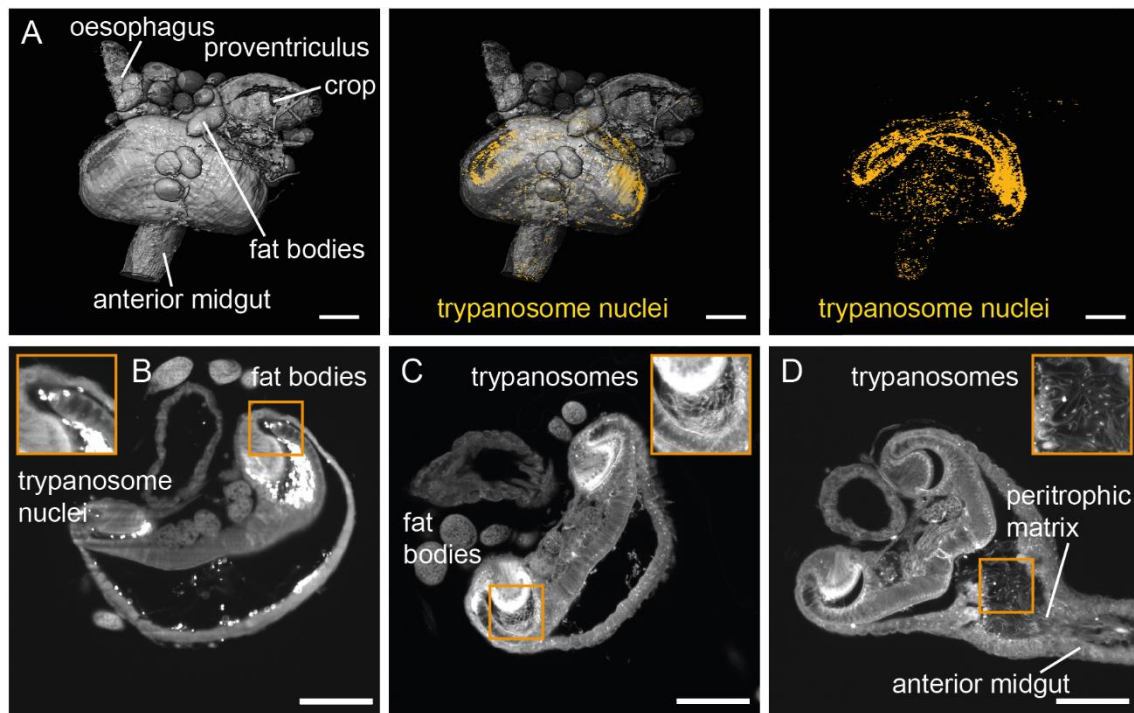
Figure 9: Multicolor light sheet fluorescence microscopy reveals the distribution pattern of trypanosomes in the proventriculus. Tsetse flies were infected with procyclic trypanosomes that express GFP in the cell nucleus (A, B) or mNeonGreen in the cytoplasm (C, D). Midguts were surgically removed and immediately fixed and further prepared for multicolor light sheet fluorescence microscopy. The proventriculus connects the anterior midgut, the crop and the oesophagus. (A) A three-dimensional reconstruction of the proventriculus. The first image shows the proventriculus surroundings (gray) rendered using the autofluorescence. The middle image shows the 3D localization of trypanosome cell nuclei (yellow) within the semi-transparent organ model (gray). Cell nuclei were highlighted using the strong GFP signal. (B, C, D) Single slices from original stacks show the distribution of trypanosomes inside. Each inset (orange) represents an enlargement of fluorescent trypanosome nuclei or trypanosomes, whereas the position is indicated in the main image. Image (B) represents the stack corresponding to the surface model shown in (A). Trypanosomes accumulated around the toroid structure of cells that produce the peritrophic matrix. Parasites were also visible between the folds of the peritrophic matrix in the junction to the anterior midgut (D). Scale bars represent 100 µm. Figure 9 A adapted from Schuster et al., 2017. Video 5 shows the original stacks (step size in z-projection 2 µm (B) or 0.5 µm (C, D)).

3.1.1.3 Fluorescent microspheres

Besides the complex topology, trypanosomes are confronted with other physical challenges while inside of the tsetse fly. One example is peristalsis, which is a wave-like contraction of circular gut muscles that is produced to transport food for digestion to the posterior part of the midgut. In addition, the peritrophic matrix is continuously produced and secreted in the posterior direction. As the matrix is always

produced and flies take blood meals regularly, trypanosomes might have to 'swim against the stream' when migrating to the gut anterior to reach the proventriculus or keep their position inside the fly. To investigate whether it is possible to gain information about forces in the fly and active or passive motion of the parasites, tsetse flies were fed with green fluorescent microspheres. In contrast to trypanosomes, beads are not actively motile. Consequently, their displacement can be correlated to processes in the fly, e.g. inner flow or peristaltic movement. Beads with a diameter of 2 µm were used, the size corresponding to the approximate diameter of a trypanosome cell. The absence of beads in fly compartments might yield information on areas, to which trypanosomes actively migrate. Studies on mosquitos have already shown that small microspheres can be a useful tool to analyze processes in hemolymph circulation, i.e. for measurements of hemolymph flow and transport (Glenn et al., 2009; Andereck et al., 2010). Therefore, preliminary experiments on feeding and visualizing microspheres inside the tsetse system were performed. Fluorescent microspheres were recorded *in vivo* with a fluorescence stereomicroscope at different time points after ingestion, using two different approaches.

First, flies were fed with fluorescent beads and WGA to specifically label the peritrophic matrix. Next, they were adhered to a microscope slide with glue and the thorax was carefully opened, to expose the proventriculus and its connection to the crop and the anterior midgut. To prevent the tissue from drying, a drop of PBS was placed on top. This allowed the observation of peristalsis in the thorax in living tissue, with the proventriculus embedded between the flight muscles in the thorax (figure 10 A; video 6 A). Beads moved from the crop via the proventriculus into the anterior midgut, as expected for an ingested blood meal in the intact fly system. The WGA labeling shows staining inside the proventriculus and the anterior midgut, but not in the crop. However, visible muscular contractions stopped shortly after opening of the thorax.

In the second approach, infected tsetse flies were fed with beads and the alimentary tract was dissected at different time points. Trypanosomes used for these experiments expressed NLS:GFP. These experiments showed that a simultaneous visualization and discrimination of the green 2 µm beads and green fluorescent nuclei was feasible (figure 10 B and C; video 6 B and C). Even four days after a meal with microspheres, some beads were still visible inside the anterior midgut tissue next to

swimming trypanosomes. Therefore, not all microspheres had been transported to the posterior midgut via peristalsis. While some beads did not show displacement, others were shifting their position inside the tissue (figure 10 B; video 6 B). The connection from the anterior midgut to the proventriculus normally shows strong peristaltic activity right after dissection. Beads and trypanosomes were actively pumped by the muscular contractions (figure 10 C; video 6 C). However, inside the proventriculus around the annular pad, the majority of the beads did not show any displacement during observation time (maximum 30 minutes). In contrast, living trypanosomes were actively moving in this region (figure 10 C; video 6 C).
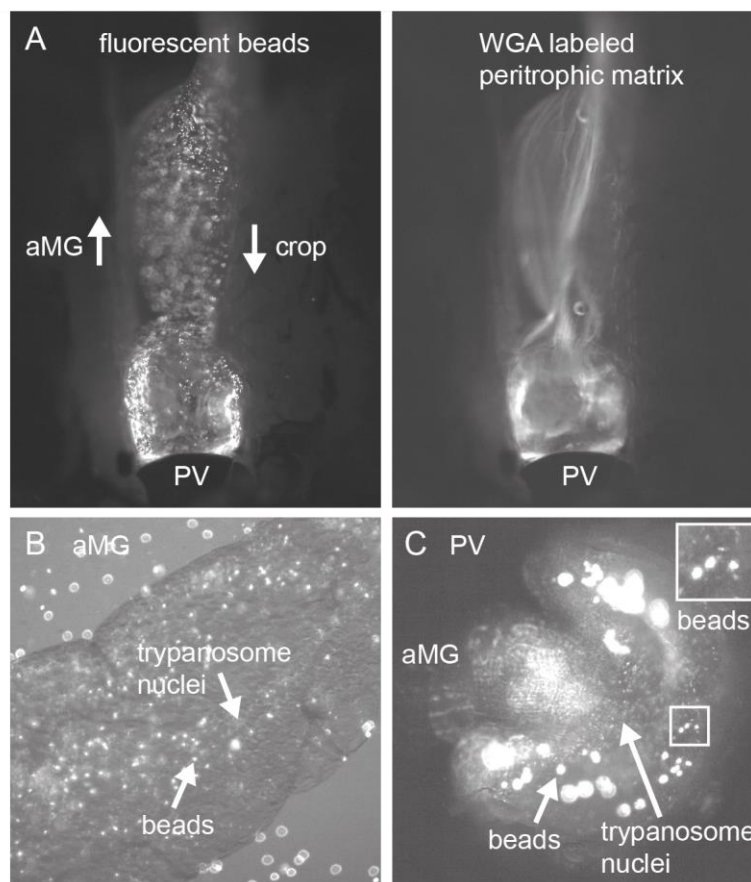
Figure 10: Fluorescent microspheres provide information about flow forces and space constraints inside the fly tissue. Flies were fed with carboxylated 2 µm green fluorescent beads and analyzed using a stereomicroscope. (A) A fly was additionally fed with rhodamine-labeled wheat germ agglutinin (WGA), glued to a slide and the thorax opened. The exposed proventriculus (PV) was covered with a drop of PBS and the circulating beads were observed. Beads were pumped from the crop over the PV to the anterior midgut (aMG), which was visible due to the peritrophic matrix staining in the aMG, which is not present in the crop. (B) Infection with beads and fluorescently labeled trypanosomes, expressing GFP in the cell nucleus. The dissected midgut showed cells and beads moving inside the aMG, two days post-infection with trypanosomes and 2 hours after feeding with beads. (C) At four days post-infection, beads were still visible inside the aMG and PV. The inset represents an enlargement of fluorescent trypanosome nuclei and beads, whereas the position is indicated in the main image. Video 6 contains the corresponding videos.

The experiments showed that microspheres can be used inside the tsetse fly tissue. As 'non-motile' particles they can give information about forces, flow and tissue constraints that can be directly compared to actively moving trypanosomes. Due to the approximately identical diameter of beads and parasites, it is possible to draw conclusions on active infection processes of the parasites or passive distribution by physical forces within the fly. Observations revealed differences in bead and trypanosome behavior and localization, however, these were preliminary experiments and further investigation is needed. Speeds and distributions can be directly compared and analyzed by particle tracking methods and will allow more insight into physical constraints of active and passive motion.

3.1.2 Three-dimensional morphology of tsetse trypanosomes

After imaging the trypanosome environment and the localization of the trypanosomes, their morphological features were next analyzed in more detail. Trypanosomes undergo a complex life cycle inside the tsetse fly vector. Several earlier studies have investigated the morphological differences between the cells in detail, e.g. by comparing cell and flagellum length as well as cell volume (Tetley and Vickerman, 1985; Vickerman, 1985; Van Den Abbeele et al., 1999; Sharma et al., 2008; Rotureau et al., 2011; Rotureau et al., 2012). Most of these studies described the trypanosome morphology by using hand drawings, electron microscopy images or photography, which are necessarily restricted to 2D. It has been shown for the bloodstream stage that details of 3D-morphology are important for the interpretation of the parasites´ swimming mechanism, which in turn plays an important role in adaptation to specific living environments (Heddergott et al., 2012; Bargul et al., 2016). Consequently, the analysis of additional morphological key parameters was performed for all free swimming developmental stages in the fly.

Trypanosomes were freshly isolated from infected fly organs, fluorescently surface-labeled with an AMCA-sulfo-NHS dye and rapidly fixed. Notably many analyzed cells showed a stronger surface staining at the flagellar tip. The cells nuclei and kinetoplasts were stained with DAPI. Several hundred cells were recorded in three-dimensional image stacks as described previously (Bargul et al., 2016) and representative examples of trypanosomes are shown in the following figures. Attached epimastigote forms from the salivary glands were not further analyzed

(Tetley and Vickerman, 1985; Vickerman, 1985; Rotureau et al., 2012). The focus was on developmental stages that are known to be active swimmers. Long epimastigote trypanosomes were excluded, as they are thought to die quickly after the asymmetric division (Van Den Abbeele et al., 1999; Sharma et al., 2008). Figure 11 shows eight different stages of interest that were classified: procyclic, long procyclic, mesocyclic, mesocyclic to epimastigote, dividing epimastigote (2K1N and 2K2N), short epimastigote and metacyclic form. Due to the continuous development of one developmental stage to another, transitional stages (i.e. long procyclic trypanosomes and mesocyclic to epimastigote cells) were also taken into account. The positions of kinetoplasts and nuclei, as well as the lengths of the free flagellar tips were determined as described in previous 2D studies (e.g. Sharma et al., 2008; Rotureau et al., 2011; Rotureau et al., 2012). Animations of the 3D-surface models are shown in video 7.

The procyclic trypanosomes exhibited a 180° right-hand turn of the flagellum around the cell body (figure 11 A). The turn of the flagellum is located anterior to the nucleus position. Cell nuclei of procyclic trypanosomes exhibited an oval cell nucleus shape. In addition to procyclic trypanosomes, long procyclic cells were classified. Long procyclic cells presumably starting to transform into mesocyclic trypanosomes, as the longer forms were frequently present at later infection time points (figure 11 B). These cells are still proliferative, have the typical pointed posterior part but are longer than the normal procyclic cell. They show the same flagellar attachment and a thickened posterior part compared to the anterior part. Pleomorphic trypanosomes morphotypes are not uniform however, and the morphological appearance can vary between individual cells of the same developmental stage. It should be noted that the morphological differences of procyclic cells described in this analysis cannot be correlated with the difference between early and late procyclic trypanosomes (Knüsel and Roditi, 2013).
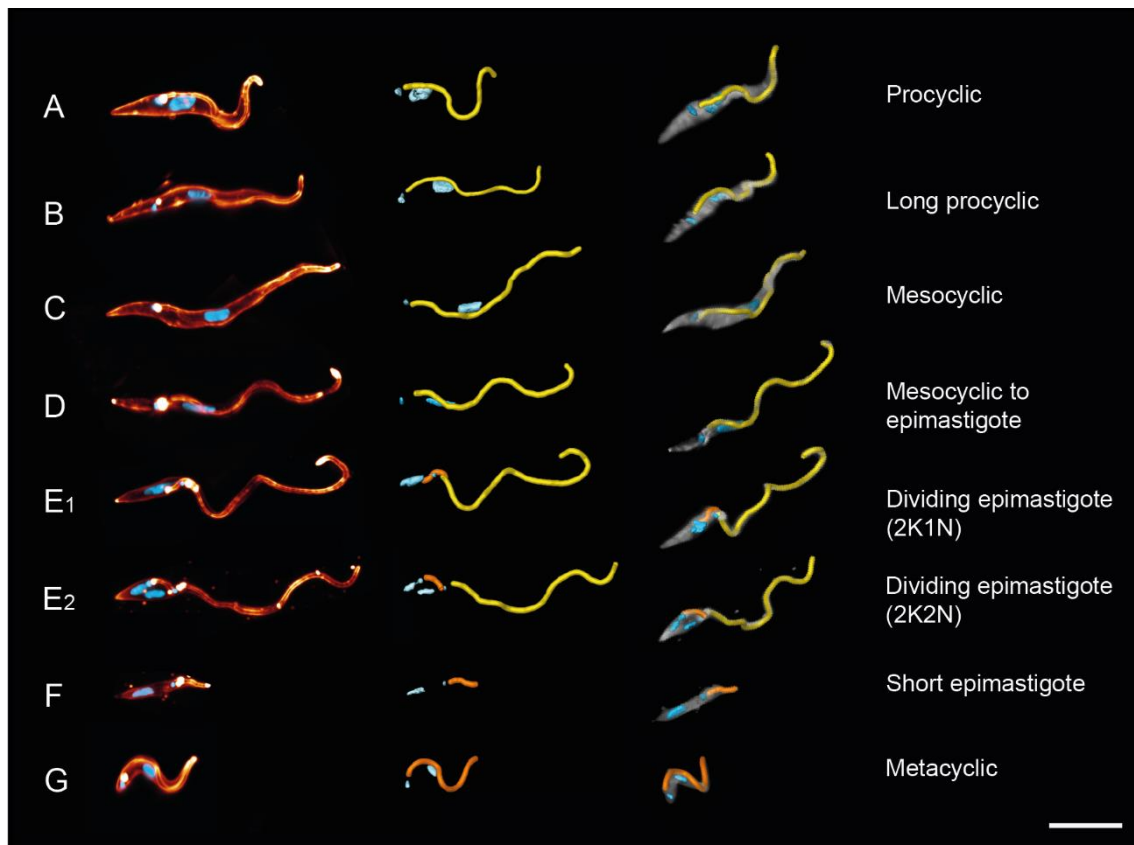
Figure 11: Three-dimensional modeling of pleomorphic trypanosomes isolated from the tsetse fly shows a characteristic morphology and corresponding flagellum attachment around the cell body. Trypanosomes were isolated from infected tsetse flies and the cell surface fluorescently labeled with an AMCA-sulfo-NHS dye. The nucleus and the kinetoplast were stained with DAPI. In the left panel, representative 3D models of selected surface-labeled developmental stages are shown. The middle panel shows the kinetoplast, nucleus and the traced flagellum in yellow or orange. The right panel shows a 3D representation of the corresponding cell from the left panel, by showing the cell body in gray and the attached flagellum in yellow or orange. The model was oriented to show the view onto the flagellar pocket at the posterior tip in order to visualize the flagellar attachment around the cell body. Scale bar represents 10 µm. (A) Representative normal procyclic and long procyclic (B) cells with a 180° right hand turn of the flagellum. (C) Mesocyclic cells show a more elongated cell body and a straighter flagellar attachment, but still fulfill the 180° right hand turn. This cell type has almost no free flagellar tip and is cell cycle-arrested. The nucleus is elongated and positioned in the middle of the cell. (D) During the transformation from the trypomastigote mesocyclic to the epimastigote stage, the nucleus elongates more and moves to the cell posterior, while the cytoplasm at the anterior tip retracts. (E_1) Epimastigote cell with a 2K1N configuration, the cell division starts after reorganization to the epimastigote stage. (E_2) Dividing epimastigote cell with 2K2N configuration shows a sperm-like appearance with almost no cytoplasm left anterior around the flagellum. The orange flagellum represents the new flagellum of the short epimastigote cell. (F) Short epimastigote cell resulting from the asymmetric division shows a drastic reduction in cell length and an extremely reduced flagellum. (G) Infective metacyclic cells re-establish the trypomastigote configuration. The flagellum exhibits again a 180° right hand turn around the cell body. Video 7 contains animations of the 3D-surface models. Figure and video adapted from Schuster et al., 2017.

The next developmental stage is represented by mesocyclic trypanosomes. Mesocyclic cells were longer and more consistent in diameter resulting in a uniform long cell body with nearly no free flagella tip left at the anterior end of the cell

(figure 11 C). The nucleus was located in the middle of the cell body and appeared more elongated in shape when compared to the procyclic nuclei. Mesocyclic cells are in cell cycle arrest at G2 stage, where the nucleus has undergone S phase but not continued to mitosis while the kinetoplast is not under division yet (Van Den Abbeele et al., 1999; Sharma et al., 2008). The turn of the flagellum was located on the posterior side of the nucleus, but still followed a 180° right turn as in procyclic trypanosomes. As soon as the mesocyclic stages reach the proventriculus, another morphological change takes place. Trypomastigote parasites differentiate into epimastigote forms, which occurs by a repositioning of the cell nucleus from the anterior to the posterior side of the kinetoplast (Hoare and Wallace, 1966). The cell nucleus elongates and migrates to the posterior, which goes hand in hand with a thinner anterior part of the cell. Here, a transition stage was classified as mesocyclic to epimastigote (figure 11 D) as described before (Subota et al., 2011). As soon as repositioning of the nucleus is finished, the cells are termed epimastigote cells. This trypanosome stage showed a sperm-like morphology with less cytoplasm left around the flagellum, eventually leading to a virtually free flagellum (figure 11 E). Due to this, the analysis of the flagellar attachment was not possible for these developmental stages. This cell type is proliferative again and called the dividing epimastigote stage (figure 11 E_1 and E_2). The posterior part of the parasites enlarges, while an asymmetric division proceeds that results in a long and a short epimastigote daughter cell (figure 11 F). Only the short cell is able to survive and colonize the salivary gland, whereas the long cell dies (Van Den Abbeele et al., 1999; Sharma et al., 2008). Short epimastigote cells had a drastically reduced total cell and flagellum length, which was intensified by the epimastigote configuration. Due to the short attachment zone, no significant attachment angle could be determined. The next stage of interest was the metacyclic form (figure 11 H), which is released by an asymmetric division of attached epimastigote cells in the salivary glands. Due to the asymmetric division, metacyclic cells re-established the trypomastigote configuration, with the nucleus again located posterior to the kinetoplast. They are free in the saliva, able to be injected into a host and represent the infective form that is pre-adapted to survive in the mammalian environment (Otieno and Darji, 1979). The flagellar attachment was again observed as a 180° turn around the cell body. This stage already showed similarities to the morphology of bloodstream forms since they were more 'curly'

compared to the other fly-specific stages. The surface staining was also more intense in this life cycle stage.

With the 3D models, it was possible to detail the flagellar attachment around the cell body and elucidate detailed overall cell morphology of every relevant microswimmer inside the tsetse system.

3.1.3 Trypanosome motility inside the tsetse fly vector

After having clarified tsetse fly topology and trypanosome morphology using state-of-the-art microscopy, the stage was set to for the investigation of the parasite motile behavior *in vivo*. Due to the complexity of this system, no quantitative analysis of motility was conducted, instead, the typical and characteristic behavior observed is described in the following.

3.1.3.1 Developmental stage-specific motion patterns

In order to further define the characteristics of each microswimmer type, the motile behavior of each developmental stage was analyzed. It was first necessary to gain an overview and visualize living trypanosomes inside specific tissues and during different time points of the infection. Flies were infected with procyclic trypanosomes and relevant organs dissected. High-speed recordings revealed typical motion patterns and cell behavior of trypanosomes in different compartments of the tsetse fly tissue.

At early time points of infection, procyclic cells were seen swimming freely between the ingested red blood cells or along the peritrophic matrix (figure 12 A, video 8 A). Their motility was comparable to the *in vitro* behavior of procyclic trypanosomes, showing persistent forward swimming in free spaces. Such free spaces could be created by dissection of the gut, where swimming behavior could be clearly analyzed. In the example shown in figure 12 A, cells could be observed orientating along the peritrophic matrix. The matrix was almost transparent, but visible due to the delimitation of the red blood cells. Procyclic cells were also seen tumbling, e.g. between densely packed red blood cells, where they were impossible to bring into focus. During establishment of an infection by infesting the ectoperitrophic space, proliferative procyclics increased in cell number and generally in size (compare figure 12 B and A). They colonized the posterior midgut region, shown in figure 12 B

(video 8 B). These parasites had a flexible cell body, though the posterior tip remained quite stiff even when making sharp U-turns (lower arrow). Cells repeatedly halted and reversed their flagellar beats in order to change direction or stay at their position, whereas a few cells swam quickly along the peritrophic matrix (upper arrow). If cells were in close contact with each other, they were able to synchronize their flagellar beats for short periods of time (middle cluster). Cells could join such clusters or leave them by simple reversal of the flagellar beat. Later during infection, procyclic cells generally increased further in cell length (figure 12 C, video 8 C). The increase in size could not be clearly shown to be linear for the entire fly population and was not considered to be indicative of late procyclic trypanosomes, however. In these experiments, accumulations of larger cells were clearly identified in several regions of the gut and classified as long procyclic cells (compare to figure 11). The morphological development towards the mesocyclic stage was apparently continuous, but the proliferative status was evident (figure 12 C, right arrow). Cells were frequently seen to poke the tissue with their anterior flagellar tip (left arrow).
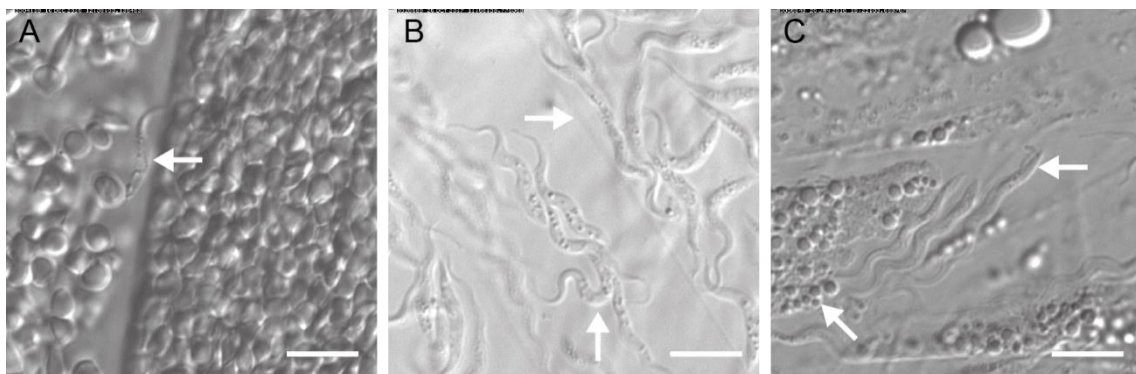
Figure 12: Procyclic trypanosomes in the posterior midgut. The panels show still images of the corresponding high-speed video 8, recorded with 250 fps. (A) Procyclic trypanosomes amongst blood cells in the endoperitrophic space early after infection (arrow). (B) Cells accumulated and proliferated in the ectoperitrophic space. They were highly flexible (lower arrow) and tended to synchronize in small clusters when they were in close contact with each other. Cells were often in contact with the peritrophic matrix (upper arrow). (C) Procyclic trypanosomes elongated during the infection process and these long procyclic cells showed some morphological similarities to mesocyclic cells, but still remained proliferative (right arrow, proliferating cell). Some cells are seen to penetrate tissue with their anterior tip (left arrow). Scale bars represent 10 µm.

Trypanosomes transform further to the non-dividing mesocyclic stage (figure 13). These cells are cell cycle-arrested and showed a very uniform morphology and flagellar oscillation. Mesocyclic cells were frequently seen to swim along the peritrophic matrix folds. Depending on the degree of confinement, these cells were

able to reduce the amplitude and wavelength in narrow channels (arrow), continuing to move forward further or maneuvering backwards by reversed waves (figure 13 A and B, video 9 A and B). They were capable of performing sharp U-turns to escape from dead ends, which revealed a high flexibility of the cell body. In the ectoperitrophic space, mesocyclic cells appeared in very high cell densities, packed tightly in peritrophic matrix folds (figure 13 B) and interstitial spaces (figure 13 C). This cell type was able to perform synchronized motion patterns in huge clusters (figure 13 C, video 9 C). Arrows indicate tissue borders where cells moved along with their anterior tip leading, showing that single cells were still able to move and reverse within these dense clusters. However, the majority of mesocyclic trypanosomes were moving in the same direction and flagellar beating was synchronized, producing visible wave patterns. During this study, this behavior was observed to be typical for this developmental stage in the anterior midgut region.
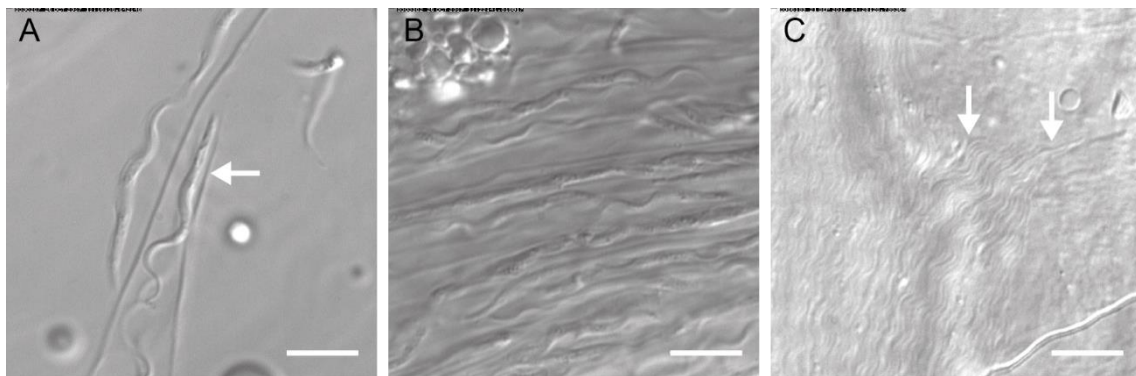

Figure 13: Mesocyclic trypanosomes in the anterior midgut. The panels show still images of the corresponding high-speed video 9, recorded with 250 fps. (A) Mesocyclic cells were fast swimmers and were often seen in close contact with the peritrophic matrix (arrow). (B) Cell population density increased during infection and mesocyclic trypanosomes were frequently observed in narrow channels. Cells were flexible and able to maneuver themselves out of narrow channels and dead ends. (C) When reaching very high cell densities, this cell type was able to perform synchronized motion patterns. The anterior tips at the tissue borders (arrows) showed that cell orientation was mostly uniform in one direction, but single cells were still able to move freely and leave the cluster. Scale bars represent 10 µm.

To develop further, mesocyclic trypanosomes have to colonize the proventriculus. They were able to reach high cell densities in this organ too, as shown in the example of figure 14 A (video 10 A). The bow-shaped structure (marked by arrows) represents a part of the ring structure inside the proventriculus, the annular pad, where cells tended to accumulate as shown before by light sheet microscopy (compare to figure 9). In this organ, mesocyclic cells undergo a transition to the thin

epimastigote stage (Van Den Abbeele et al., 1999). In figure 14 B, examples of mesocyclic cells and transition stages (right arrow) as well as dividing epimastigote (left arrow) cells are shown (video 10 B). These cells showed a sperm-like appearance and at a late stage of the division process, the cleavage furrow of the asymmetric division became visible. In video 10 B, dividing epimastigote trypanosomes moved towards or partly into the tissue, as the flexible thin part of the flagellum fitted through narrow channels, but the thick posterior part did not. Dividing epimastigote trypanosomes were highly active and revealed a flexible flagellum, resulting in a wide range of different beat amplitudes. Consistent with other developmental stages, these cells were also able to reverse the flagellar beat and maneuver themselves out of dead ends. These cells were not observed to appear in high cell densities. If they were in close contact to neighboring cells, they were not able to fully synchronize their motion over their whole body length. The short epimastigote stage produced by the asymmetric division was almost immotile. The video example shows two short epimastigote cells (video 10 C), one marked with an arrow (figure 14 C). At the cell´s posterior end, the flagellar pocket was visible, from which the very short flagellum emerged. Despite beating their flagella incessantly, the cells hardly moved forward. No huge clusters or synchronized groups of dividing or short epimastigote stages were observed during this study.
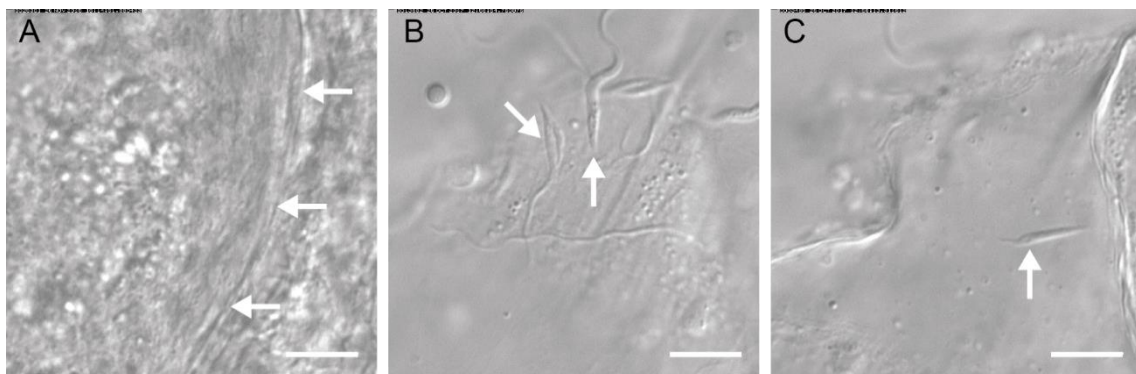
Figure 14: Proventricular trypanosomes and different epimastigote stages. The panels show still images of the corresponding high-speed video 10, recorded with 250 fps. (A) Mesocyclic trypanosomes and transition stages to epimastigote cells were densely packed in specific areas, here around the toroid structure of the annular pad (marked with arrows) in the proventriculus. (B) Transition stages (right arrow) and dividing epimastigote cells (left arrow) moved fast and sometimes became stuck in the tissue. (C) Short epimastigote stages (arrow) were almost immotile despite incessant beating of their flagellum. Scale bars represent 10 µm.

Short epimastigote cells are able to attach to the salivary gland epithelium and re-enter the cell cycle as attached epimastigote cells (Vickerman, 1985; Rotureau et

al., 2012). Cells can reach high densities and colonize the entire salivary gland. In order to visualize individual attached trypanosomes, gland regions with a low parasite burden are shown in figure 15 A and B (video 11 A and B). Due to the attachment to the gland epithelium, these cells were not free to self-organize and synchronized motion was not observed. However, attached cells were constantly moving. Figure 15 A shows a dividing cell pair, where the daughter cells are only connected at the posterior tip (lower arrow). Both cells were attached to the epithelium at opposite sides of the gland, which was possible due to its small diameter. Pre-metacyclic trypanosomes were visible between the attached epimastigote cells (A and B, upper arrows). These cells were still attached but morphologically distinguishable from epimastigote cells that possess a typical, pointed posterior end (Steiger, 1973; Tetley and Vickerman, 1985; Vickerman 1985). Eventually, the epimastigotes detach and swim freely in the salivary gland as metacyclic forms, from where they can be injected into a host via the saliva. Released free-swimming metacyclic trypanosomes were able to show a directed forward motion, but were also seen to frequently tumble (figure 15 C, video 11 C).
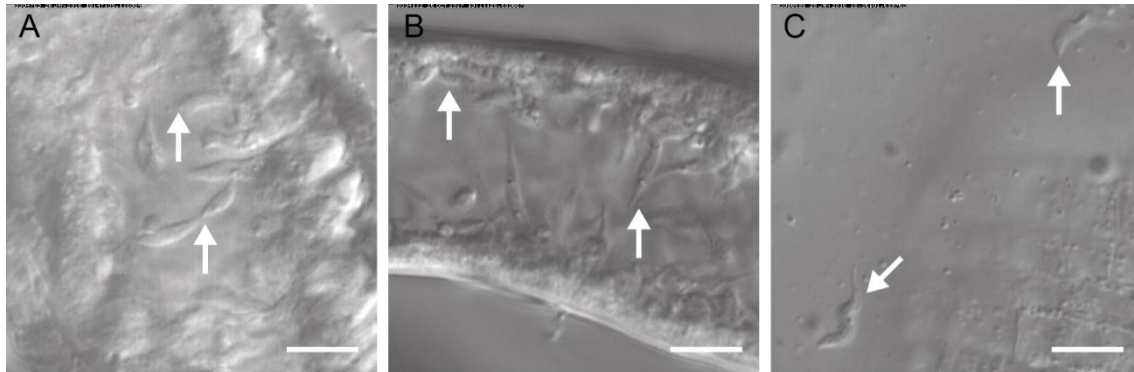
Figure 15: Trypanosome developmental stages in the tsetse salivary glands. The panels show still images of the corresponding high-speed video 11, recorded with 250 fps. (A) Trypanosomes attached to the epithelium of the salivary glands with their free anterior flagella tip. A dividing epimastigote (lower arrow) and an attached pre-metacyclic cell (upper arrow) in the gland lumen are shown. (B) Curly pre-metacyclic cells (upper arrow) were easily distinguishable from attached epimastigotes, which were characterized by a pointed posterior end (lower arrow). (C) Pre-metacyclic trypanosomes detach from the gland and develop further to free-swimming metacyclic cells (arrow). These cells were slow swimmers but pre-adapted to colonize the host skin after the infective tsetse bite. Scale bars represent 10 μm.

The trypanosome-tsetse system demonstrates the complexity of an infection process and the above data illustrates that every developmental stage has its own characteristic motion patterns. Confinement and boundary layers are present *in vivo*.

The surrounding microarchitecture of the infected region has an impact on trypanosome motion. Successful infection of the fly includes changes between solitary and collective motion behavior during development. This specific behavior was shown to be characteristic for each developmental stage.

3.1.3.2 Self-organization in cell accumulations by hydrodynamic interaction

Data from the previous chapters showed that trypanosomes occasionally form large swarms and clusters during their development in the fly. Within these accumulations, parasites are able to transiently synchronize their motion with neighboring cells. As shown before, this synchronization of parasites is possible for small clusters (figure 12 B) or for large amounts of cells (figure 13 C). In some rare events, trypanosomes were seen to perform a rapid switch between two different types of motion inside these clusters, which were termed 'chaotic' and 'synchronized' motion. In the chaotic (isotropic) motion, cells apparently moved around randomly and with no directional motion. In the synchronized motion, cells perform a visibly ordered motion pattern and seemingly self-organized next to each other. Cells could switch from chaotic to synchronized and vice versa, which is exemplified in Figure 16 and video 12. This behavior was observed in the ectoperitrophic space of the tsetse fly midgut.

In a chaotic to synchronized scenario, trypanosomes were densely packed and randomly moving within the ectoperitrophic space (figure 16 A, video 12 A). Within several seconds, cells were able to change their motion behavior and synchronize their flagella beat with that of neighboring cells. The cells had close contact with their neighbors, which resulted in visible wave motion patterns. Often, cells were seen orientated with their flagella tips at the epithelium border or in narrow corners. However, cells were not attached. Despite the quick conformation change, these arrangements were stable for at least several minutes during observation.
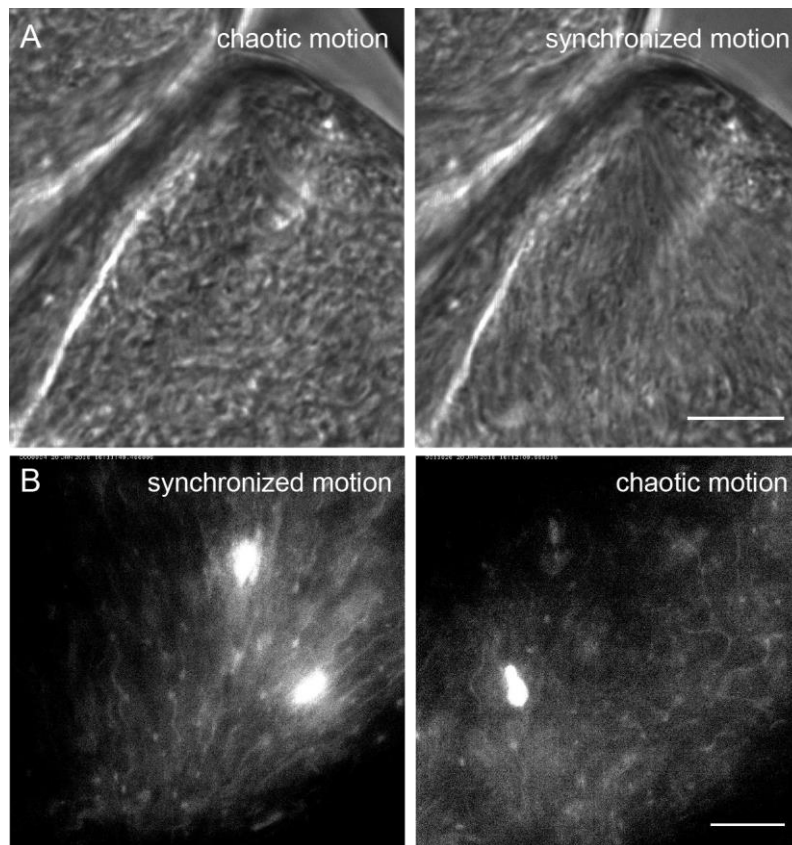
Figure 16: Rapid switching between synchronized and chaotic motion in dense trypanosome accumulations inside the ectoperitrophic space of the midgut. Infected midguts were dissected and analyzed with a microscope. The panels show still images of the corresponding high-speed video 12, recorded with 250 fps. Scale bars represent 10 µm. (A) Switch from chaotic to synchronized motion, visible in transmitted light mode. (B) Synchronized motion changed to chaotic motion within a few seconds. Trypanosomes expressed GFP in the nucleus and/or in the flagellum, which allows visualization of the motion pattern in the fluorescence mode. Figure and video adapted from Schuster et al., 2017.

This phenomenon could also occur in the reverse direction, where a synchronized swarm turned into an isotropic distribution of randomly swimming cells (figure 16 B, video 12 B). This quick change happened within a few seconds. Fluorescent cell lines, with an EGFP tag in the flagellum and/or GFP in the cell nucleus, were used to identify single cells within these swarms and confirmed the change between the motion patterns on a single cell level (figure 16 B, video 12 B). Fluorescent flagella of single trypanosomes were aligned next to each other in the synchronized state and only moments later they could be randomly distributed in the chaotic motion.

The triggers of these switching events are unknown and it was not possible to artificially reproduce this phenomenon during this study. However, the observations suggest that these swarms can be self-organized by hydrodynamic interactions in a very small timescale without the need of physical attachment.

3.1.4 Analysis of trypanosome motility

After gaining an overview of physical constraints in the vector, the morphology of different microswimmer types as well as the behavior of these parasites in their natural environment, the next goal was to develop approaches for analysis in order to be able to describe these observations quantitatively. Indeed, the complexity of this system was both interesting and problematic at the same time, why analysis was performed exemplary. The following chapters aim to show possible approaches towards quantitative analyses and provide prospects for different designated uses.

3.1.4.1 The cellular waveform of fly-specific trypanosome stages

Having produced sufficient data for the description of trypanosome motility behavior in the fly, the next step was to develop approaches for quantitative analysis at the single cell level, using the high-speed live data. Since trypanosomes are always moving, there is no static morphology per se - the cell body is constantly deforming due to the motility of the attached flagellum. In order to analyze the dynamics of the motion process correlated with morphological characteristics, the cellular waveform model for trypanosomes was developed, visualized using 3D kymographic representations (Bargul et al., 2016). These show the propagation of single flagellar beats along the time axis, resulting in a travelling wave outline of the swimming cell, at the same time allowing the measurement of speed, persistency, wavelength, amplitude and flagellar beat frequency.

This concept was now applied to fly-specific stages, in order to characterize the different microswimmer types. For this analysis, trypanosomes were recorded directly after release from the fly tissue. A large proportion of cells lose their natural ability to swim persistently forward in medium and tumble frequently (Heddergott et al., 2012; Bargul et al., 2016). Therefore, only recordings of persistently forward-swimming cells of each relevant stage were selected. For simplification, one flagellum beat of a persistently forward-moving cell was shown. The complete analysis was performed for the entire sequence of forward swimming however, in order to measure maximum swimming speed (µm/s) of the cell and the flagellar beat frequency (Hz). The cellular waveform analysis for different motile tsetse fly trypanosomes is shown in figure 17 and video 13. The cell shape was traced for one forward flagellar beat in time (t), using the z-axis and allowed the generation of a 3D model (gray). This model shows

the three-dimensional oscillation of the flagellar tip (cyan) and the corresponding travelling waves along the cell body. This provides quantifiable information about the oscillation and amplitude of exactly one flagellar beat in one illustration and allows a direct comparison between the swimmers.
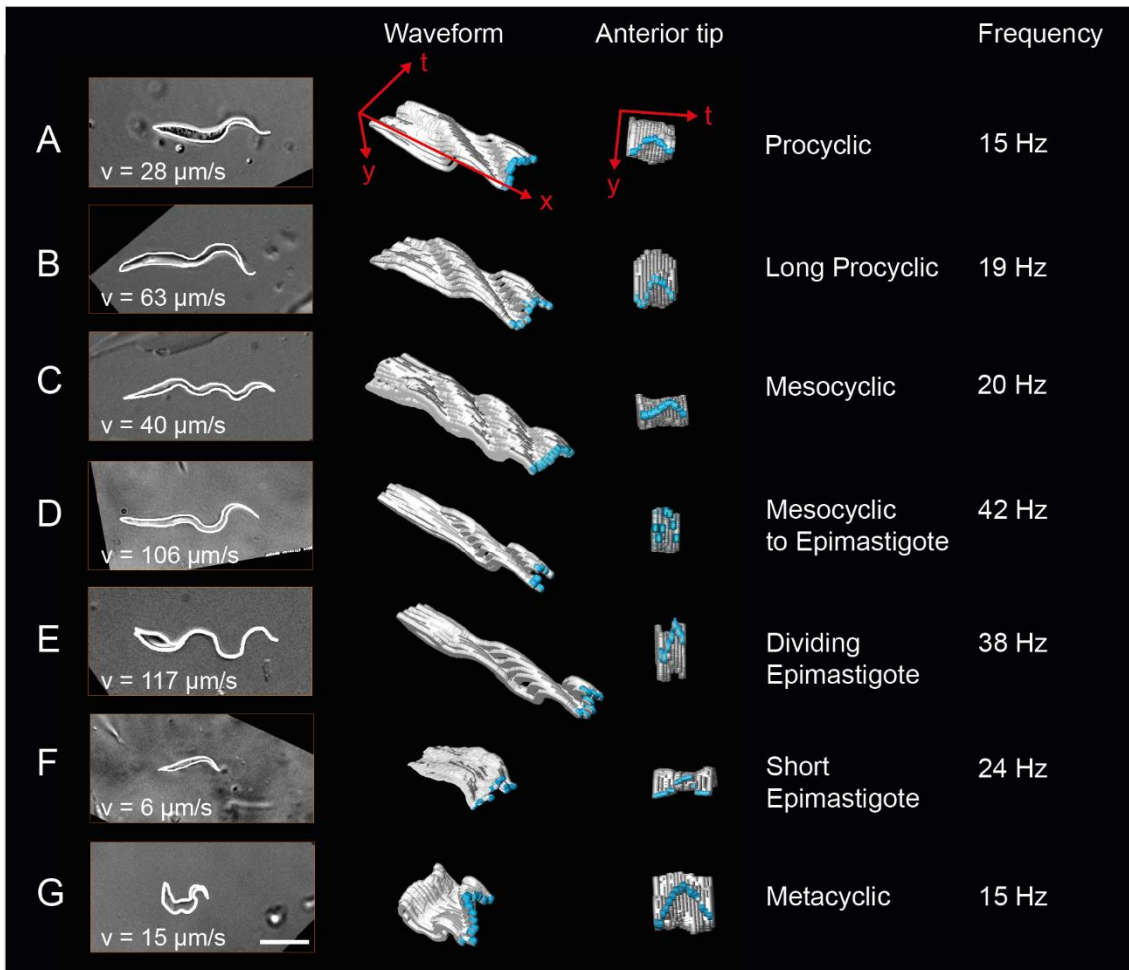
Figure 17: Generation of dynamic cellular waveform models of different trypanosome microswimmer types from the tsetse fly vector. Images in the left panels are stills from recorded high-speed videos (frame rate of 250 fps) of freshly released trypanosomes. The indicated speed (v in µm/s) represents the maximum speed reached by the cell within the analyzed sequence. The waveform model represents the outline for a single flagellar beat over time, frame by frame. The flagellar tip is highlighted in blue. The first model visualizes traveling waves on the cell body in a top-diagonal view, the second is a frontal view of the anterior tip. The frequency (Hz) of the beat is shown on the right. Procyclic (A) and long procyclic (B) cells show similar waveform models, but long procyclic cells generally swim faster and with higher beat frequency. Mesocyclic cells (C) have smaller amplitudes during flagella beating, resulting in more and smaller traveling waves. During differentiation to the epimastigote stage (D) the amplitude increased again and cells swam faster. Dividing epimastigote cells (E) were the fastest swimmers, with high amplitudes at high frequencies. Short epimastigotes (F) were almost immotile due to their very short free flagellum. Metacyclic cells (G) had a characteristically 'curly' waveform with medium beat frequencies. Scale bar represents 10 µm. Video 13 contains original video sequences and animated flagellar waveform models. Figure and video adapted from Schuster et al., 2017.

Procyclic cells are the first fly-specific life cycle stage and show a characteristic flipping forward motion, due to the more anterior localization of the flagellar pocket and the stiffness of the posterior part. This is also represented in the cellular waveform model, where the posterior part was barely transformed and remained straight. The procyclic cell shown here reached 28 μm/s and a frequency of 15 Hz (figure 17 A), whereas the long procyclic cell was able to swim significantly faster with 63 μm/s and a slightly higher beat frequency of 19 Hz (figure 17 B). Nevertheless, both cells had a similar waveform, with the long procyclic forms showing a small increase in the amplitude of the flagellar oscillation. The mesocyclic form was characterized by smaller amplitudes, resulting in small traveling waves running along the elongated cell body (figure 17 C). The loss of the free flagellar tip and the straight, worm-like appearance, produced the typical straight swimming trajectories. The transition from the mesocyclic to the epimastigote stage (figure 17 D) is accompanied by cell reorganization from the trypomastigote to the epimastigote conformation. Cytoplasm and nucleus move towards the posterior, the anterior part of the cell becomes thinner and therefore allows more flexibility for the flagellar oscillation. This leads to an increased swimming speed of above 100 μm/s with a doubling of beat frequency for this transitional stage. In this study, dividing epimastigote cells were the fastest microswimmers observed, with the epimastigote cell shown in figure 17 E reaching a speed of 117 μm/s. The sperm-like appearance allows the almost free flexible flagellum to produce large amplitudes running over the cell body to push them forward. They have a virtually completely free flagellum. After asymmetric cell division, a long epimastigote cell is produced, which was not included in this analysis. The short cell which is also generated in this division represents a completely different microswimmer type (figure 17 F). There was a decrease in cell and flagellum length, which was also mirrored in a drastic reduction of swimming performance. Short epimastigotes had a rudimentary short flagellum, beating with small amplitude and medium frequency compared to the other stages. Due to the shortness of the flagellum, no traveling waves could be observed and these cells were unable to reach speeds higher than 10 μm/s. The infective metacyclic form represents the last swimmer type in the fly´s life cycle (figure 17 G). They develop in the salivary glands and return to the trypomastigote configuration. The flagellum emerged at the very posterior end and the oscillation strongly deformed the flexible cell body. The flagellar oscillation produced high amplitudes and traveling waves propagating along the cell

body. Due to the chiral course of flagellar attachment along almost the complete body of the cell, this produced high rotational forces and the cellular waveform model differed from the models found for other fly-specific stages. Due to the 'curly' appearance, it showed more similarities to bloodstream stages than other fly forms (Bargul et al., 2016), which represent the next developmental stages in the mammalian host.

The cellular waveform analysis allowed a clear characterization of the distinct motile behavior of different fly trypanosome stages, which correlated well with their 3D morphology, taking into account and extending knowledge of trypanosomes swimming mechanism. The data determine the swimming capacity of specific morphotypes, which can now be built upon to interpret the parasites´ swimming behavior in the previously detailed tsetse microenvironments and in the described swarms of thousands of collectively moving cells.

3.1.4.2 Automated cell tracking *in vivo*

After detailing solitary swimming trypanosomes, the analysis of individual trypanosomes in dense cell accumulations was in focus. In figures 13 and 16 examples of extensive swarms were shown. Individual cell analysis was impossible in these densities using light microscopic recordings. To be able to distinguish between individual parasites in crowded areas, high-speed fluorescence microscopic recordings of a transgenic cell line expressing a bright GFP signal in the nucleus were used. An image analysis software was utilized which includes a tracking algorithm for automated particle tracking. The advantage of the fluorescent nucleus is its round shape. In contrast to the complex outline of a trypanosome, the nucleus can be easily identified and separated automatically by the software from other neighboring cells. Additionally, the form of the nucleus can yield information about the life cycle stage, as nucleus size and shape change characteristically between roundish or rod-shaped during the passage through the fly (figure 11; Sharma et al., 2008). This also allowed the identification of mixed trypanosome populations, for example procyclic and mesocyclic cells in the posterior midgut region, whereas cell populations in the anterior midgut mainly consist of mesocyclic cells.

Flies were infected with transgenic cells, dissected and fluorescent trypanosomes recorded with high-speed resolution. Representative examples of two different

compartments are shown in figure 18 and video 14. The first panel shows the trypanosomes in differential interference contrast (DIC), the middle panel shows the fluorescence signals and the third panel shows corresponding tracks of the cell nuclei generated by the Imaris tracking function. The recorded mean track speed was between 5 and 35 µm/s and is color-coded as annotated in the upper legend.
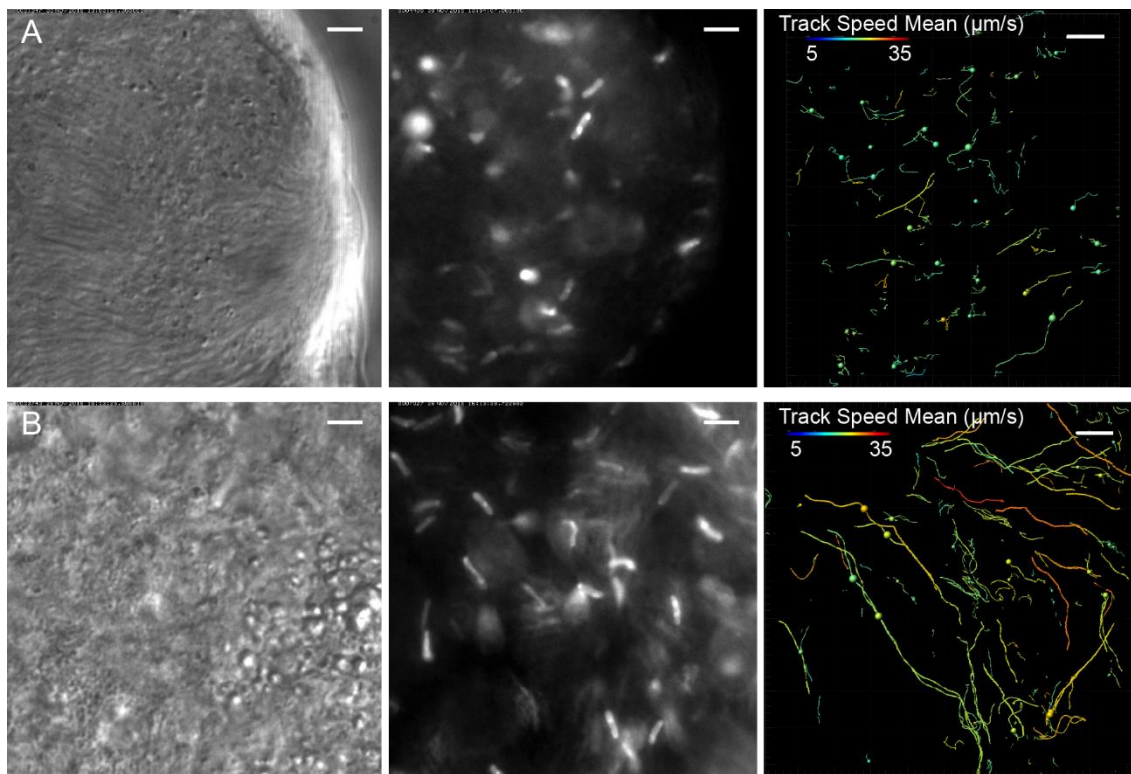
Figure 18: Automated cell tracking of fluorescent trypanosome cell nuclei inside the tsetse fly tissue. Infected midguts were dissected and areas containing a high trypanosome concentration selected. Trypanosomes expressed GFP in the nucleus and therefore provided information about single cell motion and the developmental stage. The images are stills of the corresponding high-speed videos, recorded with 250 fps. The left panel was recorded with transmitted light, the middle panel with fluorescence excitation and the right panel represents the tracking analysis of the latter performed with Imaris. Dots represent the tracked nuclei. The color code represents the mean track speed and was analyzed in a range of 5-35 µm/s. Scale bars represent 5 µm. (A) Mesocyclic trypanosomes in the ectoperitrophic space of the anterior midgut. Due to the dense cluster, trypanosomes swam more slowly and less persistently but were still free to move around. (B) Mesocyclic trypanosomes and transition stages to the epimastigote form in the proventriculus. Due to the topological structure of this region, cells were less crowded and showed more persistent swimming. Video 14 contains the corresponding videos. Figure and video adapted from Schuster et al., 2017.

Large cell accumulations were frequently observed in the ectoperitrophic space of the anterior midgut region (figure 18 A). As described previously in this work, synchronized clusters were visible, while trypanosomes were often seen arranged at epithelium borders with their anterior flagella tips. Due to the localization of the cluster in the anterior midgut and the elongated nuclear shape, cells were identified

as predominantly mesocyclic cells. The majority of these parasites hardly changed position, as forward movement was topologically restricted for the whole cluster by the epithelium border. This resulted in short tracks with low swimming speed, presumably belonging to synchronized cells in the cluster that did not reverse movement during the recorded time span. The presence of long trajectories showed free movement of single motile parasites in these dense clusters, however. In contrast, regions without a synchronization pattern showed a different trajectory profile (figure 18 B). For example, in the proventriculus, tracking data revealed a far greater proportion of persistently swimming cells with higher mean speeds, which is indicated by the different track colors. The trajectories showed a bias in direction, seemingly due to specific tissue architecture, which was in this case the peripheral region of the annular pad. This corresponds to previous observations from figure 9 and figure 14 A, showing that trypanosome accumulations occur preferentially in these regions. The elongated and thin shape of the cell nuclei confirmed predominantly mesocyclic and mesocyclic to epimastigote cells, as described previously for that organ.

The use of an automated cell tracking function allowed a quantification of solitary and collective motion of parasites in dense cell swarms *in vivo*. This approach enables the generation of comparative, quantitative datasets on the velocities of specific cell types in defined tissues and organ, at various infection time points and cell densities.

3.1.5 Trypanosome motility in artificial microenvironments

In parallel with the *in vivo* analysis of trypanosome microswimmers, another goal was the analysis of motion in artificial surroundings and to potentially influence the motile behavior *in vitro*. This kind of approach has already successfully shown that arranged pillar arrays with the same diameter as human erythrocytes are able to influence the swimming performance of the slender bloodstream stage (Heddergott et al., 2012). These experiments showed that the geometries of the surrounding environment can have a significant impact on the parasite´s motile behavior and in this case, increase swimming speed and directionality. As shown in the present work, in the tsetse fly vector trypanosomes are confronted with diverse microenvironments. They are exposed to different topologies and varying confined spaces. To take advantage of these findings, the following chapters investigate the use, benefit and limitations of

artificial geometries for fly-specific trypanosomes. With artificial systems, it might be possible to mimic processes in the tsetse fly environment due to geometric confinements and structures, which could possibly influence the parasite´s motility.

3.1.5.1 Soft lithography

Trypanosomes must traverse through narrow and convoluted channels, different viscosities, flows, and various tissue constraints. As shown in chapter 3.1.1, the tsetse fly´s inner topology is complex, especially the highly flexible conformation of the peritrophic matrix. In order to mimic the fly´s interior architecture *in vitro*, soft lithography was used. Soft lithography is broadly used in natural sciences and is based on individual mask design, fabrication of the master and final production of elastomeric stamps containing the desired three-dimensional pattern. Besides the advantage of custom-made devices, different material and controllable surface chemistries are available and are used for various biological applications (Weibel et al., 2007; Lockery et al., 2008; Knowlton et al., 2015; Shapiro et al., 2016). This technique was used to produce intricate and nature-inspired three-dimensional designs for trypanosome motility analysis *in vitro*.

The goal was to investigate the effects of different geometries on motility of tsetse fly-specific stages. The nature-inspired mask was designed with the AutoCAD software and was based on specific internal fly structures that were observed during this work (figure 19). The patterns were designed to fit onto a small coverslip (22x22 mm). Each design contained 4-5 separate designs (16x1 mm), with each of them containing individual in- and outlet ports (4x1 mm) (for further details see figure 20 A, B and chapter 5.2.6, figure 29). The designs contained single semicircular structures with different angles and sizes, as well as structures consisting of several semicircles (figure 19 A, B, D top). These structures are representative of shapes and volumes found in the fly midgut, where trypanosomes were seen to accumulate and synchronize their motion. Different triangle types and pointed structures were included, to mimic dead-ends formed by the extensive convolution of the peritrophic membrane (figure 19 A, B, E bottom). In addition, channels with various diameters were incorporated to investigate trypanosome motility and swimming speed in confined channels (figure 19 C). For one design, geometric structures at the border of the design were provided with additional

channels (4 or 10 µm), which should allow the integration of flow fields in future applications (figure 19 B), in order to mimic natural flows that occur in small volumes of the fly´s interior.
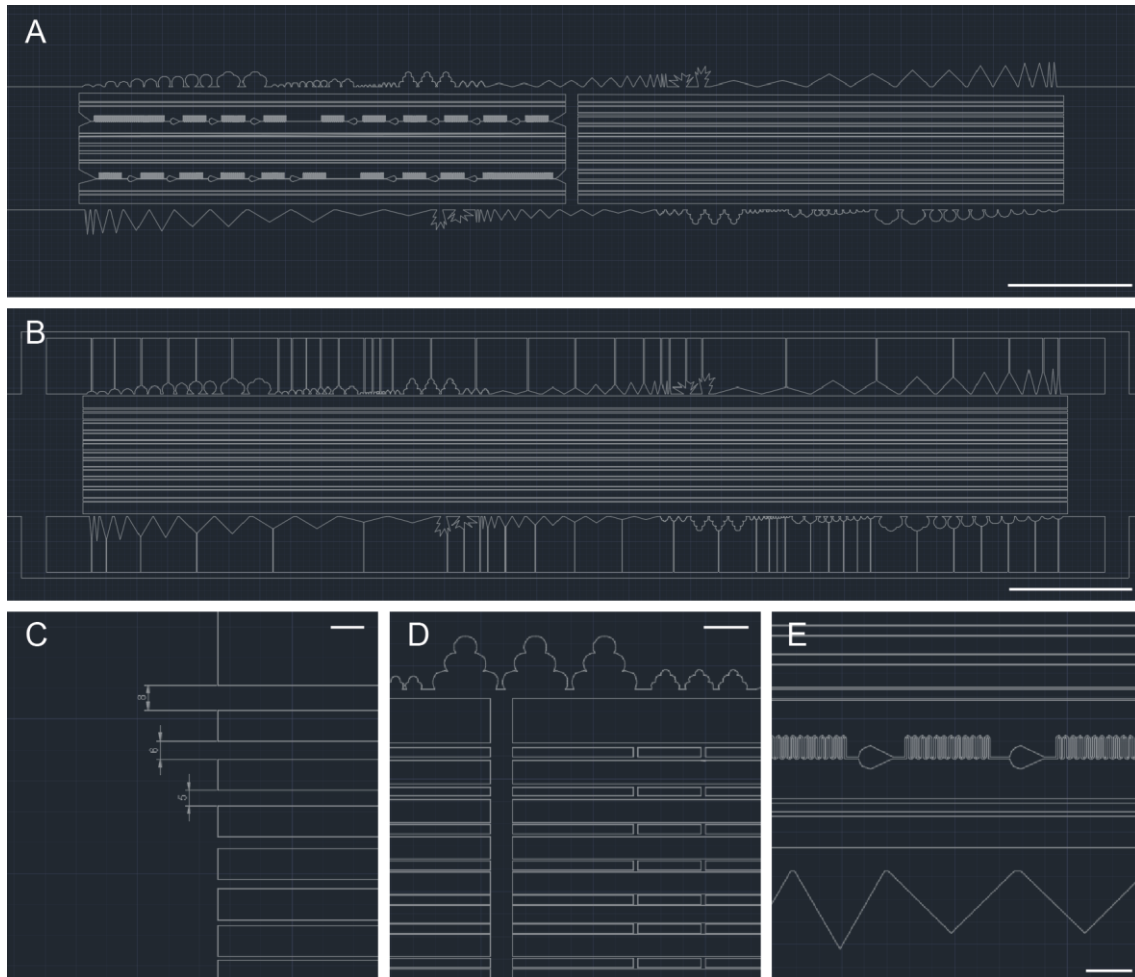
Figure 19: Custom-made design of the lithography mask, which contains nature-inspired geometries found in the tsetse fly. The mask was designed with the AutoCAD software, a vector-orientated drawing program. Scale bars represent 1,000 µm (A and B), 10 µm (C), 100 µm (D and E). Designs were equipped with large reservoirs as inlet and outlet pools on each side, containing the patterns in the middle (A and B). Channels and structures with different shapes, sizes and angles were used to mimic specific structures from the fly´s inner topology or for physical applications and measurements (A-E).

Furthermore, potentially interesting applications for physical analysis and computational modeling were included. For example, there is an increasing interest on the near-wall swimming behavior of microswimmers (Elgeti and Gompper, 2016). Lithography designs including channels with corners and curves have already been used to analyze the interaction of swimming sperm cells with walls (Denissenko et al., 2012). In order to analyze near-wall swimming of trypanosomes, channels were designed with straight or curved walls, as well as continuous channels or with

interruptions of various sizes and sharp corners (figure 19 D and E). These geometries are typically not found in the fly´s interior, but provide a controlled experimental setup with well-defined steric boundaries that are facilitated for further mathematical modeling of the swimming process.
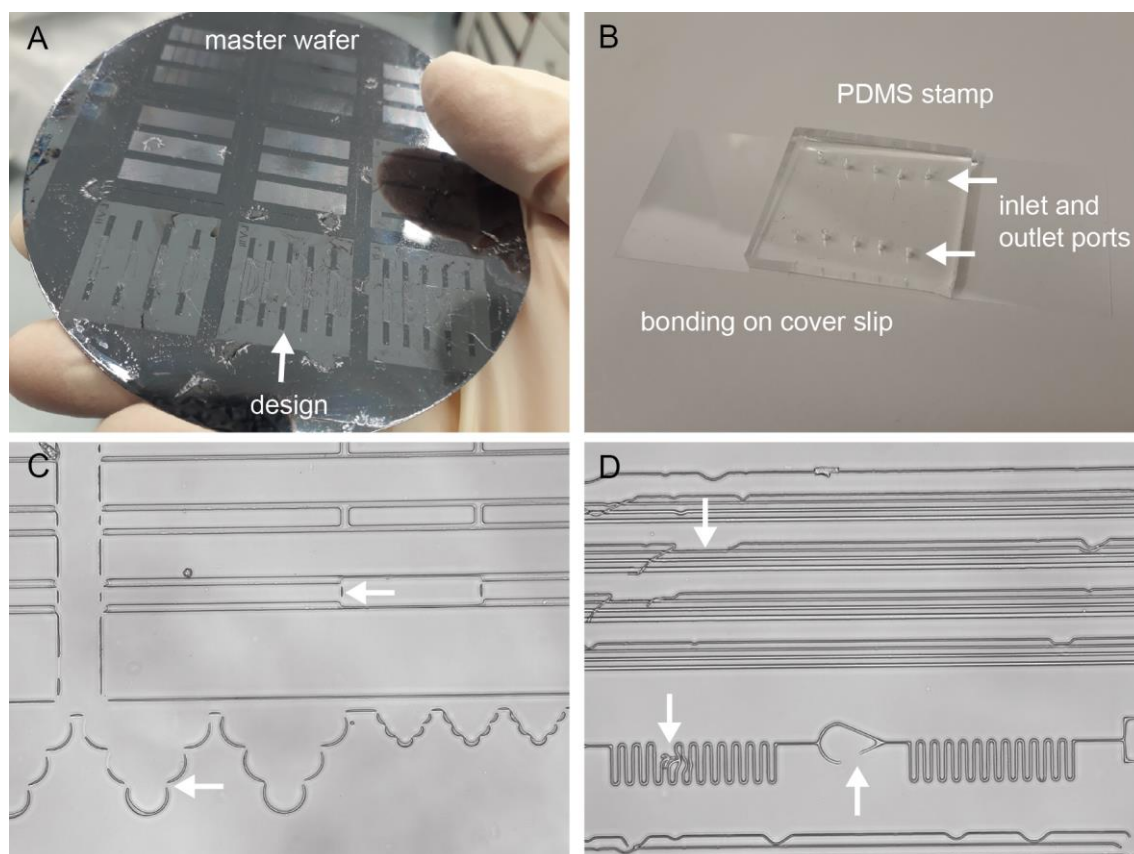
Figure 20: Problems during fabrication and application. The fabrication of a functional master wafer was not possible with the protocol recommended from the supplier company (A). Structures on the design detached during the development step (A). Bonding of the PDMS stamp to a glass substrate (here a coverslip) was not always reliable (B) and resulted in open and discontinuous structures in the PDMS stamp (C and D, arrows). It was not possible to produce a functional device.

After designing with the AutoCAD software, a photomask containing the desired pattern was ordered at a company and further used for the production of the 3D patterns (for further details see chapter 5.2.6). Soft lithography was meant to be established in the department during this work and PDMS stamps were produced using the described photomask. However, although various approaches and protocols recommended by the supplier company (BlackHole Lab) were tested, the fabrication of the master wafer did not result in a usable wafer. During the development of the master (figure 20 A), structures on the wafer detached and changed the pattern structure. This led to open and discontinuous structures in the

resulting PDMS stamp (figure 20 B), where no fluid insertion was possible (figure 20 C and D, arrows). Parameters such as the thickness of the photoresist, duration of the backing steps or the illumination time and intensity were changed in order to optimize the protocol, but without success. Later on, it was discovered that the viscous SU-8 photoresist that was used for the development had expired, which was probably the reason for the insufficient master wafer quality and the unsuccessful production of useable PDMS patterns (personal communication with laboratory members). The production of functional PDMS stamps for motility analyses was not possible during the course of this doctoral thesis. Nevertheless, the photomask has been manufactured and soft lithography equipment is now available in the laboratory for future use.

3.1.5.2 Rolled-up glass microchannels

Observations during this study showed that trypanosomes are frequently confronted with narrow channels and constrictions, e.g. those produced by the extensive folding of the peritrophic matrix or the narrow salivary gland duct. Nanomembranes allow the fabrication of three-dimensional nanostructures, for example functionalized tubes (Mei et al., 2008). These nanotubes can be designed with different diameters and various materials. Here, rolled-up glass (SiO/SiO$_2$) microchannels were chosen to visualize trypanosome motion inside the transparent tubes (Mei et al., 2008). The advantage of these tubes, besides the ease of production, is the circular and uniform diameter over the whole channel length. Some channels for testing were kindly provided by Veronika Magdanz (IWF Dresden, Germany). The tubes are well-defined in diameter (3-6 µm) and length (100-500 µm) and were arranged in large periodic arrays, containing many microchannels on one coverslip.

Trypanosomes were applied onto the coverslip containing the channels, covered with a microscope slide, and recorded microscopically. Due to their robustness and high cell numbers, procyclic cell culture trypanosomes were preferentially used. It was also possible to introduce different fly developmental stages into the arrays, though limited parasite numbers and contaminations with fly tissue were an issue, however. Trypanosomes were able to enter the channels and swim through the transparent tubes. Therefore, speed and swimming motion could be analyzed outside and inside the confinement. However, a drawback of this experimental setup was the low

chance of trypanosomes entering the narrow tubes and the lack of tools available for guiding the cells. Thus, the number of recorded cells entering the tubes over the observation time was low. Cells were at least seen to significantly increase their swimming speed in the narrow channels immediately upon contact of the flagellum with the tube walls. Figure 22 shows a procyclic trypanosome swimming directly into a 6 µm diameter microtube. The cell had an initial speed of 19 µm/s before entering the channel, briefly slowed down while threading into the tube and increased speed up to 28 µm/s while swimming persistently inside the tubular channel (video 15). The limited number of useful recordings and available arrays did not allow a full quantitative analysis, but the acceleration is presumably due to the resistance the immobile glass wall presented to the beating flagellum, which results in more force exerted in the direction of movement and thus higher forward velocity. For a full analysis, the three-dimensional rotation of the cell needs to be taken into account, but qualitatively, the experiment shows the general principal of more effective motility under constrained environmental conditions.

Figure 21: Investigation of trypanosome swimming behavior in rolled-up glass microchannels. Procyclic cell culture trypanosomes were applied on slides containing rolled-up glass microchannels. These channels are transparent and uniform in diameter. The procyclic cell swam with 19 µm/s, entered the channel (6 µm diameter) and sped up to 28 µm/s inside the confinement. Video 15 contains the corresponding video. Scale bars represent 5 µm.

3.2 Bloodstream stage infectivity and differentiation

3.2.1 Slender and stumpy bloodstream stages are infective for the tsetse fly

More than 100 years ago, Muriel Robertson stated that short stumpy cells are most likely the life cycle stage that is infective for the tsetse fly (Robertson, 1912). Her observations are still referenced in textbooks. Long before molecular markers were in use, she identified differences via morphological characteristics and described stumpy, intermediate and slender forms. The later identification of proteins from the PAD family was a breakthrough for understanding stumpy formation at a molecular level (Dean et al., 2009). The protein PAD1 is only expressed in the transmission-competent stumpy form, but not in the slender stage (Dean et al., 2009).

Preliminary experiments performed by Ines Subota and Henriette Zimmermann in our laboratory suggested that fly infections with pleomorphic AnTat 13.90 stumpy and slender cells may result in comparable salivary gland infection rates. In this reporter cell line (GFP:PAD1$_{UTR}$), a nuclear GFP signal reports on the expression of the PAD1 gene, which is massively upregulated when cells become stumpy forms. They tested salivary gland infection rates in slender (19%, fly $n = 62$) and SIF-induced stumpy (23%, fly $n = 44$) parasites. In addition, they tested a cell line that enables an inducible expression site attenuation, which leads to SIF-independent stumpy formation (Zimmermann et al., 2017). This also resulted in infections for both slender (20%, $n = 40$) and expression site-induced stumpy (7%, fly $n = 47$) cells. These observations were surprising, and challenged the original assumption that only stumpy cells can infect flies. However, as slender populations of pleomorphic AnTat always harbor a certain amount of so-called 'background' stumpy cells, or rather PAD1 positive (PAD1+) cells (on average 1-5%), further investigation was needed to distinguish whether the observed salivary gland infections were caused by these background stumpy cells or, indeed, by slender cells. Therefore, the trypanosome cell numbers used for each infection were reduced to a number small enough to statistically exclude the presence of PAD1+ stumpy cells, which are termed background stumpy trypanosomes here. The approximate volume of blood taken up during a meal by a fly is around 20 µl (Gibson and Bailey, 2003). This means that for

a concentration of 100 cells per milliliter (c/ml), theoretically the fly ingests 2 cells on average. The experiments showed that infections with 1000 slender c/ml led to 5% (fly n = 80), and infections with 100 slender c/ml led to 7.9% (fly n = 76) salivary gland infections. The infection rates were similar to those obtained using expression site-induced stumpy trypanosomes with 9.6% in 1000 c/ml (fly n = 83) and 4.5% in 100 c/ml (fly n = 89). These results further suggested an involvement of slender trypanosomes in the infection process.

To challenge this observation, additional infections with wild type (wt) pleomorphic trypanosomes containing the previously used GFP:PAD1$_{UTR}$ reporter were performed during the course of this work. The amount of cells was further reduced and flies were infected with 100, 50, and 10 c/ml SIF-induced stumpy cells (cell density > 5x10^5 c/ml, left undiluted for 48 hours) as well as 100, 50, and 10 c/ml slender cells (cell density strictly below 5x10^5 c/ml). In total, 14 different infections were performed with 761 tsetse flies that were dissected 35-40 days post-infection (table 1). Slender infections and dissections with 100 and 10 c/ml were performed by Ines Subota and are marked with an asterisk (*). To calculate the amount of PAD1+ cells as precisely as possible, every cell population was scored directly before use for infection. Stumpy populations (n = 6), contained almost 100% (2289/2290) PAD1+ cells (table 1 A-C). Slender populations (n = 8), contained 3.1% PAD1+ cells (14/459) for the 100 c/ml (table 1 D), 1% of PAD1+ (12/1155) in 50 c/ml (table 1 E) and 1.1% (3/278) for the 10 c/ml (table 1 F) infections.

The results of the infection experiments are shown in table 1. Total infection rates are shown (gray) as well as separate infection rates for male and female flies. In this work, males proved to be more susceptible to infections than females. This is consistent with published work carried out in other laboratories (e.g. Peacock et al., 2012 b). For this reason, this study was conducted with both genders, as this is also occurring in natural infection dynamics. It is important to note that all flies analyzed for these experiments showed a normal infection status in midgut, proventriculus and salivary glands. Infected organs were heavily infested by trypanosomes and all occurring developmental stages were identified. There was no visible difference between slender and stumpy infections. In almost all flies with a salivary gland infection, both glands were infected.

Table 1: Infection rates of dilution series with pleomorphic stumpy (ST) and slender (SL) trypanosomes in tsetse flies. The cell line contained a GFP:PAD1 reporter (AnTat1.1/wt/p4231 GFP:PAD1$_{UTR}$). Experiments marked with an asterisk (*) were performed by Ines Subota. The table contains the cell type used for infection, cell concentration (c/ml), cell concentration per blood meal (c/bm) as well as the theoretical calculated amount of corresponding PAD1 positive (PAD1+) cells. All cell cultures used for infections were analyzed and the amount of PAD1+ cells directly counted before infection. Stumpy cells (A-C) were averaged to 100% PAD1+ cells and slender to 3.1% (D), 1% (E) and 1.1% (F) PAD1+ cells. The blood meal is calculated with a volume of 20 µl. Male and female flies were infected in different experiments (n°) and surviving flies dissected (diss.) 35-40 days post-infection and screened for the presence of trypanosomes in the midgut (MG), proventriculus (PV) and the salivary glands (SG). The transmission index (TI) is defined as infected SG/infected MG.

	cell type	c/ml	c/bm	PAD1+ c/ml	PAD1+ c/bm	flies diss.	ratio ♀/♂	MG	PV	SG	TI	n°
A	ST	100	2	100	2	116	1.70	38.8%	29.3%	11.2%	0.29	2
						43	♂	46.5%	37.2%	27.9%		
						73	♀	34.2%	24.7%	1.4%		
B	ST	50	1	50	1	109	0.6	20.2%	18.3%	4.6%	0.23	2
						68	♂	17.6%	16.2%	5.9%		
						41	♀	24.4%	22%	2.4%		
C	ST	10	0.2	10	0.2	107	1.28	7.5%	4.7%	0.9%	0.13	2
						47	♂	12.8%	8.5%	2.1%		
						60	♀	3.3%	1.7%	0.0%		
D	SL*	100	2	3.3	0.07	129	1.43	7.8%	7.8%	4.7%	0.60	3
						53	♂	13.2%	13.2%	9.4%		
						76	♀	3.9%	3.9%	1.3%		
E	SL	50	1	0.5	0.01	186	1.11	3.2%	2.7%	1.1%	0.33	3
						88	♂	4.5%	3.4%	2.3%		
						98	♀	2.0%	2.0%	0.0%		
F	SL*	10	0.2	0.1	0.002	114	0.84	0.9%	0.9%	0.0%	0.00	2
						62	♂	1.6%	1.6%	0.0%		
						52	♀	0.0%	0.0%	0.0%		

The 100 c/ml stumpy infections, with approximately 2 ingested stumpy cells per blood meal, resulted in 38.8% midgut and 11.2% salivary gland infections (fly n = 116). In contrast, infection rates with 2 cells out of a slender culture, meaning theoretically 0.066 ingested stumpy cells (or 1 ingested stumpy cell in every 15th infection), resulted in 7.8% midgut and 4.7% salivary gland infections (fly n = 129). The percentage of infectivity for the midgut is four times lower in slender cells, whereas the salivary gland infectivity is just half reduced compared to the stumpy infection rates. Therefore, the transmission index (TI = infected salivary gland/infected midgut; Peacock et al., 2012 b) for slender infections was higher (TI = 0.60) compared to stumpy trypanosomes (TI = 0.29) when using the same cell number. The infection rates resemble the results obtained in the previous experiment by Ines Subota with 100 c/ml of the expression site inducible cell line. An infection with 50 c/ml of slender cells resulted in 3.2% midgut infections, 2.7% in a proventriculus and 1.1% in a

salivary gland infection (fly n = 186). For the 50 c/ml stumpy cells the midgut infection rate resulted in 20.2%, 18.3% for the proventriculus, and 4.6% for salivary glands (fly n = 109). Again, the TI for slender infections was higher (TI = 0.33) compared to stumpy trypanosomes (TI = 0.23). The 10 c/ml infections showed that a stumpy population is still able to infect 7.5% of the midguts and 0.9% of salivary glands (fly n = 107), with a theoretical 0.2 cells per blood meal or 1 ingested stumpy cell in every 10th fly. Under the same conditions, a slender population is able to infect 0.9% of midguts, though no salivary gland infections were observed (fly n = 114) and TI was 0.00, respectively. For slender and stumpy cells, the 1:10 dilution from 100 c/ml to 10 c/ml resulted in an approximately tenfold lower infection efficiency for midgut infections.

For both stumpy and slender trypanosomes, a reduction in cell number resulted in a reduction of infection rates. However, the observed mature infections showed a normal infection progression with a huge number of cells in infected organs. These results indicate that slender trypanosomes are able to cause infections in tsetse flies, although with lower initial infection efficiencies when compared to SIF-induced stumpy parasites under the same conditions.

3.2.2 Early infection and cell differentiation *in vivo*

According to dogma, the stumpy stage is pre-adapted to survive the conditions in the tsetse fly gut, whereas the slender stage dies soon after ingestion (Robertson 1912). Stumpy cells develop synchronously within 24 hours to the procyclic form and start to proliferate in the tsetse midgut (Fenn and Matthews, 2007). According to the data presented in this work, infection of the fly can also be initiated and maintained by the proliferative slender trypanosomes. One of the major problems analyzing the early stages of a fly infection are the very low parasite concentrations in the gut. Although cell numbers for infections that are commonly used in laboratories are much higher compared to the situation in natural infections, the remaining cell number during the first days is low, due to the fact that the fly´s innate immune system is able to eliminate most or all of the ingested parasites (Maudlin et al., 1998; Gibson and Bailey, 2003; Oberle et al., 2010). The fate of the different trypanosome populations inside the fly during the first days of infection will be investigated further in the following sections.

3.2.2.1 Slender cells become PAD1 positive after 15 hours

To answer the question if slender trypanosomes are able to infect the fly or if infections are caused by the low percentage of stumpy cells that are present in slender populations, the early fate of slender trypanosomes during the infection process was analyzed in detail. For this purpose, live cell microscopy was used. Due to low parasite numbers in the fly gut, detection of trypanosomes was easier with living parasites. This had the advantage of additional information about parasite motility, as previous data showed that slender, stumpy, and procyclic trypanosomes exhibit distinct motion patterns (this work and Heddergott et al., 2012; Bargul et al., 2016). The previously described pleomorphic GFP:PAD1$_{UTR}$ reporter cell line (chapter 3.2.1) was used for this purpose. Infections were performed with a slender culture (cell density strictly below 5x10^5 c/ml) and data are shown in figure 22. The percentage of GFP:PAD1$_{UTR}$ positive, or rather GFP-positive trypanosomes, was analyzed for time point 0 hours (cell culture population) of different infections (n = 3) and averaged to 2.43% background stumpy cells (cell n = 1152). Infections were performed with 6x10^5 c/ml in TDB, thus providing 12,000 trypanosomes per 20 µl meal on average. TDB was used instead of blood for a better visualization of trypanosomes. Flies (fly n = 30, 15 ♂ and 15 ♀) were dissected in PBS at different time points (2-4, 15-17, 24-26, 48-50 and 72-74 hours) after the infective meal. Midguts were carefully torn open and released trypanosomes stained with DAPI for cell cycle analysis. Due to their different infection capabilities (compare table 1), one female and one male fly were dissected for every time point. To keep the analyzing time frame as precise as possible, each fly had one hour of analyzing time for the microscope detection of living trypanosomes. Cell morphology, GFP:PAD1 signal and cell cycle state of all trypanosome cells found were documented and analyzed during this experiment (cell n = 782).

The cell cycle profile of *in vivo* slender parasites showed a continuously proliferating population, similar to the profile of the cultured slender cells (compare figure 24 A, 0 hours) with no apparent cell cycle arrest (figure 22 A). This suggests an asynchronous differentiation process during early infection.
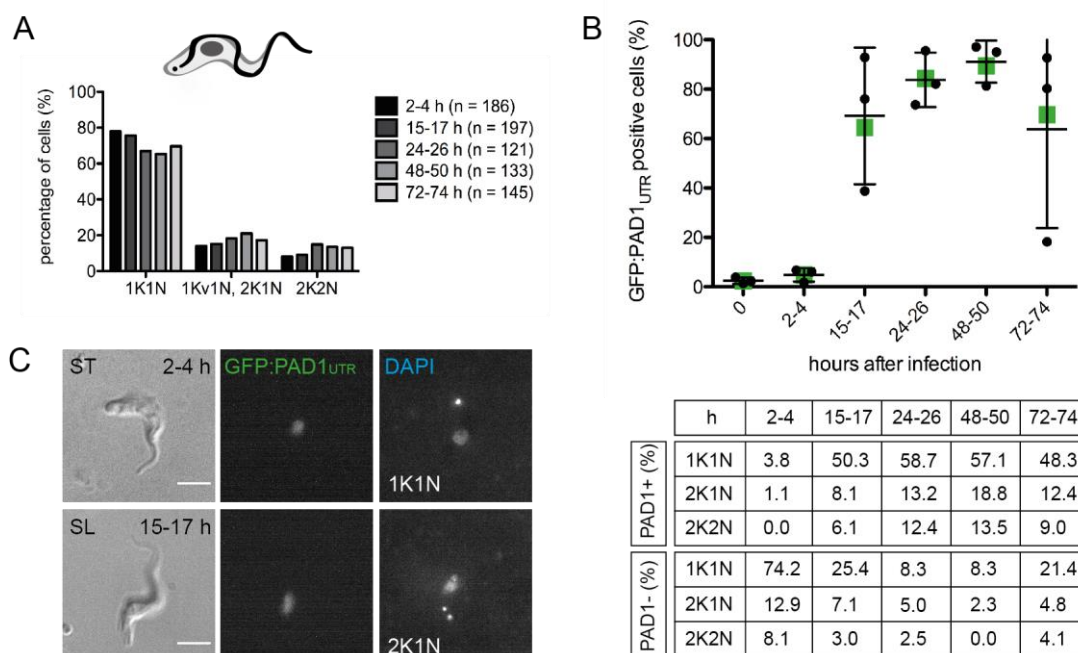
Figure 22: Slender cells continue to divide inside the tsetse fly and become PAD1 positive after 15 hours. Tsetse flies (n = 30, 15 ♂ and 15 ♀) were infected with slender cells and dissected at different time points after infection (2-4, 15-17, 24-26, 48-50 and 72-74 hours) in three different experiments. Time point 0 hours represents the *in vitro* cell population used for infection, which contained in average 2.4% GFP:PAD1 positive cells (total amount of cells analyzed n = 1152). Living trypanosomes were analyzed by microscope and documented (total amount of cell n = 782). (A) Parasites were stained with DAPI and analyzed by microscope to determine the configuration of the nucleus (N) and kinetoplast (K) to identify the cell cycle stage. (B) Trypanosomes were analyzed for the presence of a GFP-positive nucleus from the GFP:PAD1$_{UTR}$, which reflects the expression of the endogenous PAD1 protein in the reporter cell line. Each dot represents one experimental time point (1 ♂ and 1 ♀), values present average percentages (+/- SD) of three experiments. Green boxes represent the average percentage of all cells analyzed per time point. Cell cycle distribution of PAD1 positive (PAD1+) and negative (PAD1-) cells is detailed in the table. (C) The first image shows DIC mode to illustrate morphology, the second one the PAD1 signal in the nucleus and the third image nucleus and kinetoplast stained with DAPI. At 2-4 hours after infection the few PAD1 positive cells are background stumpy cells (ST), showing typical compact morphology. At 15-17 hours cells become increasingly PAD1 positive, but have typical slender morphology (SL). These cells continue to divide, and the example shows a 2K1N slender trypanosome. Images are stills of corresponding video 16. Scale bars represent 5 μm.

The number of PAD1+ cells (i.e. GFP+) slightly increased at 2-4 hours post infection, but these cells were 1K1N, morphologically stumpy trypanosomes (figure 22 C ST, video 16). The number of PAD1+ cells increased significantly in all three experiments at 15-17 hours, resulting in an average number of PAD1+ cells of 64.5% (figure 22 B). On a single cell level, PAD1+ cells showed a typical slender morphology and many trypanosomes were dividing, showing both 2K1N (8.1%) and 2K2N (6.1%) configurations (figure C SL, video 16). The fraction of PAD1+ cells peaked at 48 hours with 89.6% and decreases slightly afterwards. Even after

complete differentiation, early procyclic cells still remained PAD1+ for some days (Dean, PhD thesis, 2008).

Morphological analyses confirmed that almost all parasites showed a slender morphology and motion at the beginning, aside from the few PAD1+ 1K1N stumpy trypanosomes. After 24 hours, slender cells appeared morphologically slender/procyclic, with the stiff elongated posterior part of a procyclic from, but still revealing the flexible and wavy anterior tip from a slender trypanosome. This might be considered as a transitional stage, since after 48 hours the majority of the cells showed procyclic morphology and the typical flipping swimming pattern (described in chapter 3.1.3). Thus, the experiments suggest, for the first time, a direct transition from slender to procyclic forms, without the necessity of a stumpy stage, which runs counter to the prevailing view in the field.

3.2.2.2 Slender cells become EP1 positive after 24 hours

Data collected so far suggested that slender cells can survive inside the midgut. This indicated a direct progression to the procyclic stage. However, procyclic cells were identified solely by morphology and characteristic swimming patterns. To verify the development of mature procyclic trypanosomes, the experiment was repeated with an additional molecular marker. One of the hallmarks of differentiation to the procyclic stage is the replacement of the dense VSG coat with GPI-anchored EP and GPEET procyclins (Matthews et al., 2004). Therefore, the GFP:PAD1$_{UTR}$ reporter cell line was additionally transfected with a procyclin marker. In this case an EP1:YFP construct was used, as EP1 is expressed in early and late procyclic trypanosomes. This had two advantages: first, the construct has already been described and analyzed during the differentiation process *in vitro* (Engstler and Boshart, 2004) and second, YFP is also visible in the green UV spectrum together with GFP. The green GFP signal in the nucleus and the yellow YFP signal on the parasite surface are clearly distinguishable, therefore the two markers can be visualized simultaneously which facilitates the analysis of fast moving parasites *in vivo*.
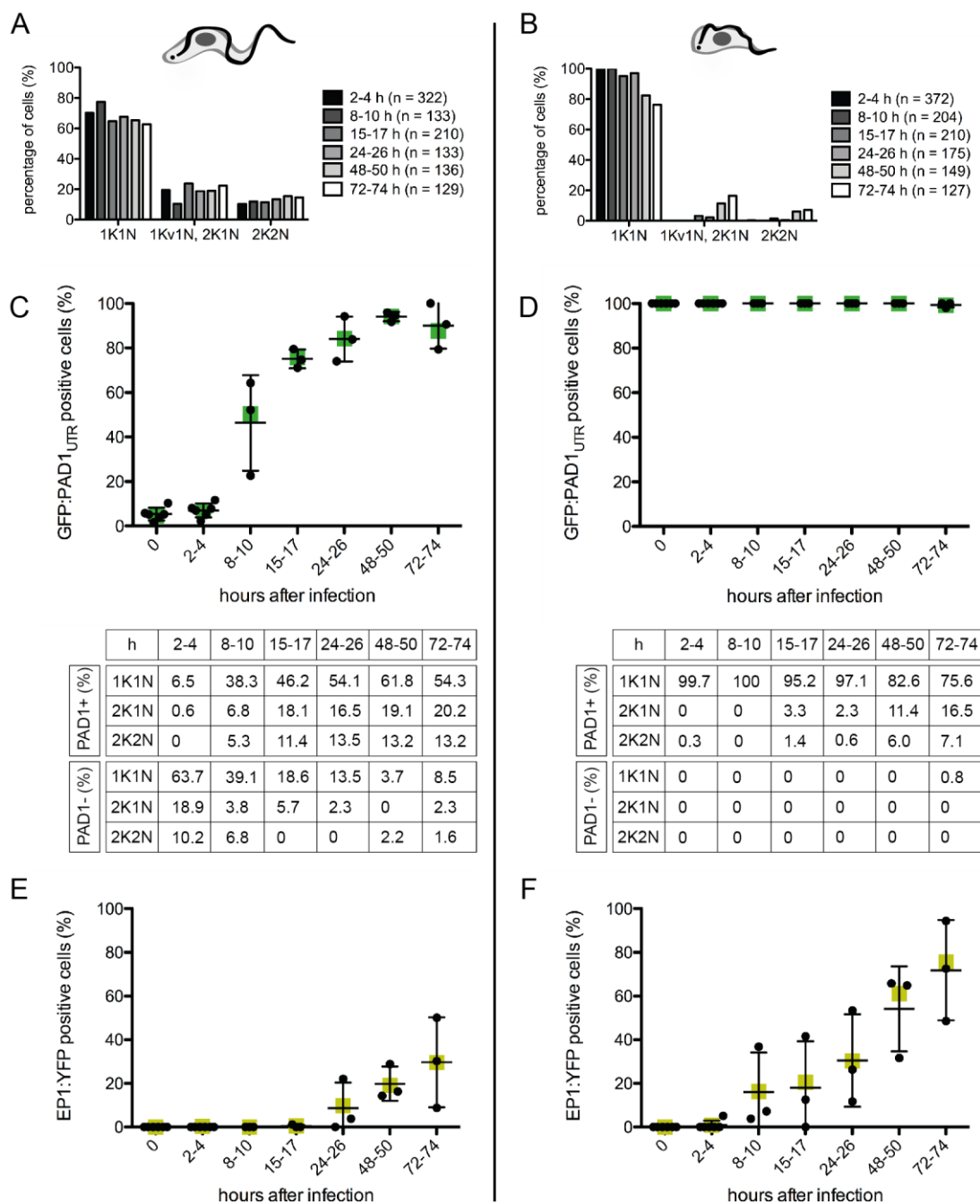
Figure 23: Both slender and stumpy cells differentiate to procyclic trypanosomes *in vivo*. Tsetse flies were infected with slender (SL) or stumpy (ST) trypanosomes. For each cell stage 42 flies (21 ♂ and 21 ♀) were dissected at different time points after infection: 2-4 (n = 6), 8-10 (n = 3), 15-17 (n = 3), 24-26 (n = 3), 48-50 (n = 3) and 72-74 (n = 3) hours in six different experiments each. Time point 0 hours represents the *in vitro* cell population used for infection, which contained on average 4.5% PAD1 positive cells (total amount of cells analyzed n = 1402). Living trypanosomes were analyzed by microscope and documented (total amount of cell n = 1380 SL, n = 1603 ST). (A, B) Parasites were stained with DAPI and analyzed by microscope to determine the configuration of the nucleus (N) and kinetoplast (K) in order to identify the cell cycle stage. (C, D) Trypanosomes were analyzed for the presence of a GFP-positive nucleus (due to GFP:PAD1$_{UTR}$), which reflects the expression of the PAD1 protein in the reporter cell line. Each dot represents one experimental time point (1 ♂ and 1 ♀), values present average percentages (+/- SD) of 3-6 experiments. Green boxes represent the average percentage of all cells analyzed per time point. Percentage of cell cycle distribution of PAD1 positive (PAD1+) and negative (PAD1-) cells is detailed in the table. (E, F) Trypanosomes were analyzed for the presence of a yellow surface coat (EP1:YFP). Each dot

represents one experimental time point (1 ♂ and 1 ♀), values present average percentages (+/- SD) of 3-6 experiments. Yellow boxes represent the average percentage of all cells analyzed per time point.

The experimental setup was the same as described in chapter 3.2.2.1, but now slender (cell density always strictly below $5x10^5$ c/ml) and SIF-induced stumpy (cell density $> 5x10^5$ c/ml, left undiluted for 48 hours) cells were analyzed for direct comparison in individual experiments (figure 23). For each cell type 30 flies (15 ♂ and 15 ♀) were analyzed as described before at 2-4, 15-17, 24-26, 48-50 and 72-74 hours after the infective meal. The percentage of GFP:PAD1+ trypanosomes was analyzed at time point 0 hours for every infection (n = 3 slender, n = 3 stumpy). For slender populations used for infections an average of 3.96% (cell n = 1085) GFP:PAD1+ trypanosomes were determined. Stumpy populations contained 100% (cell n = 1211) GFP:PAD1+ trypanosomes. It is of note that the stumpy population contained predominantly 1K1N cells (96.4%) and hardly any other cell cycle stages (no 2K1N cells and 3.6% 2K2N cells), which is in accordance with literature (Dean, PhD thesis, 2008; Dean et al., 2009). There was no EP1:YFP signal at time point 0 hours for both cell types. Living trypanosomes were detected by microscope and morphology, GFP:PAD1 signal, EP1:YFP signal and cell cycle position was documented for every single cell (cell n = 785 slender and cell n = 872 stumpy). The data showed a large increase in PAD1+ cells between 2-4 and 15-17 hours, as in the previous experiment (compare to figure 22 B), which is why additional infections were performed and cell cycle position, GFP:PAD1 signal, EP1:YFP signal and cell morphology were now also scored for earlier time points at 2-4 and 8-10 hours. An additional 595 slender and 731 stumpy trypanosomes were analyzed in triplicate experiments. Time point 0 represents the *in vitro* cell culture used for infection. The amount of GFP:PAD1+ trypanosomes was 6.62% (cell n = 317) for the slender population and 100% (cell n = 366) GFP:PAD1+ trypanosomes for the stumpy population. There was no EP1:YFP signal at time point 0 hours. For each cell type, 12 flies (6 ♂ and 6 ♀) were dissected at 2-4 and 8-10 hours post-infection. The combined data sets are shown in figure 23.

For the slender trypanosomes, the cell cycle analysis shows a continuously dividing cell population within the fly, with no detectable cell cycle arrest (figure 23 A). These results are similar to the profile of slender cells from the identical experiment previously described in figure 22 A. These profiles are in contrast to the stumpy infection (figure 23 B), where 2-10 hours after infection, trypanosomes were still

predominantly in the 1K1N position of the cell cycle; only one 2K2N cell was identified in this time window. Between 15-26 hours, the first dividing stages were detectable. The distribution of the cell cycle stages is indicative of a growing, asynchronous cell population at 72-74 hours post-infection.

The GFP:PAD1 signal increased from 7.1% at 2-4 hours, to 50.4% at 8-10 hours and to 75.7% at 15-17 hours when slender cells were used for infection (figure 23 C). The fraction of PAD1+ cells reached a peak of 94.1% after 48-50 hours and slightly decreased after 72-74 hours. This observation was in agreement with the data from the first experiment (figure 22 B). In contrast, the stumpy population remained 100% PAD1+ during the entire observation period, with only one PAD1 negative (PAD1-) cell observed at 72-74 hours (figure 23 D). It is of note that the GFP:PAD1 signals detected at the early stages of an infection with slender cells appeared weaker compared to those observed in PAD1+ stumpy cells. However, a quantification of this observation was not performed due to the motion of the cells.

In slender infections, the EP1:YFP procyclin was visible in 9.8% of the cells after 24 hours of infection, increasing to 19.1% after 48-50 hours, and 29.5% after 72-74 hours. In stumpy cell infections, the EP1 signal was visible earlier, after 8-10 hours with 16.2%, increasing to 20.5% at 15-17 hours, to 30.3% after 24-46 hours, 61.1% after 48-50 hours and 75.6% after 72-74 hours. It is of note that the early EP1:YFP signals detected in slender infections were generally weaker when compared to the signal in EP1 positive (EP1+) stumpy cells. This showed that slender parasites were able to differentiate to procyclic trypanosomes, but the differentiation and surface protein exchange was slower compared to the same process from the stumpy stage.
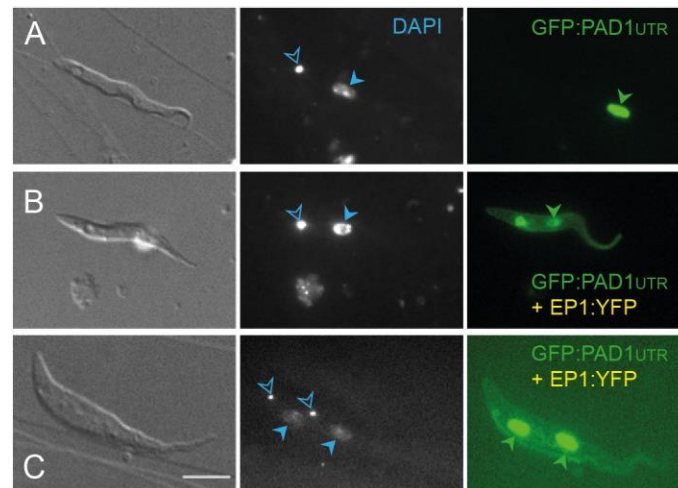
Figure 24: Procyclic trypanosomes *in vivo* 48 hours after infection with slender cells. Living trypanosomes were analyzed directly in fly gut tissues or surrounding medium. First column shows DIC images, second the blue and third the green emission wavelengths. The expression of the GFP protein (GFP:PAD1_{UTR}) is indicated by a fluorescent cell nucleus (filled green arrowheads) whereas the EP1 signal is expressed on the surface of the reporter cell line. Parasites were stained with DAPI to determine the configuration of the nucleus (filled blue arrowheads) and kinetoplast (unfilled blue arrowheads). After 48 hours almost all trypanosomes showed procyclic morphology *in vivo* (A-C). The majority of cells revealed a GFP:PAD1_{UTR} signal in the cell nucleus (A-C) and almost 20% of cells showed an additional EP1:YFP signal on the cell surface (B-C). Scale bar represents 5 µm.

Morphological examination of the parasites confirmed the data of the first experiment (compare figure 22): infected slender cells do not adapt stumpy morphology, but instead become PAD1+ and directly develop slender/procyclic morphology. The first procyclic cells were identified after 24 hours. After 48 hours the majority of cells exhibited procyclic morphology (see figure 24 for example). The stumpy population was morphologically unchanged for the first hours of infection, and showed the signs of differentiation 15-17 hours post-infection. Some procyclic cells were visible after 24 hours and almost all cells had a procyclic appearance after 48 hours.

These experiments established that slender cells do not invariably die inside the tsetse fly midgut, as textbook knowledge suggests. The direct comparison of slender and stumpy cell infections showed noticeable differences in infection progression, revealing that infections are not caused by background stumpy trypanosomes in slender populations. Instead slender cells differentiate directly to procyclic trypanosomes.

3.2.3 Analysis of the differentiation process *in vitro*

The differentiation process of stumpy to procyclic cells is well known, due to the possibility to mimic this process *in vitro*. The results so far demonstrated that slender

bloodstream stages are able to develop and differentiate to the procyclic stage in the tsetse fly, something that was only believed to be possible for the stumpy stage. After finding that slender cells can differentiate into procyclic cells in the fly, it was further addressed whether this is also possible *in vitro*. For this purpose, parallel *in vitro* differentiation into procyclic cells was performed with slender and stumpy trypanosomes. Resulting procyclic cells were used for tsetse fly infections, to analyze developmental competence.

3.2.3.1 Slender cells can differentiate to procyclic cells *in vitro*

Differentiation of pleomorphic stumpy parasites can be induced with a treatment of citrate and/or *cis*-aconitate and a drop in temperature from 37 °C to 27 °C in DTM medium (Brun and Schönenberger, 1981; Czichos et al., 1986; Ziegelbauer et al., 1990; Engstler and Boshart, 2004). Slender (cell density always strictly below $5x10^5$ c/ml) and stumpy (cell density > $5x10^5$ c/ml, left undiluted for 48 hours) cells containing the GFP:PAD1$_{UTR}$ and EP1:YFP reporters were induced to differentiate in parallel (for details see chapter 5.2.1). Cells were concentrated to a minimum cell density of $2x10^6$ c/ml at the beginning of the differentiation process. The percentage of GFP:PAD1$_{UTR}$ and EP1:YFP positive trypanosomes was analyzed for time points 0, 2-4, 15-17, 24-26, 48-50 and 72-74 hours after initiation of the differentiation. In total, slender (n = 823) and stumpy cells (n = 862) were analyzed in parallel in two independent experiments (figure 25). At 0 hours, the amount of GFP:PAD1+ trypanosomes was 1.2% for the slender population and 100% GFP:PAD1+ trypanosomes for the stumpy population. There was no EP1:YFP signal at time point 0 hours. Living parasites were stained with DAPI to determine the configuration of nucleus (N) and kinetoplast (K) to identify the cell cycle stage. To produce comparable data and fluorescence signals, the analysis by microscope was performed as previously described for the *in vivo* infections in chapter 3.2.2.

The cell cycle analysis showed a continuously dividing slender population (figure 25 A). In contrast, the profile for the stumpy parasites exhibited a cell cycle-arrested population in the first hours, containing exclusively 1K1N and a few 2K2N cells at 0-4 hours (figure 25 B). The first cells with a 2K1N configuration from the stumpy differentiation appeared after 15-17 hours, indicating a re-entry into the

cell cycle. The number of dividing cells increased until a normal cell cycle profile was reached.

At first, the slender population was largely PAD1- and only a few PAD1+ background stumpy cells were detected between 0-4 hours of differentiation (figure 25 C). However, the percentage of PAD1+ trypanosomes reached 94.9% after 15-17 hours. This PAD1+ cell population also included dividing parasites, namely 6.8% 2K1N and 17.8% 2K2N cells. Almost no dividing parasites were PAD1- at this time. Stumpy trypanosomes were 100% PAD1+ during early observation. For both cell types, PAD1 signal decreased with similar kinetics after reaching almost 100% at 24-26 hours (figure 25 C and D).

The first EP1+ cells (1.8%) arising from differentiation of slender cells were observed after 2-4 hours. This fraction increased to 14.1%, 57.7%, 89.9% and 98.3% at 15-17 hours, 24-26 hours, 48-50 hours and 72-74 hours, respectively (figure 25 E). The stumpy population expressed EP1 much earlier: 54.3% of the cells were EP1+ 2-4 hours after induction of differentiation. The number of cells with EP1 signal further increased to 79.8% at 15-17 hours and almost 100% of the stumpy population was EP1+ after 24-48 hours (figure 25 F). Other *in vitro* studies also showed that stumpy cells did not divide for about 12 hours, which coincidences with a full expression of the protein at this time point (Ziegelbauer et al., 1990). First expression of procyclin was detectable after 4 hours, which is in accordance to the finding in these experiments (figure 25 F).

After 24 hours, morphological changes became apparent in slender parasites and first cells showed morphological characteristics of the procyclic stage. After 48-50 hours, almost all cells had a procyclic appearance. The stumpy population differentiated faster and showed their first procyclic characteristics after 15-17 hours, with almost all cells being procyclic after 24-26 hours.

h	0	2-4	15-17	24-26	48-50	72-74
PAD1+ (%) 1K1N	1.2	3.7	70.3	72.3	49.6	23.1
2K1N	0.0	0.0	6.8	10.8	10.9	0.9
2K2N	0.0	0.6	17.8	13.8	7.8	1.7
PAD1- (%) 1K1N	74.1	62.0	4.2	3.1	24.0	53.8
2K1N	15.7	18.4	0.0	0.0	3.9	12.8
2K2N	9.0	15.3	0.8	0.0	3.9	7.7

h	0	2-4	15-17	24-26	48-50	72-74
PAD1+ (%) 1K1N	89.6	92.0	93.5	88.0	60.6	29.7
2K1N	0.0	0.0	4.0	7.2	4.4	5.1
2K2N	10.4	8.0	2.4	4.0	6.6	0.0
PAD1- (%) 1K1N	0.0	0.0	0.0	0.8	22.6	50.8
2K1N	0.0	0.0	0.0	0.0	2.2	4.2
2K2N	0.0	0.0	0.0	0.0	3.6	10.2
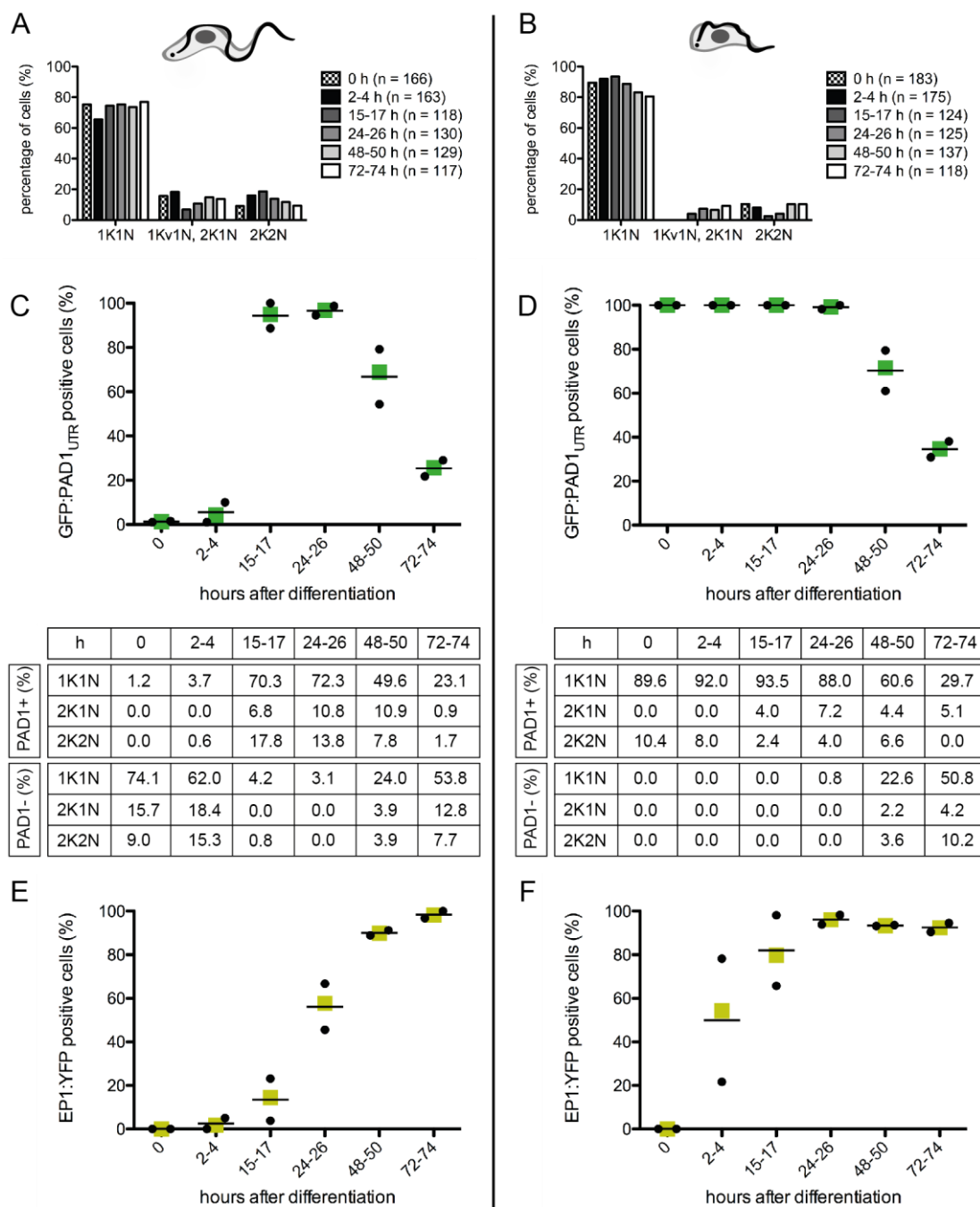
Figure 25: Both slender and stumpy cells differentiate to procyclic trypanosomes *in vitro*. Slender (SL) and stumpy (ST) trypanosomes were differentiated *in vitro* in parallel and analyzed at different time points (0, 2-4, 15-17, 24-26, 48-50 and 72-74 hours) in two different experiments. Living trypanosomes were analyzed by microscope and documented (total amount of cell n = 823 SL, n = 862 ST). (A, B) Parasites were stained with DAPI and analyzed by microscope to determine the configuration of the nucleus (N) and kinetoplast (K) to identify the cell cycle stage. (C, D) Trypanosomes were analyzed for the presence of a GFP-positive nucleus (due to GFP:PAD1$_{UTR}$), which reflects the expression of the PAD1 protein in the reporter cell line. Values are calculated as average percentage (with mean) of two experiments. Green boxes represent the average percentage of all cells analyzed per time point. Percentage of cell cycle distribution of PAD1 positive (PAD1+) and negative (PAD1-) cells is detailed in the table. (E, F) Trypanosomes were analyzed for the presence of a yellow surface coat (EP1:YFP). Values are calculated as average percentage (with mean) of two experiments. Yellow boxes represent the average percentage of all cells analyzed per time point.
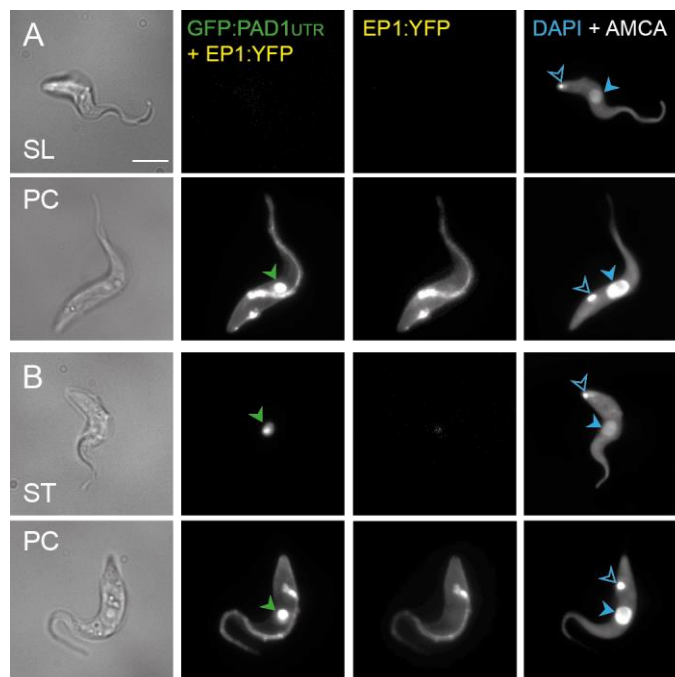
Figure 26: *In vitro* **differentiation of slender and stumpy trypanosomes to procyclic cells.** Slender (A, SL) and stumpy (B, ST) trypanosomes were differentiated *in vitro* using 6 mM *cis*-aconitate and a temperature drop to 27 °C. Some parasites were chemically fixed before differentiation and 48 hours later (A, PC and B, PC). The expression of the GFP PAD1 reporter protein (GFP:PAD1$_{UTR}$) was indicated by a fluorescent cell nucleus (filled green arrowheads) whereas the EP1 signal was expressed on the surface of the reporter cell line. First column shows DIC images, second the green, third the yellow and fourth the blue emission wavelengths. For latter images, cells were stained with DAPI (DNA) and AMCA-sulfo-NHS (cell surface). Configuration of the nucleus (filled blue arrowheads) and kinetoplast (unfilled blue arrowheads) were determined. After 48 hours almost all cells showed procyclic morphology (PC) and an EP1:YFP signal on the surface, which was visible in the green and yellow fluorescence channel. Numerous procyclic cells additionally revealed a GFP:PAD1$_{UTR}$ signal in the cell nucleus early after differentiation, which was only visible in the green channel. Scale bar represents 5 μm.

Figure 26 illustrates the morphological differences of the trypanosome populations during *in vitro* differentiation. Slender, stumpy and corresponding procyclic cells that resulted from the differentiation were surface stained with AMCA-sulfo-NHS, fixed, and stained with DAPI. In early procyclic trypanosomes the GFP signal of the PAD1 reporter was still visible.

To summarize, the data clearly confirm that an *in vitro* differentiation is possible for the slender stage, albeit with slower kinetics of procyclic development, when compared to the stumpy form. Differentiated cells from both bloodstream stage populations show procyclic morphology and a normal cell cycle profile at 72-74 hours.

3.2.3.2 Procyclic trypanosomes differentiated from slender cells can complete the life cycle *in vivo*

To test whether procyclic cells differentiated from the slender bloodstream stage are developmentally competent, flies were infected with procyclic parasites generated from both slender and stumpy stages (table 2). For this purpose, tsetse flies were infected with procyclic trypanosomes 6 days post-differentiation at a low concentration of $2x10^6$ c/ml. Parasites were fed once to 29 flies for the slender and 30 flies for the stumpy differentiation in SDM-G medium. Fly dissections were performed by the master student Jaime Lisack 35-40 days after infection and screened for the presence of trypanosomes in the midgut (MG), proventriculus (PV) and salivary glands (SG).

Table 2: Infection rates of differentiated procyclic trypanosomes from bloodstream stages. Male and female flies were infected once with $2x10^6$ c/ml procyclic trypanosomes, 6 days post-differentiation, and generated from slender (slender diff.) or stumpy (stumpy diff.) stages. Surviving flies were dissected 35-40 days post-infection and screened for the presence of trypanosomes in the midgut (MG), proventriculus (PV) and the salivary glands (SG). For one fly (**), the infection status of the PV and SG could not be determined.

cell type	n° of infection	flies infected	flies dissected	ratio ♀/♂	MG	PV	SG
procyclic cells (slender diff.)	1	29	20	0.67	30%	25%	20%
		18	12	♂	33.3%	25% **	25% **
		11	8	♀	25%	25%	12.5%
procyclic cells (stumpy diff.)	1	30	12	0.71	25%	25%	25%
		19	7	♂	42.9%	42.9%	42.9%
		11	5	♀	0%	0%	0%

Even though male flies are more sensitive to infections compared to female flies, infections with procyclic trypanosomes from a slender differentiation resulted in mature infections in both sexes. The procyclic trypanosomes were able to infect the salivary glands in 20% (4/20 flies) for the slender-derived and 25% (3/12 flies) for the stumpy-derived parasites. The low number of flies was not sufficient to make a strong quantitative statement about infection rates, but the results demonstrate that procyclic cells from a slender differentiation are able to infect the fly up to the mammalian-infective stage in salivary glands. Thus, procyclic trypanosomes generated from slender cells also possess full developmental competence.

4 Discussion

4.1 The trypanosome-tsetse system is a versatile and accessible model system for microswimmer research

Microbial motility is a topic that is attracting more and more interdisciplinary attention. Motility of parasites is of particular interest as they are medically important, but a major problem for research is the accessibility of the parasite inside the host. A recent study was able to visualize swimming *Trypanosoma carassii* in the bloodstream of a cold-blooded live vertebrate host, a transparent zebrafish (Dóró et al., 2019). However, *in vivo* imaging in mammalian hosts is difficult, and especially achieving optical access to tissues at single-cell resolution (Jelicks et al., 2013; MacLean et al., 2013). In addition, work with routinely used laboratory mammals, such as mice and rats, is complex and, importantly, they are commonly not the natural hosts of the parasites either.

A largely neglected model for parasite analysis *in vivo* is the arthropod vector. Insects transmit numerous tropical diseases, and the parasites undergo important developmental changes while inside them. For example, protists of the *Plasmodium* genus are the causative agent of malaria and are transmitted by female mosquitos (*Anopheles spp.*). A small number of mature male and female *Plasmodium* gametocytes develop in the blood of the mammalian host. Following ingestion by the mosquito, they differentiate into gametes and undergo their life cycle´s sexual phase inside the midgut lumen, before further developing the capability to migrate to the salivary glands (Josling and Llinás, 2015). Also, *Leishmania* parasites are responsible for a spectrum of diseases called leishmaniases. They undergo various morphological transformations in the female sand fly, including attached forms as well as weakly and highly motile cell stages (Dostálová and Volf, 2012). Motility plays an important role for passage through the fly and the correct positioning of the cells for further transmission (Cuvillier et al., 2003). Parasites are confronted with a variety of different habitats and barriers, which they have to adapt to, in order to complete the life cycle. Therefore, this concept is not only important in the mammalian host, but also in the insect vector, which, due its small size, is more suitable for *in vivo* analysis.

The working hypothesis for this doctoral thesis was that the type of motion and the morphological differences in trypanosomes are indispensable factors for the

completion of the life cycle inside the tsetse fly. A closer look at the tsetse fly anatomy revealed a very complex and dynamic natural habitat. Parasites undergo programmed alterations, which represent adaptations to their natural microenvironments, to ensure successful colonization of the fly. The patho-functional relevance of the motile behavior might be key for a successful outcome for the parasites, and was of major interest for this doctoral thesis.

This work details these complex host-parasite interactions in a natural vector and introduces the first tractable microswimming model system for microbial motion at low Reynolds numbers. The tsetse fly provides a comparably small and manageable space for the analysis of direct interactions of parasites and their natural microenvironment, which is beneficial for both microswimmer research and parasitology. A complete set of different methods, approaches and concepts are introduced in this work to describe the trypanosome-tsetse system. Due to the broad scope of this project, data are necessarily exemplary and only demonstrate the tractability of different parameters and the variety of analysis opportunities. Furthermore, this system approach is also applicable for other parasite-vector combinations, as the physics of parasite motility and host-parasite interactions have received broad interdisciplinary attention.

4.1.1 Mapping the tsetse fly microenvironments

To understand the swimming motion of an organism, it is important to understand its natural 3D-environment. This study introduces light sheet fluorescence microscopy (LSFM) as an advantageous technique to understand structural conditions and geometries of the tsetse fly´s inner topology (Heddleston and Chew, 2016). This technique allows three-dimensional reconstructions of basically every region of the fly, intact and with sufficient resolution to visualize internalized parasites on the single cell level (chapter 3.1.1).

A striking observation was the extensive convolution of the peritrophic matrix inside the fly gut. This turned out more as a rediscovery after a long time. Literature research yielded that Wigglesworth produced detailed drawings of anatomical tsetse fly features in 1929, including the huge surface of the peritrophic matrix (Wigglesworth, 1929). Since then, these structures have apparently been ignored by parasitologists. However, the peritrophic matrix represents an important barrier in

insects. Unlike other parasites, such as *Leishmania* and *Plasmodium*, trypanosomes are not known to secrete chitinases to degrade the peritrophic matrix (Langer and Vinetz, 2001; Rogers et al., 2008). These parasites infect mosquitos and sand flies, which secrete a Type I peritrophic matrix that is produced by the entire midgut. In contrast, tsetse flies produce a Type II peritrophic matrix, which is only produced in the proventriculus (Lehane, 1997). In fact, insects producing a type I peritrophic matrix are usually more likely disease vectors. The invasion of the ectoperitrophic space may be an adaptive strategy of the *T. brucei* subspecies, to compensate for the inability to attach and degrade the mature tsetse peritrophic matrix. Other trypanosome species like *T. vivax* do not colonize the ectoperitrophic space. Instead they attach quickly to the chitinous lining of the labrum in the middle region of the proboscis and produce infective forms (Rotureau and Van Den Abbeele, 2013). LSFM allowed us to detail the peritrophic matrix in 3D for the first time, which showed that the folded matrix fills up a great portion of the midgut. It is able to expand during the blood meal and shrink again to produce extensive folds after excretion of the liquid. Despite the fact that we still do not know the mechanism of how and where trypanosomes cross the peritrophic matrix barrier, the topological complexity of this structure inside the gut has not been appreciated (Hoare, 1931; Yorke et al., 1933; Willett, 1966; Moloo et al., 1970; Ellis and Evans, 1977; Gibson and Bailey, 2003).

The 3D visualization allows a detailed picture of the living environment where trypanosomes naturally occur and swim. The complexity of the peritrophic matrix maze is obvious by eye, but challenging to describe. The three-dimensional high-resolution maps will allow further mathematical analyses and calculations. For this approach, Philip Kollmannsberger from the Center for Computational and Theoretical Biology (CCTB) in Würzburg has conducted preliminary computations using Euclidean distance mapping (Danielsson, 1980). He was able to generate information on the degree of confinement and the connectivity of the peritrophic matrix. The average fold size was predictable by using the maximal ball concept, where spheres of fitting diameter reflect the space enclosed by the matrix in 3D. The radius of the balls and their probability distribution indicates the free space between the peritrophic matrix folds. This approach enables the use of computer-aided analysis of structural conditions and changes, in order to describe the peritrophic matrix maze quantitatively. The available data are able to form the basis for numerical simulations of trypanosomes inside their natural environment.

The high spatial resolution of LSFM allowed the detection of fluorescent trypanosomes between the peritrophic matrix folds and in different areas and organs, e.g. gut tissue, bacteriome and proventriculus. Trypanosomes are well-established models in cell biology and various genetic manipulations are feasible, including the insertion of different fluorescent proteins (MacLean et al., 2013; Gibson and Peacock, 2019). In the course of this work different fluorescence constructs were tested. A cell line with a bright green cell nucleus (NLS:GFP) was suited best for single cell localization in the LSFM recordings. A cell line with a very bright cytoplasmic tdTomato signal in living cells was tested, but the fluorescent protein was unfortunately not stable using the LSFM fixation conditions. Therefore a cell line expressing cytoplasmic mNeonGreen was used. mNeonGreen is 2.75x brighter than EGFP and 3-5x brighter than GFP (Hostettler et al., 2017), however, the cytoplasmic signal was not as strong as the signal of the accumulated GFP in the nucleus of the NLS:GFP cell line. In addition, single cell identification with a cytoplasmic marker was difficult in crowded areas. However, various different markers and fluorescent proteins are available, allowing further individual optimization. For the aim of this work, visualization of trypanosomes on a single cell level was successfully achieved with the NLS:GFP cell line. Note that due to the requirement of living symbiotic bacteria in the fly, there is no selective antibiotic treatment possible for trypanosomes *in vivo*. Cells can lose the fluorescent constructs and visible fluorescent cells might not represent the total amount of trypanosomes.

LSFM microscopy was able to refine the conventional view of trypanosome distribution in infected tsetse fly tissue (Yorke et al., 1933; Gibson and Bailey, 2003). The microscope does not allow dynamic analyses, however. In living flies the matrix convolution states change frequently, due to blood uptake, peristalsis, and the continuing production of the matrix. The peritrophic matrix is produced at a rate of approximately 1 mm/h (Willett, 1966; Harmsen, 1973) and is fully formed after 80-90 hours (Lehane and Msangi, 1991). Besides the complex topology of this maze, physical forces such as flow also might be involved in influencing trypanosome motion. Therefore, experiments were performed to visualize motile trypanosomes and fluorescent microspheres in the fly´s interior (chapter 3.1.1.3). Beads have been successfully used in experiments in mosquitos, where hemolymph flow and transport were under investigation by tracing fluorescent beads inside the mosquitos (Glenn et al., 2009; Andereck et al., 2010). Here, it was possible to simultaneously visualize

beads and living parasites inside the tsetse midgut and proventriculus. This approach can be used to gain information about inner forces or available space, e.g. by comparing the distribution of beads and trypanosomes in detail.

The first part of this work focused particularly on the geometries and physical constraints inside the tsetse fly by using LSFM. This method allowed highly detailed views of the fly´s interior topography, especially the extremely convoluted folding of the peritrophic matrix. Due to this, we are now able to correlate complex 3D structures with the two-dimensional structures observed by live cell microscopy in dissected flies. In addition, detailed three-dimensional maps will allow mathematical analyses, for example on the connectivity of channels built by the peritrophic matrix. This can be further used as basis for numerical simulations of the natural trypanosome habitat. However, the trypanosome-tsetse complex is highly dynamic, and besides geometries, other parameters like flow and viscosity need to be considered for a detailed picture. First possible approaches were highlighted in this thesis, for example the use of passive microspheres to detail flow and tissue constraints. Due to the complexity of this system, this work did not aim to unravel these aspects in detail, rather establish methods and ideas that enable further research.

4.1.2 Morphology and motility are adapted to the infection process

The trypanosome-tsetse system is, in certain aspects, ideal for the analysis of microswimming. The fly is small, compared to mammalian hosts, and it provides various natural swimmer types in their different *in vivo* environments. The development of *T. brucei* is also highly organized in time and space. Therefore, we hypothesized that varying environments might be essential for migration as well as for initiation of developmental processes. Although, what do we actually know about the parasite´s behavior inside the fly? There is a continuous selective pressure in host and vector, to which the parasites adjust with different morphological features and cell behavior. These adaptations with changing environments are not well characterized in the fly. The interaction of trypanosomes with the tsetse fly remained challenging due to technical constraints and time-consuming procedures of *in vivo* experiments (Sharma et al., 2009). In addition, the *in vitro* cultivation of all fly-specific trypanosome stages is not yet established and analysis of the individual cell types is

limited to the availability of infected flies. A study published by Kolev and colleagues, describes the *in vitro* development of fly-specific stages, including the infective metacyclic stage that expresses VSG on the surface (Kolev et al., 2012). These experiments were performed with monomorphic cells and attempts to reproduce the data our laboratory did not result in viable fly forms, however (Westphal, 2014).

One aim of this work was the three-dimensional description of the cell architecture of fly-specific stages of *T. brucei*. Although their morphological features have been described in detail (Vickerman, 1985; Sharma et al., 2009), it has been shown that the elucidation of motility mechanisms require the careful three-dimensional analysis of decisive features, like the specific flagellar attachment or the apparent elasticity of the cell body (Heddergott et al., 2012; Bargul et al., 2016). Such data has been invaluable for three-dimensional numerical simulations of trypanosomes, showing the effects of viscous fluids and the flagellar attachment on swimming velocity in bloodstream forms (Alizadehrad et al., 2015). The data presented in this thesis can be used to generate detailed 3D models and simulate all different swimmer types from the fly (chapter 3.1.2). It will allow the mathematical analysis of morphological features, which can be further used to simulate single motion as well as collective behavior and physical interaction with surfaces. The data contain important new information for computational modeling of microswimmer types, the optimal morphology of which had only been predicted in the study from Alizadehrad and colleagues. In particular, the prediction of a helical flagellar course of a mesocyclic cell, with a shallower helical progression as compared to bloodstream or procyclic forms, is in agreement with the experimentally measured mesocyclic morphology in this work (figure 11 C), underlining the predictive power of mathematical simulations. Using simulations of nature-inspired *in silico* swimmers, the study from Alizadehrad showed that the helical course of the flagellar attachment optimizes the parasite´s motility (Alizadehrad et al., 2015). Changing details of the flagellar attachment changes the swimming capacities of the swimmers and has a significant influence on the swimming performance in the models. By changing various parameters, this method allows the generation of *in silico* mutants and thereby contributes to the understanding of the trypanosome morphology. It shows that swimming velocity can be one parameter the trypanosomes adapt and the stage specific importance of flagellar course for that means.

The surface staining with the AMCA-sulfo-NHS dye revealed that metacyclic trypanosomes always showed a stronger staining, as compared to other fly-specific stages. This might be due to the fact that metacyclic forms already express metacyclic VSG (M-VSG) on their surface (Barry et al., 1998), which might be more suitable in combination with the surface dye. The AMCA-sulfo-NHS dye was already successfully used for the staining of VSG-covered bloodstream stages (Bargul et al., 2016). Due to the comparably weaker staining in fly stages, we serendipitously observed an increased surface staining at the free anterior part of the flagellar tip in some fly stages. This was especially prominent during the transformation from mesocyclic to dividing epimastigote forms (figure 11). The flagellum is very important for trypanosomes and is present in all developmental stages. The stronger staining could be due to specific surface proteins in this region. Trypanosomes probe their environment with the free tip of the flagellum and the potential role of different functions, like environmental sensing, has been discussed (Maric et al., 2010). For trypanosomes, it has been proposed that the flagellum could act as a sensory organelle, for example through the MAP kinase pathway (Rotureau et al., 2009). MAP kinase kinase 1-null mutants were able to establish midgut infections, but were unable to infect the salivary glands, suggesting that the signaling cascade is essential to complete the life cycle in the fly (Morand et al., 2012).

There are only few studies focusing on parasite motility in their respective vectors, even though dissemination in and colonization of host tissue are key events during infection processes. Quantitative *in vitro* analysis of free-swimming *Leishmania major* showed that these parasites also exhibit a tip-to-base symmetrical beat and are effective swimmers (Gadelha et al., 2007). Motility data inside the sand fly vector are fragmentary, although it is possible to visualize parasites in dissected fly guts. Even so, the multiple roles of the flagellum and cell motility in *Leishmania* have been discussed, as well as their importance for the successful infection process (Sunter and Gull, 2017). It was at least shown that motility *per se* is necessary for successful infection of the vector (Cuvillier et al., 2003). Therefore, another aim of this work was the detailed analysis of trypanosome swimming behavior by using high-speed video microscopy inside and outside of the fly tissue (chapter 3.1.3 and 3.1.4). We wanted to gain an overview of the correlation of environment, morphology and the spatiotemporal-resolved behavior of the parasites.

We were able to show that every developmental stage in the tsetse fly reveals its own characteristic motility behaviors. Some developmental stages were exclusively observed as solitary swimmers, whereas others were preferentially seen in dense swarms with close contact to neighboring cells or tissue borders. Trypanosomes were often observed swimming along the walls of the peritrophic matrix or in close contact to tissues. Interactions of microorganisms and surfaces have received considerable attention, especially in work on the surface motility of sperm cells and bacteria (Rothschild, 1963; Harshey, 2003; Berke at al., 2008; Elgeti and Gompper, 2016). Mesocyclic cells in particular were observed to perform near-wall swimming (figure 13 A and B). When mesocyclic trypanosomes were released from the fly tissue into the surrounding cell culture medium, tumbling and frequent flagellar reversals were observed. This behavior has been described for bloodstream stages in cell culture medium. Conversely, physical contact to e.g. artificial pillars or viscous medium, increased the directional motion of the parasites (Heddergott et al., 2012). Therefore, staying close to surfaces could help to guide the cells by influencing the persistence of forward motion. Trypanosomes are able to maneuver between the peritrophic matrix folds and free themselves from confinement. The elastic cell body allows sharp turns and squeezing through narrow channels, which enable the trypanosomes to assume a high degree of control in navigating through their environment.

For the dissemination within the mammalian host it has been shown that distinct trypanosome species reveal different morphological features and diverse swimming capabilities, corresponding to their preferred niches (Bargul et al., 2016). For example, *T. congolense* is a poor swimmer with a short flagellum, but it is destined for cell adherence in areas of the circulation with low blood flow. This is visualized by a short and stiff 'cellular waveform'. The cellular waveform is a concept that was introduced and used by Bargul and colleagues to describe morphological features and motility three-dimensionally. In contrast, *T. vivax* is highly motile and perfectly adapted to live in the bloodstream. The cellular waveform seems perfectly aligned to bloodstream topology. The high degree of adaptation is possibly also true for trypanosomes found in the fly, as different species have developed specific cell types to colonize different compartments inside the vector (Peacock et al., 2012 a; Rotureau and Van Den Abbeele, 2013; Ooi et al., 2016). Analysis of cellular waveforms attempts to gain mechanistic first insight into the complex correlation of

morphology and motility, and shows here that every developmental stage has specific characteristics (figure 17). For example, we have shown that dividing epimastigote trypanosomes are effective swimmers and are able to reach very high swimming speeds (figure 14 B and 17 E). For our purposes, we compared maximum speeds of different developmental stages for assessing swimming capabilities. In the current understanding of the infection process, the dividing epimastigote is thought to carry the almost immotile small epimastigote (figure 14 C and 17 F) to the salivary glands, where they attach. This is most likely to happen quickly, because during a blood meal trypanosomes can be flushed out with the saliva. Mesocyclic and different epimastigote stages can be found in the fly´s saliva during salivary gland tests during early infection (see chapter 5.2.2; Schuster, 2014). The special epimastigote cell type with the sperm-like morphology has not been observed in other species like *T. vivax* and *T. congolense*, but these species do not infect the salivary glands (Rotureau and Van Den Abbeele, 2013). Considering the observations from this thesis, this leads to the speculation that this highly motile cell type has evolved in *T. brucei* specifically for the rapid colonization of the glands.

Another interesting feature of trypanosome motility is the fact that some developmental stages reveal collective behavior. Mesocyclic trypanosomes appear in dense clusters and parasites are in close contact with each other. The synchronized motion of the cell accumulations raises the question of how these clusters are formed and organized (figure 13 C and 16). Interestingly, this high degree of collective motion was not observed for procyclic trypanosomes. Procyclic cells reach high cell densities in the posterior midgut, and small clusters were occasionally seen to synchronize but never to the same degree. The phenomenon of 'social motility' was reported to be typical for procyclic trypanosomes *in vitro* (Oberholzer et al., 2010). As this occurs in the early procyclic stage, it was speculated that this phenomenon is involved in the infection process and mimic the colonization of the midgut (Imhof et al., 2014). Observations from this work did not show any form of social motility *in vivo* however, so the colonization process still remains unclear.

Using fluorescent cell lines, single trypanosomes were identified in dense swarms and tissues. Quantitative tracking of fluorescent cell nuclei was performed using the commercially available Imaris software (figure 18). At the beginning of this work, fluorescent cells were mixed with non-fluorescent trypanosomes, for a better visualization of single signals. However, it turned out that many trypanosomes lose

fluorescence in the fly, probably due to the lack of antibiotic selection. Therefore, it was not possible to predict the number of fluorescent trypanosomes in advance. However, automated cell tracking represents a powerful tool to generate quantitative motility data inside the tsetse fly´s interior. Fluorescent flagella also enabled the visualization of single flagellar beats in dense clusters, which showed synchronization events of cells in close contact (figure 16 B). Synchronization of flagellar beating was observed in cell accumulations as well as in small clusters of just a few cells (figure 12 B). The phenomenon of synchronization has been studied with sperm flagella and was already described in 1949 by Rothschild. He observed that the flagella of bull spermatozoa tend to synchronize when they are close to each other (Rothschild, 1949). Self-organization of swimming sea urchin spermatozoa was also observed near surfaces, swimming in organized vortex arrays (Riedel et al., 2005). This leads to higher order swarm behaviors, which are of interest for modeling of single and collective flagella beating (Brumley et al., 2014; Elgeti and Gompper, 2016). Very few examples of collective motion have been analyzed in parasites. One of the swimming stages from the parasite *Trichomonas vaginalis* is also known to form large cell swarms, in a process that is in the literature described as 'swarming'. It is thought that this could represent a form of defensive reaction to the host immune response, but this remains speculative due to limited available data (Honigberg, 1990; Hirt, 2013).

During this work, we were able to isolate various developmental stages directly from the fly and use them for detailed *in vitro* studies and also visualize all stages *in vivo* directly in their microhabitats. Fluorescent trypanosomes allowed analysis of single parasites in dense clusters and procedures for quantitative tracking were demonstrated. The trypanosome-tsetse system allows direct observations over ranges of cell concentrations, different swimmer types, interactions with the natural environment and neighboring cells. Although we have shown the tractability of this system, it still remains a complete and therefore complex system, which has been shaped and optimized for function by evolution. Although this is a huge advantage in terms of the quality and quantity of attainable data it also poses a challenge for handling and processing of that data. Due to the vast multifactorial analysis opportunities, we were necessarily restricted to generate exemplary data in the scope of this work. It should nonetheless be noted that the data on maximal velocities and flagellar beat frequencies of developmental stages are based on relatively large

sample numbers. As such, they are expected to be quite accurate and represent adequate starting parameters for the analysis of environmental effects on the parasites (figure 17). For further analyses, reference frames need to be defined and specific questions need to be asked, now that we have the so far unique ability to analyze distinct microswimmers within their natural habitats. Here, we have introduced a broad set of methods, concepts and possibilities to tackle this system. Further experiments and *in silico* modeling can lead to a more comprehensive understanding of microswimmers in general and the parasite-vector interactions. To summarize, the trypanosome-tsetse system is demonstrated to be a versatile and tractable model for the analysis of microswimming and its biophysical relevance.

4.1.3 The use of artificial environments in microswimmer research

Elucidation of the motility of single cells and cell types represents an important step towards understanding the population dynamics and how the architecture of the environment influences behavior. It has been shown that specific artificial geometries are able to influence the motile behavior or swimming direction of microswimmers. This concept is not only important for protist pathogens, as the motile behavior of spermatozoa and bacteria are also in the focus of interdisciplinary research (e.g. Binz et al., 2010; Denissenko et al., 2012). For bloodstream form trypanosomes it has been shown that ordered pillar arrays, with size and spacing of red blood cells, are able to promote sufficient maximum forward velocity (Heddergott et al., 2012). This illustrated the adaptation of the parasites to their natural environment and the importance of physical contact with obstacles (Heddergott et al., 2012; Bargul et al., 2016). These observations were only possible because the complex environment of the mammalian bloodstream was partly copied in an artificial environment. Due to the natural complexity of a whole organism, in addition to the *in vivo* analysis methods described so far, there will always be the need to reproduce results in such artificial, controllable systems, i.e. simplified representations of system parts are needed (Elgeti et al., 2015). We attempted to partly abstract the trypanosome-tsetse system, in order to challenge experimental results with adjustable parameters in artificial surrounding.

To attempt to generate complex geometries, soft lithography was utilized to produce microfluidic devices. Microfluidics is widely used in microswimmer research and for

the elucidation of natural environmental factors (e.g. Binz et al., 2010; Denissenko et al., 2012; Heddergott et al., 2012; Uppaluri et al., 2012; Tung et al., 2015; Hochstetter and Pfohl, 2016; Yawata et al., 2016). For the purpose of this study, a custom-made soft lithography mask was designed, containing geometries that were inspired by natural topologies found in the tsetse fly system using LSFM and live-cell microscopy (chapter 3.1.5.1). Unfortunately, it was not possible to establish a reliable working protocol for the production of PDMS stamps. Different approaches were tested to optimize the workflow, but none of them resulted in usable patterns. Later on, members from our laboratory found that the SU-8 photoresist for the development of the pattern had expired, which was the reason for the problems during production of the devices. On account of this, analysis of trypanosomes in the designed structures was not possible during the course of this thesis. Nevertheless, the rationale for selected designs features can be briefly discussed.

An interesting observation was the near-wall swimming behavior, which was observed for mesocyclic trypanosomes swimming along the peritrophic matrix wall and discussed earlier in this work. In the case of human sperm cells, it was already shown that they rarely swim in the central part of microchannels. Instead, cells swim with their heads against the channel wall, resulting in swimming preferably along surfaces and along corners (Denissenko et al., 2012). When the channel contained a sharp curve, sperm cells departed from the wall until heading for the next wall. Specific wall shapes were able to direct motile sperm cells in preferential directions. This observation allowed the design of a one-way running track, where specific pattern shapes guide all sperm cells in one direction. If cells changed direction, they were quickly redirected (Denissenko et al., 2012). Mesocyclic trypanosomes exhibit a different morphology to sperm cells and therefore no-head -against-the-wall motion is possible (figure 13 A and B). Instead, the worm-like mesocyclic cells perform small oscillations with their flagellum, resulting in small amplitude waves, which might help them to stay close to surfaces (figure 11 C and 17 C). To analyze this in more in detail, the custom-made mask design contained different channels with varying sizes, sharp curves and different shapes. These structures were inspired from both geometries found in the tsetse fly, as well as structures used in sperm research (figure 19).

In order to analyze the self-organization of trypanosomes, different geometries such as triangles and semicircles with different sizes and angles were implemented

(figure 19). These are structures that were designed with similar dimensions and shapes as those found in the fly´s interior. However, the designs were supposed to have defined static dimensions, in contrast to the changing conditions inside the fly. The influence of distinct shapes on the self-organization of microorganisms has been described before, for example in bacteria. A combination of experimental observations in microfluidic devices and computational analysis revealed a process of self-organization that results in a high correlation of cell orientation and growth of collective cell movement (Cho et al., 2007). Interestingly, this ordered organization facilitates efficient escape of bacterial cells, where in contrast a disorganized expansion leads to blockage of cell escape. The escape of cells is important, as it improves the access of nutrients into the interior of the colony and evacuation of waste. Using a computational model, it was predicted that cell length might be optimized to maximize the self-organization of the population. The results from the present work might also emphasized that self-organization could be influenced by the shape of the surrounding and shape of the parasites. Mesocyclic trypanosomes are cell cycle-arrested and exhibit a 'tubular' morphology, which results in a quite uniform cell population. Huge clusters were observed, that were able to synchronize their motion (see chapter 3.1.3). The orientation of individual cells becomes aligned with the orientation of neighboring cells, which might be facilitated by the uniform elongated cell shape. However, single parasites were observed to move free within these cluster and escape or enter, as it was described to be beneficial for organized bacterial colonies (Cho et al., 2007). To date, we can only speculate on the relevance of these fascinating phenomena, therefore the reproduction of confined structures inducing this kind of behavior and comparison to known analogous behavior in other microswimmers would be a primary goal.

Microfluidics has many potential applications and for future directions a number of aspects might be of interest. For example, some microfluidic devices allow cell sorting. A combination of ratcheting microchannels and sorting junctions was used to build a sorting device for motile *E. coli* cells by length (Hulme et al., 2008). The device directs the motion of swimming cells, resulting in a successive isolation of shorter cells within the population. Other studies emphasized the sorting of sperm microswimmers with microfluidics, where motile sperm is successfully separated from non-motile sperm through specific surface-modified microchannels (Huang et al., 2014). These approaches might be potentially used to sort fly-specific stages as well,

due to varying motile behaviors and cell lengths. Soft lithography systems are also available for connection with flow fields and chemical gradients. It was shown that sperm upstream navigation is facilitated by rheotaxis (Kantsler et al., 2014). Rheotaxis is a form of taxis influenced by currents, for example in fish which turn to face into oncoming current to hold their position. Considering that trypanosomes swimming against the continuously produced peritrophic matrix and peristalsis, rheotaxis experiments with trypanosomes are an obvious project of interest. The connection to a pump system would allow the analysis in controlled flow regimes and a direct comparison to *in vivo* observations. As mentioned in chapters 3.1.1.3 and 4.1.1, the use of fluorescent microspheres as 'non-motile' particles for direct comparison to motile trypanosome behavior would be prudent. In terms of the infection process, it is still not known how trypanosomes manage to navigate through the fly. Therefore simplified experiments with controllable flow fields might give insights into their long-range orientation capabilities. Concerning orientation capabilities, another possible approach is the insertion of chemical gradients in the devices. Chemotaxis is known to be a strategy for sperm cells to reach the egg efficiently, as it is the case for sea urchin sperm in moving water. Studies have shown the validity of microfluidic models for quantitative chemotaxis studies (e.g. Xie et al., 2010; Chang et al., 2013; Bhagwat et al., 2018).

Concerning trypanosome behavior in narrow channels, another approach besides soft lithography was tested. Glass microchannels with adjustable diameters in the micrometer range were applied for the analysis of trypanosomes motion (chapter 3.1.5.2). These narrow channels can mimic confined conditions, for example the tubular and thin salivary gland duct, which is especially narrow at its origin. Trypanosomes swimming through the confined tubes showed an increase of swimming speed. From a biological point of view, it is important for trypanosomes to reach their destinations soon to complete the life cycle with a limited time span, why an increased velocity under confined conditions seem useful for the parasites. The glass channels have the big advantage of a uniform round diameter, which makes them controllable in three-dimensional space. They represent a very reproducible system, in which the trypanosomes are easy to trace for measurements and calculations. However, a disadvantage that needs to be overcome is the low probability of single cells actually entering the thin tubes. Microstructures to assist entry of cells need to be designed for further experiments. This fact and the low

number of available devices did not allow a quantitative analysis, but we could show in this work as a proof of principle that this approach seems promising for further investigation.

In conclusion, the use of artificial and controllable microenvironments facilitates microswimmer research, even though it was not possible to establish the desired approaches for the trypanosome-tsetse system during this doctoral thesis. Due to individual mask designs and the possibility of implementing features like flow control or chemical gradients, soft lithography offers a broad spectrum of artificial manipulations of the surrounding. This enables the simulation of natural environmental constrains and therefore multifunctional experimental setups for biological and physical applications. Due to the complexity of a natural system, a relative reduction of single aspects - such as the influence of geometries - is necessary to understand to motile behavior of parasites inside their host or vector. A big advantage of the trypanosome-tsetse system is the availability of different microswimmer types that can be isolated from the fly and analyzed *in vitro*. This approach might also be interesting for other swimming parasites, such as the highly motile promastigote stage of *Leishmania*. Further investigation of the trypanosome-tsetse system is needed, as many interesting applications will elucidate detailed parasite motility behaviors that need to be compared to and validated in the *in vivo* system, as we have extensively introduced and demonstrated in this work.

4.2 Slender trypanosomes are able to infect the tsetse fly

Several essential processes during trypanosome development have been described over the past 100 years, however, some puzzling and contentious issues still remain (Krüger et al., 2018). Besides the two commonly-recognized forms occurring in the bloodstream, long brain forms and fat tissue-adapted trypanosomes have been described, as well as a renewed appreciation of the importance of the skin as reservoir in the mammalian host (Mogk et al., 2014 a and b, 2017; Caljon et al., 2016; Capewell et al., 2016; Trindade et al., 2016). The present study underlines these findings from other laboratories, showing that the trypanosome behavior in the vector is also far more complex than described until recently.

There are only a few laboratories working with tsetse flies and studies dealing with trypanosome infections directly in the fly are limited, because the handling of these delicate insects is not trivial. The first days of the parasite infection within the fly gut were largely neglected in previous publications, due to the fact that the differentiation process from the bloodstream stage to the procyclic midgut stage can be accomplished *in vitro*. Therefore, early events occurring in the fly have not been investigated in detail. In addition, a big problem in tsetse fly work is the fact that every laboratory uses different conditions for fly infections, which adds many variables: cell lines, trypanosome and fly strains, trypanosome developmental stages, fly sexes, fly age and the general composition of the infective meal (e.g. Vassella et al., 2000; Acosta-Serrano et al., 2001; Gibson and Bailey, 2003; Domenicali Pfister et al., 2006; Peacock et al., 2006; Sharma et al., 2008; Rotureau et al., 2011; Walshe et al., 2011; Weiss et al., 2013). The detailed analysis of these parasite-vector interactions allowed us to gain new insights into the biology of trypanosomes in their vector and propose a new developmental pathway that occurs during the infection process. The data from this thesis sheds a new light on the developmental competence of bloodstream stages and the infectivity for the tsetse fly vector.

4.2.1 Infection rate of bloodstream stages

We decided to use male and female flies for our experiments as well as bloodstream forms from a pleomorphic trypanosome strain, which possesses full developmental competence. These were used to design experiments that mimicked natural

conditions as close as possible, while still being under controllable laboratory conditions (Le Ray et al., 1977; Vassella and Boshart, 1996). Even though pleomorphic parasite strains more closely resemble those found in nature, many groups only work with monomorphic trypanosomes. This is most likely due to the fact that the handling of pleomorphic bloodstream trypanosomes is more difficult, as they cannot be cultured in normal HMI-9 trypanosome medium. These cells need to be cultured on agarose plates or, as is performed in our laboratory, in viscous medium supplemented with 1.1% methylcellulose (Vassella and Boshart, 1996; Vassella et al., 2001, Zimmermann et al., 2017). Due to their sensitivity to SIF (stumpy inducing factor), cell density must always be strictly monitored. In addition, these cells show an increased sensitivity to environmental changes and stress, such as temperature change or slight variations in media composition (laboratory observation). As an example, the direct transfer of cells from old to freshly prepared medium or a different batch of medium can result in growth defects and slower doubling times. A transfer was always performed stepwise by mixing the two media and allowed the parasites to adapt to the new conditions. For this reason, many groups only use the pleomorphic procyclic trypanosomes for fly infections, which can be cultured in normal SDM-79 medium and are easy to handle, while still others use the pleomorphic bloodstream forms directly from freshly thawed blood stabilates. In the latter case, exact cell numbers as well as the amount of slender, intermediate or stumpy trypanosomes are difficult to predict. A recent study from Rose and colleagues detailed significant differences in infection kinetics by using different cell types from the same cell line (Rose et al., 2019). Many laboratories also use only one tsetse fly gender to generate infection rates and numbers. However, this and other studies have proven that the infection properties of male and female flies are not equal (e.g. Maudlin et al., 1990; Walshe et al., 2011; Peacock et al., 2012 b).

During early infection, only a few parasites survive the attack by the fly´s immune system. The low number of surviving trypanosomes makes data generation challenging. Commonly used methods for cell population analysis such as fluorescence-activated cell sorting (FACS) are not feasible in this case. For this reason, we used fluorescent reporter cell lines and live cell microscopy in this study. Proteins of the PAD (proteins associated with differentiation) family were the first markers described as being specific for stumpy trypanosomes (Dean et al., 2009). Therefore, a PAD1 reporter cell line was used to clearly distinguish between slender

and stumpy trypanosomes. A sequence motif in the 3´UTR mediated the early increase of the PAD1 transcript abundance during differentiation to the stumpy form (MacGregor and Matthews, 2012). As a stumpy marker, PAD1 positive (PAD1+) cells should uniformly have a 1K1N configuration, while all 2K1N or 2K2N cells can be assigned as slender forms (Shapiro et al., 1984; Dean et al., 2009). However, Dean et al. also identified around 10% of PAD1+ 2K2N slender cells (but no 2K1N cells), which might represent intermediate cells that have committed to stumpy formation. This means that stumpy populations are 100% PAD1 positive, whereas slender cultures are not 100% PAD1 negative. Slender cultures always harbor a certain amount of stumpy cells or rather PAD1+ cells. For a long time it was unclear how these cells are formed, as at low parasite densities no SIF response should occur that triggers the stumpy formation. Recently, a density-independent pathway for stumpy formation was discovered, which is linked to antigenic variation (Batram et al., 2014; Zimmermann et al., 2017). This mechanism is solely controlled by the transcriptional status of the expression site coding for the parasite´s VSGs. The authors hypothesized that an unsuccessful VSG switch can result to a synchronous differentiation to the stumpy stage *in vitro*. They suggested that this alternative mechanism might answer the question of how trypanosomes ensure their transmission, even at low cell densities, when SIF is not able to accumulate to an effective concentration. In fact, based on mathematical simulations from previously published data, the existence of a cell density-independent mechanism, termed the background differentiation rate, has been suggested before (Savill and Seed, 2004). This is in accordance with the findings from this work, in that the amount of PAD1+ trypanosomes in a low-density slender population varied but on average between 1-5% were PAD1+ cells. These trypanosomes were termed background stumpy cells. They were, for the most part, morphologically stumpy (and only 1K1N or 2K2N), but some cells also showed characteristics of an intermediate form.

These facts were important for the dilution experiments in chapter 3.2.1, and therefore every cell population used was also checked for the exact amount of background PAD1+ trypanosomes. This information was further used to estimate the amount of ingested cells and cell types per blood meal (table 1). If we compare infections with 50 c/ml, 1 ingested stumpy cell on average (table 1 B) per blood meal resulted in 20.2% (22/109) midgut infections and 4.6% (5/109) salivary gland infections. In contrast, 1 ingested slender cell on average (table 1 E) per blood meal

resulted in 3.2% (6/186) midgut infections and 1.1% (2/186) salivary gland infection. Considering the 1% background stumpy rate from these cell cultures, this means that 0.01 stumpy cells were ingested on average per feeding, which means that only 1 in every 100 flies ingested a stumpy cell. On account of this, the salivary gland infection rates could be caused by the two hypothetical background stumpy cells that were ingested by the 186 flies. However, there is never a 100% of infection success rate. Due to this, it could not explain the midgut infections. It is important to keep in mind that in some tsetse-infested areas, less than 0.1% of wild flies are infected with trypanosomes (Aksoy et al., 2003; Brun et al., 2010; Kagbadouno et al., 2012). Even under laboratory conditions, tsetse flies are refractory to infection. If every ingested stumpy cell would be able to establish an infection, the infection rates for stumpy cells would be much higher, hypothetically 100%, but this is clearly not the case. Other infection experiments performed by Ines Subota showed that even with high cell concentrations, there is a peak of infectivity, which never reaches 100% effectiveness. Even the addition of glutathione (MacLeod et al., 2007), which boosts infection success, resulted in a maximum of 34% salivary gland infections (n = 469). For infections with 2 stumpy cells on average per blood meal for each fly (table 1 A), we reached 38.8% (45/116) midgut infections and only 11.2% (13/116) salivary gland infections. In addition, we used for our calculation 20 µl of ingested blood per blood meal for every fly (Gibson and Bailey, 2003). Male flies normally take up less blood than female flies however, and therefore less trypanosomes, even though male flies showed generally higher infection rates compared to females. In addition, younger flies take up less blood shortly after hatching, compared to flies that are a few days old (Walshe et al., 2011). It is important to note that we used the lectin inhibitor N-acetyl-D-glucosamine for our infections, which is broadly used in research on tsetse fly infections (Peacock et al., 2006). Further experiments without this supplement should be conducted, to keep the infection process as natural as possible. Interestingly, the TI (transmission index; Peacock et al., 2012 b) revealed that slender-derived trypanosomes perform better than stumpy parasites in the fly, even though stumpy parasites are more likely to establish an initial infection, which will be discussed later.

Taken together, the infection numbers strongly suggest an involvement of slender forms in infection and that one single trypanosome cell might be sufficient to colonize a tsetse fly. In fact, it was proposed before that a single *T. congolense* trypanosome

is sufficient to cause a tsetse fly infection (Maudlin and Welburn, 1989). For the experiments presented here, the probability that all positive flies are only caused by stumpy cells is rather unlikely but, of course, cannot be formally excluded with this dataset. That is why further experiments were conducted to answer the question if slender trypanosomes are able to survive in the fly gut, which are discussed in the following section.

4.2.2 Adaptions to the new environment

To verify the previously-mentioned observations, live cell microscopy was performed using fluorescent reporter cell lines that were directly visualized in infected fly tissue. The usage of PAD1 as a marker has allowed the precise correlation between PAD1 expression and differentiation capacity of stumpy trypanosomes (Dean et al., 2009; MacGregor et al., 2011; Trindade et al., 2016; Zimmermann et al., 2017; Silvester et al., 2018). Dean and colleagues, who identified PAD1 as a stumpy marker, mention that their results support the classical observations from Robertson in 1912, which suggest that the stumpy forms are the essential transmissible stage (Robertson, 1912). However, Robertson did not exclude the possibility that slender or intermediate cells are capable of causing infections, instead saying that it "... apparently does not occur". Another study, performed by Turner and colleagues, described that slender forms are killed more rapidly than stumpy forms in the tsetse midgut (Turner et al., 1988). They fed tsetse flies on infected mice and analyzed living trypanosomes as well as trypanosomes in air-dried gut smears. Interestingly, they also did not exclude the survival of some slender cells, they only stated that their result "... suggests that stumpy trypanosomes are primarily responsible for transformation to procyclics."

The *in vivo* experiments from the present work showed that the slender trypanosomes did not die in the tsetse midgut and were able to develop to the procyclic midgut stage (figure 22 and 23). The increasing GFP fluorescence in the cell nuclei over time provided indirect evidence for the presence of PAD1 mRNA. The number of PAD1+ cells slightly increased in all experiments after 2-4 hours compared to 0 hours. This does not necessarily mean an increase in PAD1+ cells, instead, the background stumpy cells may just have a better chance to survive compared to the slender cells, and thereby account for a larger fraction of the total. In all, the number

of cells found in the flies infected with stumpy trypanosomes (n = 1603) was slightly higher than for the slender infections (n = 1380), by analyzing 42 flies (21 ♂ and 21 ♀) for each slender and stumpy infection. However, this could be caused by the fact that during early infection stumpy trypanosomes are weak swimmers and were therefore easier to analyze, in contrast to fast swimming slender parasites, which sometimes 'escaped' before analysis of all parameters was complete. For slender infections, the results showed a strong increase of the PAD1+ cells after 15-17 hours with 64.5% (figure 22 B) and 75.7% (figure 23 C) in two different experiments using different cell lines. For that reason, additional infections were performed later, revealing the presence of 50.4% (figure 23 C) PAD1+ cells already after 8-10 hours. What is striking about these observations is the fact that most of the PAD1+ cells showed slender morphology and continued to divide (figure 22 A-C, figure 23 A and C). In contrast, the stumpy infections showed a slow re-entry to the cell cycle, with around 5% dividing cells after 15-17 hours, with a normal cell cycle profile only reached after 72-74 hours (figure 23 B and D). It is important to mention that the intensity of the PAD1 signal in stumpy cells was, on average, stronger compared to that of the slender cells. This can be explained by the fact that GFP is a very stable protein (Cubitt et al., 1995; Shaner et al., 2005) and stumpy cells have had time to translate PAD1 mRNA during stumpy development, in contrast to the slender cells, which only began to express PAD1 after they had been ingested by the tsetse fly. This direct comparison allows the conclusion that the colonization of the midgut in slender infections is not due to the background stumpy cells, as these cells showed a different infection profile and PAD1 signal intensity compared to the slender cells. However, the PAD1 marker used here does not directly report on PAD1 protein levels. For this reason, further experiments using anti-PAD1 antibodies would be beneficial to determine the presence of the PAD1 protein in stumpy and slender trypanosomes from the tsetse midgut.

The *in vitro* experiments showed a similar development (figure 25 C), as PAD1+ trypanosomes were observed to increase in slender cultures. Interestingly, the PAD1 signal increased much faster in the *in vitro* experiments compared to the *in vivo* experiments. Normally, *in vitro* differentiations of pleomorphic strains are performed using only stumpy trypanosomes, because they are the only stage believed to be developmentally competent for transforming to the procyclic stage. However, a report from 1991 had already noted that an *in vitro* differentiation of bloodstream

trypanosomes to procyclic cells does not require intermediate or stumpy forms (Bass and Wang, 1991). They were able to differentiate long slender forms from the pleomorphic *T. brucei* strain TREU667 directly to procyclic trypanosomes when incubated in Cunningham´s medium at 26 °C. It is also possible to differentiate monomorphic cells from the slender form directly to the procyclic stage, even though monomorphic cells have lost the ability to develop into the stumpy stage (Czichos et al., 1986). However, the resulting procyclic trypanosomes from monomorphic cultures do not establish stable cultures. Therefore, in the study of Bass and Wang it was not clear if the resulting procyclic trypanosomes are fully developmentally competent or were only 'procyclic-like' such as the procyclic cells generated from monomorphic cells. With the fly experiments in this work we could observe that they developed further after becoming procyclic and could complete the entire life cycle. Experiments performed by Ines Subota also showed that monomorphic cells are able to establish midgut infections. However, cell numbers in the gut were much lower compared to pleomorphic infections and they were not able to develop to the salivary glands.

From the morphological point of view, the observations in the current work also show that slender cells can differentiate directly to the procyclic form. Occasionally a transitional stage was observed, which possessed characteristic features of both slender and procyclic trypanosomes. To confirm the development of mature procyclic forms, an additional molecular marker was used. The replacement of VSGs on the procyclic cell surface by the procyclins GPEET and EP represents one of the hallmarks in differentiation, and therefore an EP1:YFP marker was used to transfect the GFP:PAD1$_{UTR}$ reporter cell line. Engstler and Boshart showed that after a cold shock *in vitro,* only stumpy trypanosomes were able to route procyclin quickly to the cell surface, whereas slender trypanosomes retained the protein intracellularly (Engstler and Boshart, 2004). The EP1 protein accumulated in the endosomal compartment but was not transported to the surface. They concluded that cell cycle arrest, or rather the stumpy form itself, is required to allow transit of the EP1 to the cell surface, meaning this process is developmentally regulated and not temperature-dependent. However, they used a temperature drop to 20 °C and cultivated trypanosomes on agar plates for 12 hours, conditions that differ from the experimental setup in this study (figure 23 and 25). The results from the present study showed that, *in vivo*, EP1 appears on the cell surface in around 9.8% of the slender cells after 24-26 hours and continued to increase to 19.1% after 48-50 hours

and 29.5% after 72-74 hours (figure 23 E). In contrast, stumpy cells already showed EP1 on the surface after 8-10 hours with 16.2%, continuously increasing to 75.6% after 72-74 hours (figure 23 F). This observation was not surprising, considering that the endocytosis rate of stumpy cells is much higher and they can quickly exchange the VSG with EP1. Indeed, an accumulation of EP1 signal close to the flagellar pocket was observed in a few slender trypanosomes, as described before (Engstler and Boshart, 2004). However, slender cells were able to route the EP1 procyclin to their surface, but with slower kinetics than the stumpy cells. It is important to keep in mind that the GPEET protein is predominantly present in early procyclic cells. As such, control experiments using a GPEET marker would be beneficial to further detail the procyclin diffusion on the cell surface during differentiation from bloodstream to procyclic forms *in vivo*. The observations from the *in vivo* experiments were also confirmed by the *in vitro* experiments, where slender cells started to express EP1 on the surface at 15-17 hours with 14.4%, reaching almost 100% after 72-74 hours (figure 25 E). Stumpy trypanosomes were 45% EP1 positive (EP1+) already after 2-4 hours with and reached almost 100% after 24-26 hours (figure 25 F), which is in accordance with other *in vitro* differentiations using pleomorphic trypanosomes (Engstler and Boshart, 2004; Dean et al., 2009). The work conducted for this thesis shows that EP expression in stumpy trypanosomes was initiated before release of the cell cycle arrest and therefore can be uncoupled from the commitment to the differentiation process, a fact that has been reported before (Engstler and Boshart, 2004). Dean and colleagues performed experiments with mixed populations of stumpy and slender trypanosomes and exposed both cell types to *cis*-aconitate, then checked for EP-procyclin expression. They confirmed a co-expression of both EP and PAD1 for 96% of the cells, therefore identifying stumpy trypanosomes as the cells competent for differentiation to the procyclic stage. They analyzed the cells only 6 hours after exposure to *cis*-aconitate, however. Data from this thesis showed that neither PAD1 nor EP was increased after 2-4 hours, signals were instead visible between 15-17 hours, which is why a closer look between these time points could be beneficial for further analysis.

Interestingly, a high cell density for slender and stumpy cells for the *in vitro* differentiation experiments was necessary to generate a reliable procyclic population. If cell density was too low, the cells differentiate into procyclics within the same time frame but did not continue to grow well (data not shown). It is a known fact that

procyclic trypanosomes prefer high cell densities or, rather do not tolerate low density, which is why (for example) conditioned medium is used for transfections to generate clonal populations. Conditioned medium is prepared from a mid-long phase procyclic culture, where cells are removed from the medium by filtration. The specific components inside the conditioned medium that promote the parasite growth are unknown. This phenomenon seems not to occur in the tsetse fly midgut, as even low cell numbers were able to establish infections, inviting speculation on potential chemical triggers inside the gut lumen that influence the division process.

Beside the internal parameters of the fly system, environmental triggers can also be easily mimicked. For example, a temperature drop can induce hypersensitivity of stumpy trypanosomes to *cis*-aconitate, making it possible to induce differentiation at low concentrations (Engstler and Boshart, 2004). In natural situations*, cis*-aconitate is present in the tsetse midgut at 15.9 µM (Hunt et al., 1994) and at ~130 µM in ingested blood (Jacobs and Lee, 1964), which is much lower than the concentrations used for *in vitro* differentiations. It is not known whether the drop in temperature is the specific reason for trypanosomes being able to differentiate *in vivo*, but it is likely, considering the naturally occurring variation of temperatures. Under natural conditions, trypanosomes would commonly be exposed to cooler temperatures. Specifically, when flies take a blood meal early in the morning or at the latest during the first night after ingestion (Engstler and Boshart, 2004). Although colonized laboratory flies are mainly held at a constant range of 25-27 °C, this parameter is easy to change in an experimental setup, which might be useful for further experiments dealing with the influence of temperature. Considering the natural situation, we decided to use mixed populations of flies with both genders and different ages. A study by Walshe and colleagues has shown that the post-eclosion age of the fly has considerable influence on the infection capabilities (Walshe et al., 2011). The susceptibility for an infection quickly decreases with increasing fly age. For our experiments, flies were infected a few hours after hatching until up to 3 days post-eclosion. This might be an important epidemiological factor and is possibly close to the natural situation, as it is not clear or predictable how soon after emergence flies have their first blood meal in the wild. For further analysis, however, infections with slender and stumpy trypanosomes with separate flies at different ages, for example <24 hours and 48 hours post-eclosion, might be of interest. This allows direct comparison and if the age of the fly favors or hinders an infection comparable

for slender and stumpy trypanosomes. In addition, experiments with older flies that already received blood meals, might be interesting, even though fly numbers probably need to be very high due to the low infection efficiency.

By using mixed populations of tsetse flies and pleomorphic trypanosomes, we were able to connect *in vitro* cell culture and the natural circumstances in the relevant vector. Even considering the fact that every fly represents a complex and unique microenvironment and cannot be as standardized as cell culture cultivation, this system is open for several manipulations. For example, the influence of temperature changes or varying infection time points after hatching, which can be correlated to natural conditions that occur in the wild, is worth further analysis. We used a pleomorphic trypanosome strain, which is accepted in the scientific field and frequently used for experiments. We cannot completely exclude adaptations of these parasites due to cell culture conditions however, even though cells show complete developmental competence. Trypanosomes cultivated from laboratory mice or even from corresponding fresh blood stabilates might also show different infection kinetics in tsetse flies compared to real infections, as rodents do not belong to the repertoire of natural hosts of *T. brucei* (Turner, 1990). Therefore, further investigation using fresh trypanosomes from animals in the field would be beneficial to address details during the infection process, but obtaining the data and analysis of these samples pose a considerable challenge.

4.2.3 Beneficial effects of the *T. brucei* slender form for transmissibility

In terms of infection kinetics and biological adaptation, it is beneficial for the parasites that both bloodstream stages are capable of infecting the tsetse fly vector. The development of stumpy parasites inside the host is triggered by high cell numbers, however, the chances for transmission generally seem to be low, considering the fact that parasitemia is not always high in infected individuals. Actually, the opposite case with low parasite numbers is much more prevalent. Chronic infections that persist over years with *T. b. gambiense* normally show low parasitemia and aparasitaemic, asymptomatic infections in humans shown almost no detectable parasite load (Capewell et al., 2016; Capewell et al., 2019). Against the long-standing belief that trypanosomiasis is always fatal, studies are being to suggest that trypanotolerance in

humans exists and that these individuals are able to tolerate at least *T. b. gambiense* parasites, while being serologically positive but microscopically negative for trypanosomes (Jamonneau et al., 2010; Jamonneau et al., 2012). The parasite load in African wildlife is also usually very low. Parasites and wild game had time to co-evolve over millions of years, and consequently these hosts developed a degree of tolerance and do usually not show typical symptoms of illness (Lambrecht, 1985). Nonetheless, wild animals as well as asymptomatic human individuals serve as important reservoirs for trypanosomes to ensure future transmission (Anderson et al., 2011; Auty et al., 2012; Jamonneau et al., 2012). There is however little evidence that the proportion of stumpy parasites in an infected individual dominates the likelihood of transmission. Aside from this, the fact that even under favorable laboratory conditions, e.g. using only teneral flies for infections, the numbers of infected flies with mature salivary gland infections are low. Even if a fly ingests trypanosomes with the blood meal, this does not automatically result in a successful infection. In addition, the survival of stumpy cells is limited to a few days, which seems to pose a risk for the parasites if they would only rely on these forms for transmission competence.

The stumpy development is important in order to regulate the cell density of *T. brucei* and ensure long-term survival of the host (Vassella et al., 1997). Infections with monomorphic trypanosomes, which have lost the ability to differentiate to stumpy cells, result in the quick death of susceptible animals due to the overwhelming parasite density reached within a short time (Turner, 1990; Magez et al., 2008). These cells still secrete SIF but are thought to be unable to respond to SIF anymore (Vassella et al., 1997). Interestingly, other trypanosome species (e.g. *T. congolense* and *T. vivax*) are not found to have a morphologically distinguishable stumpy bloodstream form (Vickerman, 1969; Rotureau and Van Den Abbeele, 2013; Bargul et al., 2016). However, early reports from *T. vivax* infections pointed to pleomorphism of cells in the bloodstream (Gardiner and Wilson, 1987) and a stationary cell population analogous to the *T. brucei* stumpy stage (Shapiro et al., 1984). There are no obvious morphological changes visible in *T. congolense*, but early work reported pleomorphism of bloodstream stages with trypanosomes varying in cell body length (Nantulya et al., 1978). Even without a morphological stumpy stage, it was shown for *T. congolense* that they are able to respond to high cell densities with an accumulation of a cell cycle-arrested stage (Silvester et al., 2017). Therefore, this

species also exhibits a proliferation control mechanism, when parasites reach a cell density of approximately 8×10^7 c/ml in mice. Some molecular markers have also been identified, suggesting a morphology-independent pathway for its further development in the tsetse fly (Silvester et al., 2018). Strikingly, *in vitro* experiments showed that conditioned medium generated from bloodstream *T. congolense* trypanosomes is able to promote growth arrest and activation of stumpy reporter gene expression in *T. brucei*. In contrast, *T. congolense* did not respond to conditioned medium generated from *T. brucei* cultures, which is why they seem unperturbed by the presence of *T. brucei* SIF in the medium. Co-infections with both species *in vivo* in mice also showed that the amount of PAD1+ cells was strongly increased in *T. brucei* trypanosomes (50% PAD1+) when mixed with *T. congolense*, compared to the control mono-infection with *T. brucei* only (<10% PAD1+). However, the cell density of *T. brucei* cells in mixed infections was lower compared to *T. brucei* infections alone. This generates a potential for evolutionary conflicts, considering the involvement of quorum-sensing mechanisms and the cross-talk between different species. Alongside these observations, it also needs to be taken into account that the probability of mixed infections between different trypanosome species is significant, considering the high frequency of trypanosome infections in animal reservoirs (Anderson et al., 2011). This makes the entire infection process even more complex, as various factors are involved in influencing the slender-stumpy ratio of *T. brucei* in the host. Regardless, direct evidence in livestock and wildlife is still limited or fragmentary.

Considering the development inside the vector, the data produced in the course of this thesis have shown that slender cells are able to survive and further develop in the tsetse fly. However, the efficiency and infection profiles from slender and stumpy cells revealed differences. Stumpy trypanosomes are considered to be the pre-adapted trypanosome stage with the ability to quickly respond to the environmental changes subjected to within the fly (e.g. Nolan et al., 2000; Engstler and Boshart, 2004; Dean et al., 2009; Rico et al., 2013; Matthews et al., 2015). The work presented here has also shown that stumpy parasites produce higher infection rates and differentiate faster to the procyclic stage, which is able to colonize the midgut (chapter 3.2.2). This is probably a huge advantage considering that the fly´s immune system is trying to eliminate the parasites immediately after ingestion. Stumpy parasites are more efficient at establishing an initial midgut infection

compared to slender parasites (chapter 3.2.1). Infections with a low number of stumpy trypanosomes resulted in higher infection rates as compared with the same amount of slender parasites. Surprisingly, the TI data showed that after successful infection of the midgut, slender parasites were actually more efficient in establishing a salivary gland infection than stumpy trypanosomes. This unexpected finding invites speculation. One major difference between infections with slender and stumpy parasites is the motile behavior of the parasites within the first days. Stumpy trypanosomes are weak swimmers until they develop to the procyclic midgut stage 1-2 days after ingestion. In contrast, slender trypanosomes are efficient swimmers and highly active right from the beginning of the infection process. How trypanosomes reach the ectoperitrophic space, however, is still controversial. A recent study from Rose and colleagues strongly suggests that trypanosomes might pass through the proventriculus within the first days of infection (Rose et al., 2019). The ectoperitrophic space is located between the peritrophic matrix and the gut epithelium and protects the parasites from the fly´s immune system, which allows them to colonize the gut and establish a permanent infection (Gibson and Bailey, 2003; Oberle et al., 2010). The authors suggest that trypanosomes pass via the newly secreted peritrophic matrix in the proventriculus, rather than directly crossing the mature matrix or circumnavigating via the posterior gut. Therefore, slender trypanosomes might potentially be able to colonize the proventriculus earlier than stumpy trypanosomes. Interestingly, an infection of the salivary glands is not possible during the whole infection process. There is a limited time span to proceed further in infection from the midgut and colonize the glands. Flies can be infected in the midgut for their whole life, but never develop a salivary gland infection. In addition, there is the so-called 'teneral phenomenon'. Teneral flies are easier to infect, probably because the peritrophic matrix is not fully mature, and thus facilitates crossing of the parasites (Walshe et al., 2011). Therefore, susceptibility for infection deceases with fly age and motility might give slender trypanosomes a time advantage. Another difference in infection with slender and stumpy parasites is the cell cycle status. Stumpy parasites are cell cycle-arrested and re-enter the cell cycle a few days after ingestion when differentiated to procyclic trypanosomes. In contrast, slender trypanosomes continue dividing and a single cell is able to produce a small population within a short time. Considering the fact that the number of ingested parasites is potentially low in nature and the fly´s immune system is trying to

eliminate the parasites, slender cells might increase their chances of infecting the fly by producing more parasites within the first critical days. This potentially results in more survivors that are able to colonize the fly more quickly after ingestion, even though slender cells develop to mature procyclic trypanosomes with a time-delay in comparison to stumpy cells.

The evolutionary development of stumpy forms in *T. brucei* is undoubtedly beneficial (Matthews et al., 2015), but their main task during infection is most likely cell density regulation in the host. Regulation of parasitemia via cell cycle arrest is known to occur in other trypanosome species, but without a morphologically distinguishable stumpy form. The proliferative forms are able to infect the fly and no additional pre-adapted stage is known in closely related species such as *T. congolense* and *T. vivax*. From an evolutionary point of view, the occurrence of cell cycle-arrested stumpy trypanosomes seems to be a comparably 'new' invention of *T. brucei* (Haag et al., 1998; Steverding, 2008). So, why should proliferative *T. brucei* slender cells not have or have lost the ability to infect the fly over time? This was probably previously overlooked due to the fact that cell cycle-arrested stumpy cells are pre-adapted, already expressing important proteins for differentiation such as PAD1 and PAD2 and are quickly able to express procyclic specific proteins on their surface. As slender parasites still need to switch on the PAD1 pathway before they are able to develop to the procyclic form, this gives stumpy trypanosomes an advantage for quick adaptation to the new environment. Taken together, there are many potential benefits for both bloodstream stages being infective, which favor the balancing act between survival and transmission.

4.2.4 A revised life cycle model for *T. brucei*

To summarize, we demonstrated in this work that pleomorphic slender bloodstream forms are able to passage through tsetse flies and that a single cell is sufficient to cause a mature infection. We performed numerous fly infections, predicting the amount of ingested cells as precisely as possible and were able to draw a detailed picture of early developmental events happening inside the tsetse fly vector. Interestingly, most of the published studies mentioned above are not in disagreement with the observations presented here. The present work also proves that stumpy cells are pre-adapted and are able to develop more quickly to the procyclic midgut stage

than slender cells, in both *in vivo* and *in vitro* experiments. As discussed before however, experimental designs vary in different laboratories and this can impede and complicate the direct comparison of datasets. We designed experiments to represent natural conditions and therefore analyzed trypanosomes directly in the relevant vector. A lack of tsetse fly colonies and the rare use of pleomorphic strains in other laboratories probably promoted the fact that the survival capabilities of slender cells were overlooked until now.

The beneficial purpose of the stumpy stage is without question, but they are not essential for tsetse transmission. Stumpy cells are adapted to the fly´s gut environment and can colonize it efficiently. However, slender cells are also able to develop to the midgut stage and cause mature infections. They express a reporter for PAD1 mRNA, which supports the importance of the PAD1 pathway and protein for the differentiation process. Thus far it was thought that expression of PAD1 was restricted to stumpy trypanosomes. The data obtained here suggest that the protein PAD1 is not as closely connected to the stumpy stage as previously thought, but is nonetheless essential for the survival and further development in the tsetse fly gut. Given that we did not check if the PAD1 protein was expressed however, we can at present only speculate on this point based on the reporter cell line. The use of delicate pleomorphic cells, fluorescent reporters and the establishment of a tsetse fly colony, allowed us to firmly establish the trypanosome-tsetse system and gain unexpected insights into the infection process and trypanosome biology in general.

As a result of this work, a revised life cycle for *T. brucei* is proposed, where slender and stumpy cells are both able to infect the tsetse fly (figure 27). This is in contrast to current opinion in the field but emphasizes once more the evolutionary success of these parasites. The balancing act between maintenance of an infection, the survival of the host, and the permanent transmissibility is challenging, especially in ensuring maximized long-term survival and parasite spread. Our findings add an important piece of knowledge regarding the transmission capabilities of the parasite and might help to solve the so-called transmission paradox, which has surrounded the disease for a long time (Capewell et al., 2019). Low levels of parasitemia, as are found in African wild game or humans with chronic *T. b. gambiense* infections, raise the question of how these parasites are able to ensure transmission success. Considering the findings presented in this thesis, that one ingested trypanosome -

slender or stumpy form - is able to establish a mature infection in the vector, the transmission paradox scenario becomes less problematic. Elucidating these findings further could solve puzzling questions on how African trypanosomes can infect and spread so successfully in a variety of different hosts. With this new perception we are able to shift perspectives in parasite biology and epidemiology.
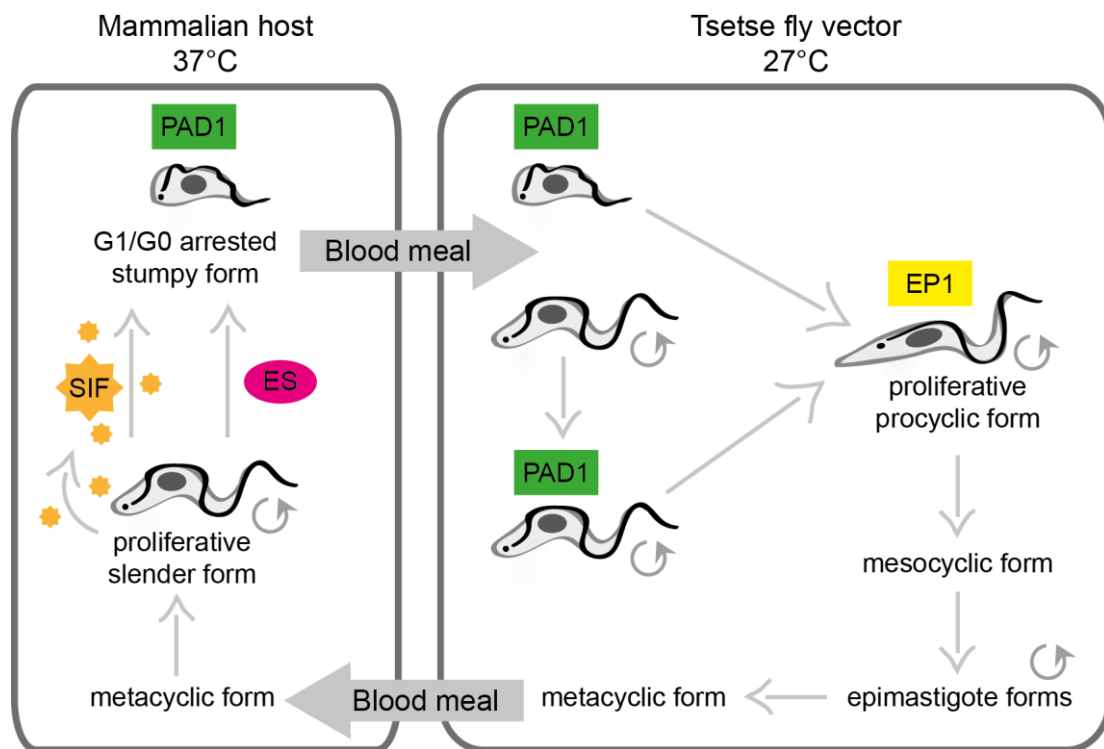

Figure 27: A revised life cycle for the parasite *T. brucei*. Circular arrows indicate proliferative forms. In the mammalian host, two main life cycle stages exist – the proliferative slender form and the G1/G0 arrested stumpy form. At least two different triggers are known to initiate stumpy development and the PAD1-pathway (PAD1), via the stumpy inducing factor (SIF) or expression site attenuation (ES). During a blood meal, the fly ingests both bloodstream forms. Stumpy trypanosomes are able to develop to the proliferative procyclic midgut stage, which expresses EP1 on the cell surface. Data from this work show that proliferative slender trypanosomes are also infective to the tsetse fly. They are able to initiate the PAD1 pathway without undergoing cell cycle arrest and directly differentiate to the procyclic stage. This work reveals that both bloodstream stages are infective for the tsetse fly and that a single parasite, either slender or stumpy, is able to establish a mature infection up to the transmissible metacyclic stage.

5 Materials and Methods

5.1 Materials

5.1.1 Buffers and solutions

DNA analyses

1x Tris-acetate-EDTA (TAE) buffer
40 mM Tris, 40 mM acetic acid, 1 mM EDTA (pH 8.0)

***E. coli* cultivation**

Agar plates
1.5% agar in LB-medium, 100 µg/ml ampicillin

LB-medium (for 1 l)
10 g Bacto-Tryptone, 5 g yeast extract, 10 g NaCl, pH 7.4 (autoclaved)

Microscopy analyses

1x Phosphate buffered saline (PBS)
10 mM Na_2HPO_4, 1.7 mM KH_2PO_4, 137 mM NaCl, 2.7 mM KCl, pH 7.4

8% (w/v) formaldehyde (FA)
8 g paraformaldehyde (PFA), 100 ml 0.1 M HEPES (pH 7.2)

Clearing solution (BABB)
1:2 (v/v) benzyl alcohol:benzyl benzoate

***Trypanosoma brucei* cultivation**

DTM medium (for 1 l)
One liter medium contains 6.8 g NaCl, 0.4 g KCl, 0.2 g $CaCl_2$, 0.14 g NaH_2PO_4, 0.2 g $MgSO_4$, 7.94 g HEPES, 2.2 g $NaHCO_3$, 1 ml phenol red (10 mg/ml), 20 ml MEM amino acids solution 50x (ref.no. 11130036), 10 ml MEM non-essential amino acids solution 100x (ref.no. 11140035), 1.63 g L-glutamine, 0.293 g L-glutamic acid hydrochloride, 730 µl glycerol, 10 ml MEM vitamin solution 100x (ref.no. 11120037), 14 µl *β*-mercaptoethanol, 114 mg Na-pyruvate, 14 mg hypoxanthine, 28.2 mg

bathocuproin, 7.5 mg hemin, 640 mg proline and 182 mg cysteine. The medium was prepared using ddH$_2$O and adjusted to pH 7.5. Afterwards, 150 ml heat-inactivated (1 hour, 56 °C) fetal calf serum (FCS) (Sigma-Aldrich, USA) was added, the medium filter sterilized and stored at -20 °C.

Hemin solution

2.5 mg/ml hemin (Serva, DE), 0.05 N NaOH, stored at -20 °C

HMI-9 medium (1x for 1 l or 1.6x for 0.625 l)

The medium consists of 17.6 g "Hirumi's modified Iscove's medium 9" powder (IMDM, pH 7.5), 3 g sodium bicarbonate, 136 mg hypoxanthine, 28.2 mg bathocuproine sulfonate, 14.3 µl *β*-mercaptoethanol, 39 mg thymidine, 100,000 U penicillin, 100 mg streptomycin, 182 mg L-cysteine and 10% (v/v) FCS (Sigma-Aldrich, USA), which was heat-inactivated for 1 hour at 56 °C before use. The medium was prepared using ddH$_2$O and adjusted to pH 7.5, filter sterilized and stored at -20 °C.

MC-HMI-9 medium (1.6x HMI-9 medium containing 1.1% methylcellulose)

11 g methylcellulose (Cat. No. 94378-500G; Sigma-Aldrich, USA) and 366 ml ddH$_2$O were directly mixed before being autoclaved in a 1 l bottle containing a large magnetic stir bar (minimum 8 mm). Afterwards, it was stirred gently for at least 24 hours at 4 °C until it became transparent. Right before usage, a bottle of 1.6x HMI-9 medium was thawed, poured into the methylcellulose and stirred for 24 hours at room temperature (400 rpm). The medium was then stored at 4 °C under constant stirring and used for one month maximum. For cell culture, small volumes of medium were stored in 100 ml bottles directly in the incubator at 37 °C with the lid slightly untwisted.

SDM-79 medium (for 1 l)

The medium stock consists of SDM 79-CGGGPPTA powder (powder for 1 l in 800 ml H$_2$O; ordered via a trypanosome consortium), 2 g NaHCO$_3$, 1.8 g dextrose, 513.4 mg L-proline, 100 mg sodium pyruvate, 406.8 mg L-threonine, 10.5 mg L-glutamic acid, 50 mg glucosamine HCl and the pH was adjusted to 7.3 with 10 M NaOH (filling up to 900 ml). The medium was filter sterilized and stored at 4 °C. Right before use, 100 ml

of heat inactivated (1 hour, 56 °C) FCS (Sigma-Aldrich, USA) and 3 ml hemin (Serva, DE) were added.

SDM-G medium (for 1 l)
The SDM-79 medium was additionally complemented with 1,224 ml 50% glycerol (in ddH$_2$O, filter sterilized).

Trypanosome dilution buffer (TDB)
20 mM Na$_2$HPO$_4$, 2 mM NaH$_2$PO$_4$ (pH 7.7), 20 mM glucose, 5 mM KCl, 80 mM NaCl, 1 mM MgSO$_4$, pH 7.6 (filter sterilized)

2x freezing mix for BSF
80% (v/v) HMI-9, 20% (v/v) glycerol (filter sterilized)

2x freezing mix for PCF
80% (v/v) SDM-G, 20% (v/v) glycerol (filter sterilized)

5.1.2 Equipment and devices

Cell culture

Airstream Class II BSC	Esco global, Hoyland (UK)
Amaxa Nucleofector II	Lonza, Basel (CH)
Bottle top filter unit	Roth, Karlsruhe (DE)
CO$_2$ Incubators	Binder, Tuttlingen (DE)
Neubauer chamber	Marienfeld, Lauda-Königshofen (DE)

Centrifuges, shakers and stirrer

Centrifuge Spectrafuge^{TM} Mini	Labnet International Inc., Edison (USA)
Centrifuge Z 216 MK	Hermle Labortechnik GmbH, Wehingen (DE)
Centrifuge Z 383 K	Hermle Labortechnik GmbH, Wehingen (DE)
Magnetic stirrer RSM-02HP	Phoenix Instrument, Garbsen (DE)
Shaker Ceromat R	B. Braun Biotech International, Melsungen (DE)

Chemicals

The chemicals used for this work were obtained from Carl Roth (Karlsruhe, DE), AppliChem (Darmstadt, DE) or Sigma-Aldrich (St. Louis, USA) if not otherwise stated in the text.

Consumables

24-well tissue culture plates	Sarstedt, Nümbrecht (DE)
Circular (MN 615 Ø 50 mm) and pleated filters (MN 615 ¼ Ø 185 mm)	Macherey-Nagel, Düren (DE)
Coverslips, Menzel-Gläser	Thermo Fisher Scientific, Waltham (USA)
Cryo tubes	Sarstedt, Nümbrecht (DE)
Eppendorf tubes	A. Hartenstein, Würzburg (DE)
Falcon tubes	Sarstedt, Nümbrecht (DE)
Glass Pasteur pipettes	Sarstedt, Nümbrecht (DE)
Heparin tubes, sodium heparin 170 I.U.	BD Vacutainer, Plymouth (UK)
Lens paper	Karl Hecht GmbH, Sondheim (DE)
Microtubes orig. Eppendorf	A. Hartenstein, Würzburg (DE)
Object slides, Menzel-Gläser	Thermo Fisher Scientific, Waltham (USA)
Pasteur pipettes, without cotton stopper	Carl Roth GmbH+Co. KG, Karlsruhe (DE)
Plastic petri dish	Sarstedt, Nümbrecht (DE)
Serological pipettes	Sarstedt, Nümbrecht (DE)
Soft-Ject single-use syringe, 3 ml	Henke Sass Wolf, Tuttlingen (DE)
Sterile syringe filter, 0.2 µm cellulose acetate membrane	VWR International, Radnor (USA)
Test tubes	A. Hartenstein, Würzburg (DE)
Type F Immersion liquid	Leica Microsystems, Wetzlar (DE)
Vented cell culture flasks	Greiner Bio-One, Frickenhausen (DE)
Welted glasses with snap-on lid, 5 ml	A. Hartenstein, Würzburg (DE)

DNA analyses

6x Loading Dye	Thermo Fisher Scientific, Waltham (DE)
Gel chamber Cti	Bio-Rad Laboratories Inc., Hercules (USA)
GEL iX Imager	Intas Science Imaging Instruments, Göttingen (DE)
GeneRuler™ DNA Ladder mix	Thermo Fisher Scientific, Waltham (DE)
Power-Pac™ Basic	Bio-Rad Laboratories Inc., Hercules (USA)
Tecan Infinite M200 NanoQuat	Tecan Group, Männerdorf (CH)

Enzymes and enzyme buffers

All enzymes and corresponding buffers used for this work were obtained from Thermo Fisher Scientific (Waltham, USA).

Fly maintenance and work

Bovine blood, heparinized with 170 I.U., sterile	Different veterinarians, freshly taken from slaughtering
Breeding net	Slovak University of Technology, Bratislava (SK)
Feeding membrane	Slovak University of Technology, Bratislava (SK)
Feeding plates (210x154x20 mm and 580x210x20 mm)	Carl Roth GmbH+Co. KG, Karlsruhe (DE)
Glass petri dish	A. Hartenstein, Würzburg (DE)
Heating plate	VWR International, Nynashamn (SE)
Pupae sieve, self-made	Central workshop Biocenter, Würzburg (DE)
Roubaud cages, self-made	Central workshop Biocenter, Würzburg (DE)
Sheep blood, defibrinated, sterile	Acila, Mörfelden-Walldorf (DE)
Trays for breeding, self-made	Central workshop Biocenter, Würzburg (DE)
Tweezers, Dumont #3C	Dumont, Montignez (CH)

Microscopes, cameras and equipment

Biomed	Leitz, Wetzlar (DE)
Canon EOS 80D	Canon, Tokyo (JP)
Canon EFS 18-135 mm	Canon, Tokyo (JP)
DMI6000B wide-field	Leica Microsystems, Mannheim (DE)
Eclipse TS100	Nikon, Tokyo (JP)
iMIC	FEI-TILL Photonics, Gräfelfing (DE)
Intensilight C-HGFI	Nikon, Tokyo (JP)
Leica DFC 365 FX	Leica, Wetzlar (DE)
Leica MZ16FA	Leica Microsystems Ltd, Heerbrugg (CH)
Light sheet fluorescence microscope, custom built	Department of Medicine II and Interdisciplinary Center for Clinical Research, University Hospital Würzburg (DE)
Light sheet fluorescence microscope	LaVision BioTec, Bielefeld (DE)
Olympus CX41	Olympus Corporation, Tokyo (JP)
pco.camera, type pco.1600	PCO, Kelheim (DE)
sCMOS pco.edge	PCO, Kelheim (DE)
Wild M3Z	Wild Heerbrugg, Gais (CH)
Wilovert, inverted	Helmut Hund GmbH, Wetzlar (DE)

Kits

Amaxa Basic Parasite Nucleofector Kit 1   Lonza, Basel (CH)

NucleoSpin Plasmid Kit   Macherey-Nagel, Düren (DE)

5.1.3 Fluorescent probes and dyes

Table 3: Fluorescent dyes and probes used in this work. The names of the fluorescent dye/probe, the supplier, the target and the fluorescent color are indicated.

Fluorescent dyes and probes	Supplier	Labeled target and color
Atto 488 NHS-Ester, dye	Atto-tec GmbH, Siegen (DE)	cell surface, green
DAPI, dye	AppliChem, Darmstadt (DE)	DNA, blue
FluoSpheres carboxylated, 2 µm, 2% solids, probe	Life Technologies, Oregon (USA)	yellow-green
Propidium iodide, dye	Sigma-Aldrich, St. Louis (USA)	DNA, red
AMCA-sulfo-NHS, dye	Thermo Fisher Scientific, Waltham (DE)	cell surface, blue
WGA labeled with rhodamine, dye	Vector Laboratories, Burlingame (CA)	peritrophic matrix, red

5.1.4 Organisms

Bacterial strain

Escherichia coli (E. coli) Top 10

Genotype: F-mcrA Δ(mrr-hsdRMS-mcrBC) Φ80lacZΔM15 ΔlacX74 recA1 araD139 Δ(araleu)7697galU galK rpsL(StrR) endA1 nupG

Competent bacteria were generated using the method of Chung and colleagues (Chung et al., 1989).

Trypanosomes

Wild type strain

For this work, all developmental stages of the pleomorphic parasites *Trypanosoma brucei brucei*, strain EATRO 1125 (serodome AnTat1.1) were used (Le Ray et al., 1977).

Transgenic cell lines

Table 4: Cell lines used during this work. All used cell lines based on the pleomorphic *Trypanosoma brucei brucei*, strain EATRO 1125 (serodome AnTat1.1). Represented are the names of the cell lines, the parental trypanosome cell line, construct, the selection and the origin of the cell line. All cell lines were generated in our laboratory and cultured as BSF (bloodstream form) or PCF (procyclic form).

Name	Parental cell line	Construct	Selection	Origin
GFP:PAD1$_{UTR}$	Antat1.1	p4231 PAD1:NLS (p4231 Sunter and Carrington, unpublished)	Blas	Ines Subota
GFP:PAD1$_{UTR}$ + EP1:YFP	Antat1.1 GFP:PAD1$_{UTR}$	pGaprone(ble)_EPGFG_rev GPY PARPYFP (Markus Engstler)	Blas, Phleo	Sarah Schuster, this work
mNG	Antat1.1	pTSARib(puro)_ mNeonGreen	Puro	Christian Reuter
NLS	Antat1.1	pHD67E NLS:GFP (pHD67E Bingle et al., 2001 + NLS:GFP from p4231 Sunter and Carrington, unpublished)	Hygro	Sarah Schuster, Master thesis 2014
PFR	Antat1.1	pPC PFR nt EGFP PFRAtag Adhiambo et al., 2009	Puro	Sarah Schuster, Master thesis 2014
PFR+NLS	Antat1.1 PFR	pHD67E NLS:GFP	Hygro, Puro	Sarah Schuster, Master thesis 2014
tdT	Antat1.1 GFP:PAD1$_{UTR}$	pTSARib(bla)_ tdTomato	Blas, Puro	Julia Weingart, Bachelor thesis 2018

Transgenic cell lines were selected with the following antibiotics.

Antibiotic	Abbreviation	Manufacturer	Selection in µg/ml	
			BSF	PCF
Blasticidin	Blas	Invivogen, San Diego (USA)	5	10
Hygromycin	Hygro	AppliChem, Darmstadt (DE)	5	25
Phleomycin	Phleo	Invivogen, San Diego (USA)	2.5	2.5
Puromycin	Puro	AppliChem, Darmstadt (DE)	1	1

Tsetse flies

For this work *Glossina morsitans morsitans* were used. At the beginning of this work, fly pupae were received from the laboratory of Philippe Bastin and Brice Rotureau in Paris (FR), Pasteur Institute. Flies were further bred in our laboratory and a stable tsetse fly colony was established during this doctoral thesis.

5.1.5 Soft lithography

Equipment

Air gun	BlackHole Lab, Paris (FR)
Biopsy punch with plunger, 1 mm	BlackHole Lab, Paris (FR)
Glass stab	BlackHole Lab, Paris (FR)
Hot plate	BlackHole Lab, Paris (FR)
Oven, STZ 5.4	Flac Instruments, Treviglio (IT)
Plasma cleaner, PDC-002-CE	Harrick Plasma, Ithaca (USA)
Razor blade	BlackHole Lab, Paris (FR)
Sonicator Elmasonic P30H	Elma, Singen (DE)
Spin coater, Model WS-650Mz-23NPPB	Laurell Technologies, North Wales (USA)
UV Kub 2	Kloé, Montpellier (FR)
Vacuum desiccator	Kartell Labware, Noviglio (IT)

Consumables

Hellmanex solution	Hellma Analytics, Müllheim (DE)
Petri dishes	BlackHole Lab, Paris (FR)
Plastic cubs	BlackHole Lab, Paris (FR)
Plastic tubes	BlackHole Lab, Paris (FR)
Silicon elastomer curing agent, Sylgard 184	Dow Corning, Midland (USA)
Silicon elastomer, Sylgard 184	Dow Corning, Midland (USA)
SU-8 developer	MicroChem, Newton (USA)
SU-8 negative resist	MicroChem, Newton (USA)
Terumo syringe with needle (0.50x16 mm), 1 ml	Terumo Europe N.V., Leuven (BE)
Wafer	University Wafer Inc., Boston (USA)

5.1.6 Software

Adobe Illustrator Creative Suite 6	Adobe Systems Incorporated, San Jose (USA)
Amira	Thermo Fischer Scientific, Waltham (USA)
Andor iQ Software	Andor Technology Ltd, Belfast (UK)
AutoCAD	Autodesk, San Rafael (USA)
CLC Main Workbench 6	CLC bio-Qiagen, Aarhus (DK)
GraphPad Prism	GraphPad Software, La Jolla (USA)
Huygens Essential	Scientific Volume Imaging B.V., Hilversum (NL)
iControl	Tecan, Männedorf (CH)
ImageJ, Fiji	National Institute of Health, Bethesda (USA)

Imaris	Bitplane, Zurich (CH)
INTAS Gel Capture Software	INTAS, Göttingen (DE)
Keynote	Apple, Cupertino (USA)
LA Aquisition	FEI-TILL Photonics, Gräfelfing (DE)
Leica Application suite AF	Leica, Wetzlar (DE)
Microsoft Office	Microsoft, Redmon (USA)
pco.CamWare	PCO, Kehlheim (DE)
WISE Database Viewer	WISE Software Solutions, Newberg (USA)
XMedia Recode	Sebastian Dörfler, https://www.xmedia-recode.de/ (DE)
Zotero	Corporation for Digital Scholarship, Vienna (USA)

5.2 Methods

5.2.1 Working with trypanosomes

Cultivation of pleomorphic BSF trypanosomes

The cultivation of pleomorphic BSF trypanosomes was performed in viscous HMI-9 medium (Hirumi and Hirumi, 1989), supplemented with 10% (v/v) fetal bovine serum and 1.1% (w/v) methylcellulose (Sigma 94378), referred to as MC-HMI-9 medium (Vassella et al., 2001). Cells were kept in vented cell culture flasks at 37 °C and 5% CO_2 in a cell culture incubator. Generally, working with pleomorphic BSF cells demands for quick handling and avoidance of temperature drops. Cells were counted frequently using a Neubauer chamber. For normal cultivation, cell density was held strictly below $5x10^5$ cells/ml to avoid the *in vitro* differentiation to the stumpy stage (McCulloch et al., 2004). Cultures were diluted to the appropriate number with pre-warmed MC-HMI-9 and suitable antibiotics.

For harvesting cells from cell culture the methylcellulose had to be removed. The culture was diluted 1:4 with pre-warmed TDB (37 °C) and filtered using two different approaches, depending on the volume. For 10 ml of cell culture a sterile, TDB pre-wetted pleated filter (MN 615 ¼ Ø 185 mm, Macherey-Nagel, DE) was used and the filtrate collected in a falcon tube. Volumes larger than 10 ml of culture were filtered with a sterile bottle top filter unit (Carl Roth, DE), containing a circular filter (MN 615 Ø 50 mm, Macherey-Nagel, DE). After filtration, cells were centrifuged 1,400x *g* for 15 minutes at 37 °C in falcon tubes and the supernatant discarded. For

larger volumes, pellets of all falcon tubes were combined. During filtration around one third of the cells were lost.

Cultivation of pleomorphic PCF trypanosomes

The cultivation of pleomorphic PCF trypanosomes was performed in SDM-79 medium (Brun and Schönenberger, 1979), supplemented with 10% (v/v) fetal bovine serum (Hirumi and Hirumi, 1989) and 0.06% (v/v) glycerol (Vassella et al., 2000), referred to as SDM-G medium. The glycerol prevents the differentiation from early to late procyclic forms. Cells were kept in vented cell culture flasks at 27 °C with 5% CO_2 in a cell culture incubator. Cells were counted frequently using a Neubauer chamber. For normal cultivation cell density was preferentially kept between $5x10^5$ and $1x10^7$ cells/ml, but exceptions were possible. Cultures were diluted to appropriate cell densities with room temperature SDM-G and suitable antibiotics.

For harvesting, cells were washed in TDB and centrifuged for 1,400x g for 10 minutes at room temperature in falcon tubes.

Generating and thawing of cryo-stabilates

Generation of cryo-stabilates used the same procedure for BSF and PCF trypanosomes. A stabilate of BSF contained ideally $5x10^6$ cells/ml and for PCF trypanosomes ideally $8x10^7$ cells/ml. Cells were harvested and resuspended in an appropriate volume of corresponding ice-cold cell culture medium (500 µl for each stabilate). The same volume of ice-cold 2x freezing mix (20% glycerol, 80% medium) was added to each tube, resulting in 1 ml per tube with a final glycerol concentration of 10% glycerol. Cryo-stabilates were placed on ice and quickly transferred to -80 °C. For long-term storage, the stabilates were transferred to -150 °C after at least 24 hours.

Thawing of cryo-stabilates uses the same procedure for BSF and PCF trypanosomes. A stabilate was quickly thawed in a 37 °C water bath and cells were transferred immediately to 10 ml of pre-cooled medium and centrifuged (1,400x g, 10 minutes, 4 °C). The pellet was resuspended in pre-warmed 500 µl of SDM-G or HMI-9 medium and cells were transferred into cell culture bottles containing SDM-G or MC-HMI-9 medium. One hour after thawing, the cell concentration was

determined, the culture diluted to an appropriate cell density and required antibiotics were added.

Generation of transgenic trypanosome cell lines

To generate transgenic parasites the Amaxa Nucleofector II (Lonza, CH) and the Amaxa Basic Parasite Nucleofector Kit 1 (Lonza, CH) were used. Cooling of cells was strictly avoided for the whole procedure. For one transfection of pleomorphic BSF trypanosomes $5x10^7$ cells were harvested at 37 °C (procedure described above). Trypanosomes were resuspended in 100 µl of Basic Parasite Solution 1 and mixed with 10 µg of linearized DNA (dissolved in 10 µl sterile H_2O). The mixture was quickly transferred into an electroporation cuvette and transfections were done by electroporation using the program X-001 of the AMAXA Nucleofector II (Lonza, CH). Immediately afterwards, cells were transferred to 5 ml pre-warmed HMI-9 and added to 35 ml of MC-HMI-9 medium containing parental antibiotics and gently mixed (pool). Cells were diluted (1:5 and 1:10) and dilutions as well as the undiluted culture were transferred to 24-well plates, each well with a volume of 1 ml. All remaining cells were transferred into cell culture flasks. After 6 hours (approximately one cell cycle) 1 volume of medium containing 1x parental selection and 2x new selection were added to each well and to the flasks. Parasites were detected 4-7 days after the transfection by screening every well on a Neubauer chamber for the presence of trypanosomes. The methylcellulose impeded the visualization of trypanosomes and direct screening of wells was not sufficient with these low cell numbers. Every growing population (clone) was transferred into a flask and treated in cell culture as described for the pleomorphic BSF.

Differentiation of slender parasites to the stumpy stage

For the differentiation of slender to stumpy parasites, cells from a culture with a starting population density of $5x10^5$ c/ml were incubated without dilution. The accumulation of the stumpy inducing factor SIF in the medium triggers the differentiation to stumpy cells after 48 hours. The specific morphology was verified by eye to confirm stumpy development before each experiment.

Differentiation of BSF to the procyclic stage

For the differentiation to procyclic forms, both slender and stumpy trypanosomes were used. Cells were harvested as described above at room temperature and the pellet resuspended in 500 µl of DTM medium (Overath et al., 1986). Cells were counted with a Neubauer chamber. Additional DTM medium was added to reach a cell density of at least $2x10^6$ cells/ml. To trigger the differentiation to procyclic forms, either *cis*-aconitate was added to a final concentration of 6 mM or *cis*-aconitate and citrate were added at 3 mM each (Brun and Schönenberger, 1981; Overath et al., 1986) and cells were transferred from 37 °C to 27 °C (cold shock). If the volume was below 5 ml, the cell flasks were placed upright. As soon as cells reached $2x10^7$ cells/ml for the first time they were diluted with SDM-G medium. Freshly differentiated trypanosomes were kept at high densities between $3x10^6$ and $2x10^7$ cells/ml for the first few days.

5.2.2 Working with tsetse flies

Establishment and maintenance of a tsetse fly colony

General

One aim of this doctoral thesis was to establish a stable tsetse fly colony in our laboratory together with Ines Subota. Initially, pupae of *Glossina morsitans morsitans* were received from the laboratory of Philippe Bastin and Brice Rotureau in Paris (FR) at the Pasteur Institute. The following describes the protocols that were established to maintain the colony and perform quality management. Datasheets were designed to document the daily work with the flies, including separation for breeding, pupae and infections sheets. All corresponding documents, protocols and Excel files are stored on servers at the Department of Cell and Developmental Biology, University of Würzburg.

Maintenance and cleaning

Tsetse flies were kept in an insectary at 27 °C with a relative humidity of 70% and a day/night rhythm of 12 hours each. Flies were maintained in self-made Roubaud cages with a maximum of 40 flies per cage for breeding, with a female/male ratio of 3:1. Six cages were placed per tray, with flies sorted by age. Generally, flies were caught and transferred between cages using a test tube. In case of euthanizing

animals, a drop of chloroform was added to the test tube. All dead flies were autoclaved and discarded.

A cleaning schedule was used to ensure cleanliness of the insectary and health of the flies. Nets and trays were changed and cleaned once a week.

Feeding

At the beginning of this work, flies for breeding were fed three times a week through a silicon membrane (Moloo, 1971) with heparinized cow blood (received from different veterinarians, freshly taken from slaughtering). Later on, we switched to defibrinated sterile sheep blood (Acila, DE). Sheep blood was received every two weeks, aliquoted under sterile conditions, and stored at 4 °C until use. Blood was only fed to the flies within the first 21 days after it had been taken from the animal. For feeding, a thin layer of blood was spread on a feeding plate, covered by a silicon feeding membrane and warmed to 37 °C on a heating plate. Cages were placed on the membrane and flies were allowed to feed for at least 10 minutes.

Pupae

Fly pupae were collected each morning on working days (peak larviposition occurs in the afternoon) and collected in a glass petri dish for each calendar week. Pupae that appeared not to be correctly or fully developed (e.g. mutants or abortions) were discarded and the number of such pupae was monitored in the quality management. Fly larvae that were not yet pupated were left alone until the next day. Due to the sensitivity of pupae during the first days of development, collected pupae from each calendar week were left alone for one week. In the second week, pupae were sorted by size via self-made pupae sieves and categorized as following: category E (3.2 mm), D (2.8 mm), C (2.5 mm), B (2.2 mm) and A (< 2.2 mm). Depending on the number of flies needed for experiments and breeding, the corresponding number of pupae was transferred into cages, preferentially the largest ones. Usually, category B and A were discarded. The size distribution of the pupae is a valid marker for the health of the colony and was also monitored in an Excel file for quality management purposes.

Breeding

The pupae hatch three weeks after pupation. The condition in which they emerge (e.g. normal, too small, crippled wings), emergence rate, as well the male/female ratio at hatching was noted and recorded in the quality management Excel file. All pupae that had not hatched were autoclaved and discarded.

Newly-hatched flies were isolated from the pupae on each working day and sorted into different cages by sex. This was done manually on the basis of visual abdominal characteristics (figure 28 A and B). Flies were fed once before male and female flies were placed together into breeding cages with a female/male ratio of 3:1. The initial separation of male and female flies ensures the complete development of sexual organs as well as a sufficient supply with energy before breeding. During the time male flies mated with the females, they were not able to receive a blood meal.

Infection and maintenance of infected flies

Flies were infected with trypanosomes no longer than 72 hours post-eclosion (ideally <48 hours) by feeding for at least 10 minutes (Walshe et al., 2011). For every infection, 60 mM N-acetyl-D-glucosamine was added (Peacock et al., 2006). After infection flies were fed 2-3 times a week as described above. A maximum of 50 infected flies were placed in one cage.

During this work, different conditions for infection were tested. Depending on the experiment and the cell line, flies were either infected with procyclic, slender, or stumpy cells. Infections were performed in antibiotic-free medium, TDB or blood.

Infections with procyclic cells were performed using antibiotic-free SDM-G medium. To generate infections resulting in a high number of salivary gland infections, stumpy parasites were harvested (as described above), transferred to blood and additionally 12.5 mM glutathione was added (MacLeod et al., 2007).

In contrast, if the aim of the experiment was to visualize parasites immediately after infection in the tsetse midgut, slender or stumpy cells were harvested (as described above), transferred to TDB, and concentrated to $6x10^5$ cells/ml.

For dilution experiments with low cell numbers, cell density of either stumpy or slender trypanosomes was calculated and the dilutions made in blood. Due to the viscosity of the medium, pipetting of small amounts could be inaccurate. Therefore, cells were diluted 1:100 in pre-warmed TDB and counted again, and the corresponding volume was added to the pre-warmed blood.

For some experiments, tsetse flies were fed 40 µg/ml wheat germ agglutinin (WGA) or 0.013% solid microspheres in SDM-G medium or TDB heated to 37 °C.

Test for salivary gland infection

To test whether the flies developed a salivary gland infection, a non-invasive method was used. After 5 weeks of infection, single flies were isolated into a cage and placed onto a glass objective slide. The slide itself was on a heating plate at 37 °C. This increase in temperature triggers the fly to 'bite' on the slide and to leave saliva that can be analyzed using a microscope. The presence of metacyclic trypanosomes confirms a salivary gland infection.
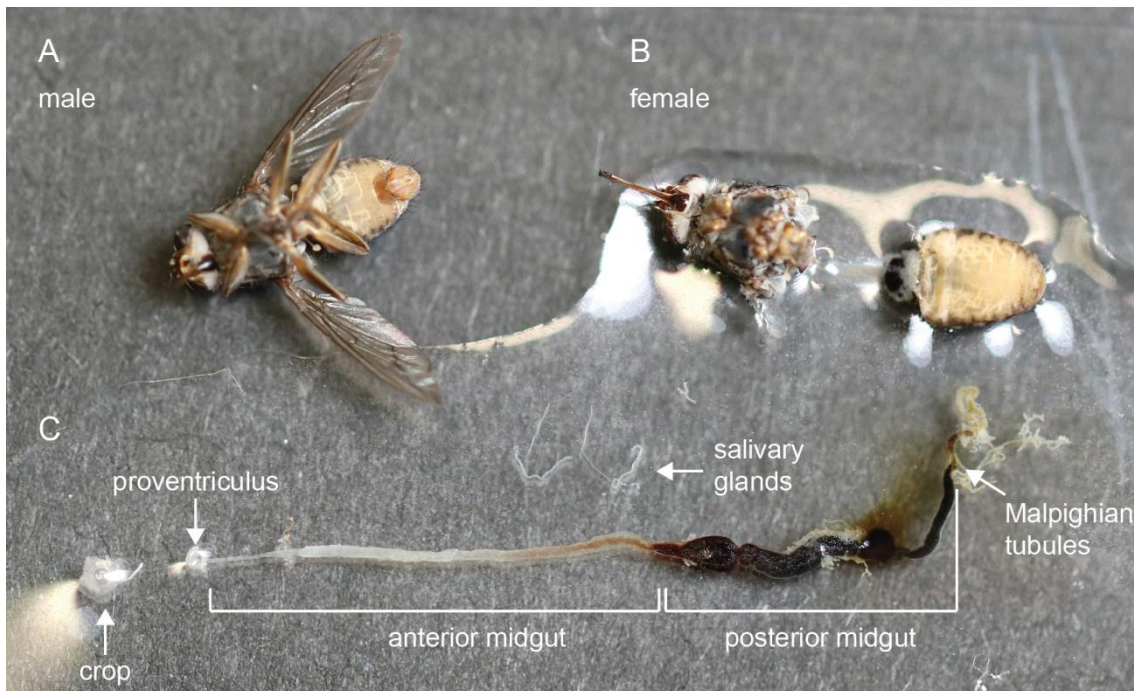
Figure 28: Dissection of a tsetse fly. Tsetse flies were euthanized with chloroform (A, male fly). Wings and legs were removed and the connection between the thorax and the abdomen disconnected in a drop of PBS to prevent drying of the tissue (B, female fly). The complete alimentary tract was removed and spread out lengthwise from the proventriculus (and the attached crop) to the Malphigian tubes. The two salivary glands were arranged next to it.

Dissection of flies

For dissection (figure 28), flies in a test tube were euthanized with a few drops of chloroform. Wings and legs were removed and the fly placed on a microscope slide in a drop of PBS. Dissections were performed using high precision tweezers (Dumont, CH) and a stereomicroscope (Wild Heerbrugg, CH). Whole tsetse alimentary tracts, from the proventriculus to the Malpighian tubules, as well as the

salivary glands were dissected and arranged lengthwise (figure 28 C). Attached fat bodies, as well as other unneeded tissues, were carefully removed and discarded. Depending on the experiment, the tissue was left intact or ripped at the region of interest to check for the presence of trypanosomes. For further analysis at the microscope the tissue was covered with a coverslip.

5.2.3 Working with *E. coli*

Transformation of chemically competent *E. coli* with plasmid DNA

Competent *E. coli* Top 10 were thawed on ice. Then, 10 ng plasmid DNA was added and the mixture was incubated on ice for 45 minutes. Bacteria were exposed to heat shock at 42 °C for 30 seconds and cooled again for 3 minutes on ice. Afterwards 1 ml LB-medium was added and the bacteria were incubated on a shaker (150-200 rpm) for 1 hour at 37 °C. Next, 100 µl and 300 µl of bacteria suspension were spread on agar plates containing ampicillin (100 µg/ml) and incubated overnight upside down at 37 °C. Until further use, plates were sealed with parafilm and stored at 4 °C.

Bacteria culture

Single bacteria colonies were picked from agar plates and cultured in LB-medium containing ampicillin (100 µg/ml) on a shaker (150-200 rpm) overnight at 37 °C. Usually, five colonies with 5 ml of LB-medium each, were incubated.

5.2.4 Molecular biological methods

Agarose gel electrophoresis

Agarose gel electrophoresis was used to separate and visualize DNA or DNA fragments after enzyme digestion. DNA samples were loaded onto a 0.8% agarose gel (Sigma-Aldrich, USA) in TAE buffer. Each sample was mixed with 6x loading dye. GeneRuler DNA Ladder Mix (Thermo Fisher Scientific, USA) was used as a marker. The gel was stained in an ethidium bromide bath (3 µg/ml) for 20 minutes, illuminated with UV light (310-350 nm) and imaged using the gel documentation system GEL iX Imager (Intas Science Imaging Instruments, DE).

Isolation of plasmid DNA from bacteria

Plasmid DNA was extracted using the NucleoSpin Plasmid Kit (Macherey-Nagel, DE) following the manufacturer´s instructions. DNA concentration and purity were determined using the Tecan Infinite M200 (Tecan Group, CH) by measuring the absorbance at 260 nm and 280 nm. Plasmid DNA was stored at -20 °C.

Restriction enzyme digestion

Restriction enzyme digestion was used to linearize plasmids for transfection into trypanosomes. Suitable enzymes were determined using CLC Main Workbench (CLC bio, NL) and digestion was conducted according to the manufacturer´s instructions.

Isopropanol precipitation of DNA

Isopropanol precipitation was used to isolate DNA from aqueous solutions. For this, 1 volume of isopropanol was added to the dissolved DNA along with 0.1 volume 3 M sodium acetate (representing 10% of total volume). After inverting the tube several times, the sample was pelleted by centrifugation (20,000x g, 20 minutes, 4 °C). The supernatant was discarded and the DNA pellet washed twice with 1 ml 70% ethanol (20,000x g, 5 minutes, 4 °C). After the last centrifugation step, the supernatant was discarded and the remaining pellet dried under sterile conditions. Finally, the pellet was eluted in an appropriate amount of ddH$_2$O (10 µg in 10 µl for transfection). The final DNA concentration and purity were determined using the Tecan Infinite M200 (Tecan Group, CH) by measuring the absorbance at 260 nm and 280 nm.

5.2.5 Microscope analyses

Fixation of trypanosomes and fluorescence staining

Cells were either obtained from cell culture or from fly tissue. Cultured parasites were harvested as described above. In the case of fly-specific stages, corresponding organs were dissected as described above and transferred into a fresh drop of PBS. Then, the tissue was ripped to free the trypanosomes. Cells were collected in a test tube and pelleted by centrifugation for 60 seconds in a picofuge. The supernatant was discarded, leaving a small volume in which to concentrate to cells. In order to stain living parasites, a surface dye (AMCA-sulfo-NHS or Atto 488 NHS-Ester) was

added at this step and the parasites incubated for 10 minutes on ice in the dark. After staining, the parasites were fixed overnight using 4% (w/v) FA and 0.05% (v/v) glutaraldehyde in the dark at 4 °C. Before analysis, trypanosomes were washed once in PBS and DNA visualized with DAPI.

Microscopy of fixed trypanosome cells and data analyses

Images of trypanosomes were recorded using the iMIC wide field fluorescence microscope (FEI-TILL Photonics, DE). This microscope was equipped with a CCD camera (Sensicam qe, pixel size 6.45 µm, PCO, DE) and filter cubes ET-mCherry-Texas-Red, ET-GFP, ET-YFP and DAPI (Chroma Technology CORP, USA). A 100x (NA 1.4) objective was used (Olympus, DE) for the acquisition of Z-stacks. Stacks were generated using the Live Acquisition Software (TILL Photonics, DE) and 100 or 150 Z-planes were recorded automatically at a step size of 100 nm. The analysis of the stacks was performed with ImageJ/Fiji software (National Institute of Health, USA).

For further image processing the stacks were deconvolved using the Huygens Essential software (Scientific Volume Imaging B.V., NL). Fluorescent images are shown as maximum intensity projections of stacks and differential interference contrast (DIC) images are shown as single image. Some images were false colored for better visualization. 3D models were computed with the Amira software (Thermo Fischer Scientific, USA) using an edge detection filter (Sobel) and volume models using the Voltex display function. In addition, flagella were traced using the volume model and Amira´s filament editor.

Live cell imaging of trypanosomes with a high-speed camera

High-speed recordings of trypanosomes were performed with the DMI6000B wide field fluorescence microscope (Leica microsystems, DE). This microscope was equipped with a DFC365FX camera (pixel size 6.45 µm, Leica microsystems, DE) and a 100x oil objective (NA 1.4) or 63x glycerol objective (NA 1.3) was used. All microscope and fluorescence settings were managed using the Leica Application suite AF software (Leica, DE). For high-speed recordings the microscope was additionally connected to an sCMOS camera pco.edge (pixel size 6.5 µm, PCO, DE) and all settings for high speed recordings were managed using the pco.CamWare

software (PCO, DE). If not mentioned otherwise, images were taken at frame rates of 250 fps and 800x800 pixels. Image acquisition did not normally exceed 1 hour of recording time per sample.

Videos were saved as TIFF stacks (Tagged Image File Format) and further analyzed using the ImageJ/Fiji software (National Institute of Health, USA). Due to high data volumes, long videos were reduced from 16-bit to 8-bit files and brightness and contrast adjusted appropriately. Videos were saved as .avi files and further converted to the size-reduced mp4. format using the Xmedia Recode software (Sebastian Dörfler, DE). Multivideos containing several videos and text were generated using Keynote (Apple, USA) and exported as .mp4 files.

Sample preparation for light sheet fluorescence microscopy

The samples were prepared for LSFM by modified protocols, which were adapted and optimized for tsetse fly and trypanosome analysis on the basis of published procedures (Brede at al., 2012; Smolla et al., 2014).

Flies were numbed at 4 °C and extremities such as wings, head and legs removed before the remaining fly body was fixed in 4% FA in PBS for at least 2 days and stored at 4 °C until further use. As a test, complete flies were also fixed. The fixation for teneral or young flies was more difficult than for older flies. All solutions were replaced with transfer pipettes, leaving the sample within the same glass vial to prevent injury to the tissue. Whole flies were washed in PBS (2x 10 minutes) and incubated in an aqueous solution of 30% hydrogen-peroxide for 7-9 days. During this treatment the thick cuticle of the insect turned from dark brown to a light yellowish color. The bleaching process produced bubbles inside the tissue in some cases, for further experiments only bubble-free flies were used. After bleaching, the flies were washed in PBS (3x 10 minutes) and dehydrated in a dilution series of ethanol (30%, 50%, 70%, 80%, 90% each 2 hours; 2x 100% 12 hours minimum). For a complete dehydration of the tissue, ethanol was replaced by 100% n-hexane and flies were incubated for 2 hours. After contact with n-hexane, air exposure was strictly avoided. The n-hexane solution was removed stepwise in exchange with clearing solution (3x solution exchange). The clearing solution (BABB) consists of 1 part benzyl alcohol and 2 parts benzyl benzoate. After incubation for at least 2 hours, at room temperature, tissues became optically transparent and suitable for imaging. Transparent flies were stored at 4 °C.

For the preparation of the digestive system, flies were starved for 1, 6, 24 or 48 hours before being dissected. For peritrophic matrix staining, flies were fed with 40 µg/ml of wheat germ agglutinin (WGA) labeled with rhodamine (Vector Laboratories, US) in preheated (37 °C) SDM-79 medium or TDB. Dissection time was chosen depending on the region of interest, as the stained tissue moved posterior with the production of new peritrophic matrix. Whole alimentary tracts, from the proventriculus to the Malpighian tubules were dissected in a drop of PBS (compare figure 28 C). With infected flies, the midgut was observed under a microscope for the presence of trypanosomes. Fresh tissue was immediately placed in 4% FA in PBS and incubated for at least 24 hours and stored at 4 °C until further use. In some cases, midguts were additionally stained with 10 µg/ml propidium iodide. For the alimentary tracts, no bleaching was needed. The remaining protocol was performed as described above for flies, except for the n-hexane treatment, which was performed for 30 minutes.

Image acquisition at the light sheet microscope and data analysis

Cleared fly samples were imaged using a non-commercial home-built scanning light sheet fluorescence microscope form the Department of Medicine II and Interdisciplinary Center for Clinical Research, University Hospital Würzburg (Brede et al., 2012; Stegner et al., 2017) or at a commercial scanning light sheet fluorescence microscope (LaVision BioTec, DE).

Samples were clamped using tweezers and suspended in a self-made cover glass chamber filled with freshly prepared BABB solution. All settings were managed with the Andor iQ software (Andor Technology Ltd, UK) in consultation with an authorized technician from the Department of Medicine II, Würzburg. Three-dimensional stacks were generated with 2 µm or 0.5 µm step size and automatically saved as TIFF stacks. Stacks were additionally opened directly with the Imaris software (Bitplane, CH) to verify the 3D tissue constitution.

Stacks were deconvolved using the Huygens Essential software (Scientific Volume Imaging B.V., NL), or directly analyzed in detail using ImageJ/Fiji (National Institute of Health, USA) and Amira (Thermo Fischer Scientific, USA) for 3D visualization.

5.2.6 Soft lithography

Soft lithography is a technique that allows the production and replication of three-dimensional patterned microstructures (Qin et al., 2010). A photomask, containing the desired designs, is used to produce a mold, which can further be used to produce elastomeric stamps with well-defined dimensions and structures on the micrometer scale. The multifunctionality of this method allows usage for numerous applications and is widely used in various biological fields (e.g. Weibel et al., 2007; Lockery et al., 2008; Knowlton et al., 2015; Shapiro et al., 2016).

Mask design using AutoCAD

The Autodesk AutoCAD (Computer-Aided Design) software (Autodesk, USA) was used for the design of a custom-built photolithography mask. The software is a vector-orientated drawing program and contains a command-based platform as well as a 2D visual design platform.

We used a circular chrome photomask, 10.6 cm (4 inches) in diameter, made of soda lime glass and coated with a thin layer of chromium. For precise pattern transfer and handling, the design process necessarily considered correct dimensions, resolution and alignment (Qin et al., 2010). Individual designs were created to fit on a glass slide with dimensions of 22x22 mm, so that 9 different designs could be fitted on one photomask (figure 29 A). This left enough space for PDMS cutting as well as for fluid inlet and outlet ports. To test the usage of this system for different experiments, the photomask was shared with the departmental student Elisabeth Meiser (design numbers I-VI). The drawings were divided into different layers, i.e. one separate layer for text, outer boundaries and inner boundaries. The layering was essential to designate chrome mask polarity, as the photomask would later contain regions of transparent and opaque regions. Here, it needed to be considered whether a positive or negative photoresist would be used. For this study, the wafer was later coated with a negative photoresist.
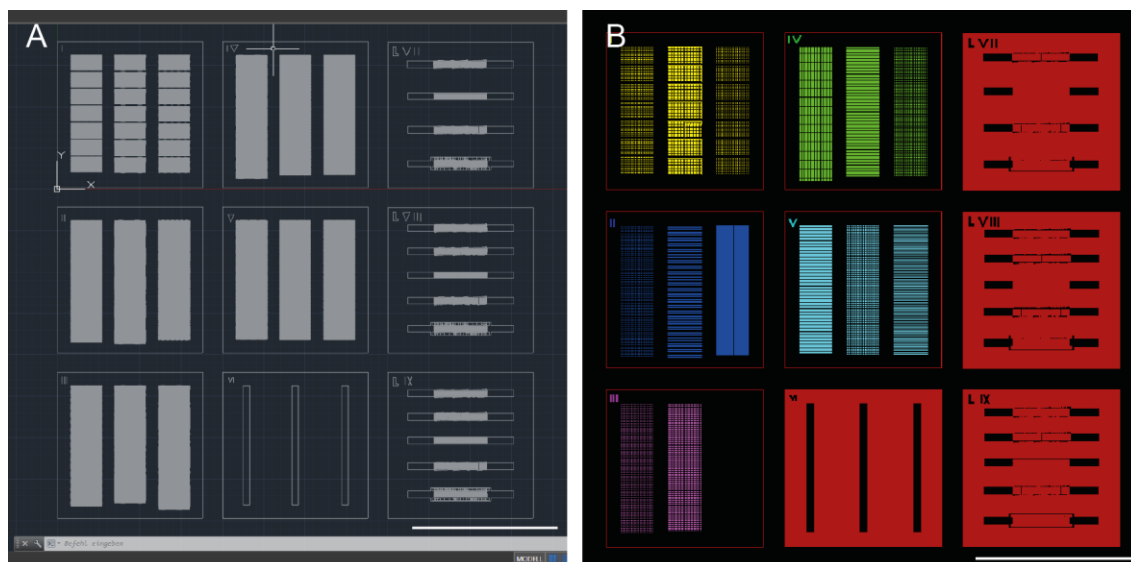
Figure 29: Design of the photomask for lithography. Scale bars represent 22 mm. (A) The desired patterns were designed using the AutoCAD software. (B) The VisualCAM file was opened with the WISE Database Viewer for final approval. Mask polarity was specified in different layers, with colored regions representing chrome on the photomask. Designs I-V are filled with chrome whereas structures VI-IX are bordered with chrome.

The designed AutoCAD drawing was sent to JD Photo Data and their manufacturing business JD Photo-Tools (UK) as an AutoCAD .dwg file, where it was checked and edited by their design team. The file was sent back as a VisualCAM .vcam database file for final approval. The .vcam file was opened using the WISE Database Viewer 16.0 (WISE Software Solutions, USA), as shown in figure 29 B. Colored regions mark structures that are later filled with chrome, meaning structures on designs I-V are filled with chrome and structures VI-IX are bordered with chrome. The optimal dimensions of the final chrome mask were compared with measured dimensions and certified by JD Photo-Tools.

Preparation of the wafer and spin coating with SU-8

All lithography equipment was supplied and installed by BlackHole Lab (FR). The mask was used as a template to produce a mold. For an equal distribution of the photoresist on the wafer, a spin coater was used. The spin coater was located under a fume hood without direct light exposure. For the desired thickness of the photoresist layer, the amount of photoresist and the spinning speed were calculated. The wafer was cleaned with acetone and isopropanol. To evaporate all the solvents and dehydrate it completely, the wafer was placed on a hot plate with the shiny part facing up (15 minutes, 120 °C). It was then covered with a petri dish to avoid

contamination. After cooling, the wafer was placed in the spin coater (Model WS-650Mz-23NPPB; Laurell Technologies, USA). For a desired thickness of 2 µm, for example, 4 ml of the viscous SU-8 photoresist (1 ml photoresist per inch of wafer diameter) was transferred on the wafer and a two-step spinning program was started. 1. low speed spinning (10 seconds, 500 rpm), 2. high speed spinning (35 seconds, 35,000 rpm). The spin coater was cleaned with acetone.

Making a mold from the master wafer

In the next step, the pattern of the photomask was transferred onto the wafer with the SU-8 negative photoresist. By using a negative photoresist, a photo-acid is formed during illumination which crosslinks to the resist upon exposure to high temperatures. Areas that were exposed to UV light were not crosslinked and could be removed with developer solution.

The mask was placed on top of the wafer and was illuminated, using hard (direct) contact between mask and wafer. The hard contact results in a better resolution (maximum resolution 2 µm), hence reducing light scattering during illumination. Cross linkage was performed in an oven at 95 °C until the pattern became visible to the naked eye, but minimally for 5 minutes. The wafer was then covered drop-wise with SU-8 developer, which was immediately removed using an air gun. The standard protocol for developing the structures used a petri dish filled with SU-8 developer. However, this resulted in the detachment of the structured photoresist and the wafer was not usable, so a to drop-wise developing approach was used instead. Afterwards, the wafer was cleaned with isopropanol and dried. A hard bake step (15 minutes, 150 °C) was performed followed by a silanization step for the further use with PDMS. Silanization prevents the PDMS from adhering to the master. This step was performed by Elisabeth Meiser. The resulting master wafer was further used to produce the PDSM devices.

Production of wafer pattern in PDMS and bonding on glass slide

The wafer was placed in a plastic petri dish, with the pattern of the wafer on top. If not in use, the petri dish was always closed, to avoid dust on the wafer. To fill a new dish with PDMS, 80 g of silicon elastomere and 8 g of silicon elastomere curing agent were needed. If the pattern had already been cut out and the dish had a PDMS

border, only 40 g of silicon elastomere and 4 g of silicon elastomere curing agent were used.

Both reagents were mixed in a plastic cup using a glass rod, which was cleaned of dust beforehand with an air gun. To get rid of air bubbles, the mixture was placed in a vacuum for 30 minutes. Afterwards, the mixture was gently poured over the entire wafer without creating bubbles by staying close to the wafer surface. The petri dish was then placed into an oven (2 hours, 80 °C) to allow the PDMS to harden. The arrays were carefully cut out with a razor blade and removed from the wafer. They were trimmed to the right size and two holes were punched at opposite endings of each design using a biopsy punch (1 mm).

The PDMS stamps were bonded to glass slides, coverslips or small glass petri dishes. For visualization at the microscope, coverslips were best suited. To clean the PDMS stamps quickly, arrays were cleaned with isopropanol, dried with the air gun and placed into a clean petri dish (pattern on top). Alternatively, PDMS stamps and slides or coverslips were placed in a glass cuvette (lid on top) containing 2% hellmanex solution in H_2O, an effective cleaning solution for glass. The cuvette was then placed in an ultrasonic bath (37 kHz, 320 W, 10 minutes). Next, everything was cleaned with water, the cuvette filled with isopropanol and sonication was repeated. Slide and pattern were cleaned with water, dried and placed in a clean petri dish, with the pattern on top.

After thorough cleaning, the arrays were plasma cleaned for 3 minutes. This step is essential, because plasma cleaning makes the surface of the arrays and the glass dish hydrophilic. For bonding, the arrays were pressed carefully (pattern facing down) onto the glass substrate. Some patterns were additionally placed in the oven (15 minutes, 80 °C), to test which procedure resulted in the best pattern quality. For storage, the petri dishes were covered with lids and placed in the dark at room temperature. They were used for several months.

To apply liquid into the channels, small plastic tubes were inserted into the holes that were previously punched. A syringe was inserted into the tubes, and channels carefully filled with liquid. The volume applied to a specific channel and the quality of bonding was carefully monitored.

6 Bibliography

Acosta-Serrano, A., Vassella, E., Liniger, M., Kunz Renggli, C., Brun, R., Roditi, I., and Englund, P.T. (2001). The surface coat of procyclic *Trypanosoma brucei*: programmed expression and proteolytic cleavage of procyclin in the tsetse fly. Proceedings of the National Academy of Sciences of the United States of America *98*, 1513–1518.

Adhiambo, C., Blisnick, T., Toutirais, G., Delannoy, E., and Bastin, P. (2009). A novel function for the atypical small G protein Rab-like 5 in the assembly of the trypanosome flagellum. Journal of Cell Science *122*, 834–841.

Aksoy, E., Vigneron, A., Bing, X., Zhao, X., O'Neill, M., Wu, Y., Bangs, J.D., Weiss, B.L., and Aksoy, S. (2016). Mammalian African trypanosome VSG coat enhances tsetse's vector competence. Proceedings of the National Academy of Sciences *113*, 6961–6966.

Aksoy, S. (1995). *Wigglesworthia* gen. nov. and *Wigglesworthia glossinidia* sp. nov., Taxa Consisting of the Mycetocyte-Associated, Primary Endosymbionts of Tsetse Flies. International Journal of Systematic Bacteriology *45*, 848–851.

Aksoy, S., Gibson, W.C., and Lehane, M.J. (2003). Interactions between tsetse and trypanosomes with implications for the control of trypanosomiasis. Advances in Parasitology *53*, 1–83.

Alizadehrad, D., Krüger, T., Engstler, M., and Stark, H. (2015). Simulating the Complex Cell Design of *Trypanosoma brucei* and Its Motility. PLoS Computational Biology *11*, e1003967.

Amiguet-Vercher, A., Pérez-Morga, D., Pays, A., Poelvoorde, P., Van Xong, H., Tebabi, P., Vanhamme, L., and Pays, E. (2004). Loss of the mono-allelic control of the VSG expression sites during the development of *Trypanosoma brucei* in the bloodstream: Transcription inactivation in *T. brucei*. Molecular Microbiology *51*, 1577–1588.

Andereck, J.W., King, J.G., and Hillyer, J.F. (2010). Contraction of the Ventral Abdomen Potentiates Extracardiac Retrograde Hemolymph Propulsion in the Mosquito Hemocoel. PLoS ONE *5*, e12943.

Anderson, N.E., Mubanga, J., Fevre, E.M., Picozzi, K., Eisler, M.C., Thomas, R., and Welburn, S.C. (2011). Characterisation of the Wildlife Reservoir Community for Human and Animal Trypanosomiasis in the Luangwa Valley, Zambia. PLoS Neglected Tropical Diseases *5*, e1211.

Auty, H., Anderson, N.E., Picozzi, K., Lembo, T., Mubanga, J., Hoare, R., Fyumagwa, R.D., Mable, B., Hamill, L., Cleaveland, S., et al. (2012). Trypanosome Diversity in Wildlife Species from the Serengeti and Luangwa Valley Ecosystems. PLoS Neglected Tropical Diseases *6*, e1828.

Babu, S.B., and Stark, H. (2012). Modeling the locomotion of the African trypanosome using multi-particle collision dynamics. New Journal of Physics *14*, 085012.

Bargul, J.L., Jung, J., McOdimba, F.A., Omogo, C.O., Adung'a, V.O., Krüger, T., Masiga, D.K., and Engstler, M. (2016). Species-Specific Adaptations of Trypanosome Morphology and Motility to the Mammalian Host. PLoS Pathogens *12*, e1005448.

Barry, J. (1998). VSG gene control and infectivity strategy of metacyclic stage *Trypanosoma brucei*. Molecular and Biochemical Parasitology *91*, 93–105.

Barry, J.D., and Emergy, D.L. (1984). Parasite development and host responses during the establishment of *Trypanosoma brucei* infection transmitted by tsetse fly. Parasitology *88 (Pt 1)*, 67–84.

Bates, P.A. (2007). Transmission of Leishmania metacyclic promastigotes by phlebotomine sand flies. International Journal for Parasitology *37*, 1097–1106.

Bates, P.A. (2008). Leishmania sand fly interaction: progress and challenges. Current Opinion in Microbiology *11*, 340–344.

Berke, A.P., Turner, L., Berg, H.C., and Lauga, E. (2008). Hydrodynamic Attraction of Swimming Microorganisms by Surfaces. Physical Review Letters *101*.

Bhagwat, S., Sontakke, S., K, D., Parte, P., and Jadhav, S. (2018). Chemotactic behavior of spermatozoa captured using a microfluidic chip. Biomicrofluidics *12*, 024112.

Bingle, L.E.H., Gibson, W.C., Bailey, M., and Eastlake, J.L. (2001). A novel GFP approach for the analysis of genetic exchange in trypanosomes allowing the *in situ* detection of mating events. Microbiology *147*, 3231–3240.

Binz, M., Lee, A.P., Edwards, C., and Nicolau, D.V. (2010). Motility of bacteria in microfluidic structures. Microelectronic Engineering *87*, 810–813.

Branche, C. (2006). Conserved and specific functions of axoneme components in trypanosome motility. Journal of Cell Science *119*, 3443–3455.

Brede, C., Friedrich, M., Jordán-Garrote, A.-L., Riedel, S.S., Bäuerlein, C.A., Heinze, K.G., Bopp, T., Schulz, S., Mottok, A., Kiesel, C., et al. (2012). Mapping immune processes in intact tissues at cellular resolution. Journal of Clinical Investigation *122*, 4439–4446.

Breidbach, T., Ngazoa, E., and Steverding, D. (2002). *Trypanosoma brucei*: *in vitro* slender-to-stumpy differentiation of culture-adapted, monomorphic bloodstream forms. Experimental Parasitology *101*, 223–230.

Broadhead, R., Dawe, H.R., Farr, H., Griffiths, S., Hart, S.R., Portman, N., Shaw, M.K., Ginger, M.L., Gaskell, S.J., McKean, P.G., et al. (2006). Flagellar motility is required for the viability of the bloodstream trypanosome. Nature *440*, 224–227.

Brokaw, C.J. (1965). Non-sinusoidal bending waves of sperm flagella. Journal of Experimental Biology *43*, 155–169.

Bruce, D. (1895). Preliminary Report on Tsetse Fly Disease or Nagana in Zululand. London School of Hygiene and Tropical Medicine. Bennett and Davis, Durban, *18* pp.

Brugerolle, G. (1991). Flagellar and cytoskeletal systems in amitochondrial flagellates: Archamoeba, Metamonada and Parabasala. Protoplasma *164*, 70–90.

Brumley, D.R., Wan, K.Y., Polin, M., and Goldstein, R.E. (2014). Flagellar synchronization through direct hydrodynamic interactions. eLife *3*.

Brun, R., and Balmer, O. (2006). New developments in human African trypanosomiasis: Current Opinion in Infectious Diseases *19*, 415–420.

Brun, R., and Schönenberger, M. (1979). Cultivation and in vitro cloning or procyclic culture forms of Trypanosoma brucei in a semi-defined medium. Short communication. Acta Tropica *36*, 289–292.

Brun, R., and Schönenberger, M. (1981). Stimulating effect of citrate and *cis*-aconitate on the transformation of *Trypanosoma brucei* bloodstream forms to procyclic forms in vitro. Zeitschrift Für Parasitenkunde. Parasitology Research *66*, 17–24.

Brun, R., Blum, J., Chappuis, F., and Burri, C. (2010). Human African trypanosomiasis. Lancet *375*, 12.

Caljon, G., Van Reet, N., De Trez, C., Vermeersch, M., Pérez-Morga, D., and Van Den Abbeele, J. (2016). The Dermis as a Delivery Site of *Trypanosoma brucei* for Tsetse Flies. PLoS Pathogens *12*, e1005744.

Capewell, P., Atkins, K., Weir, W., Jamonneau, V., Camara, M., Clucas, C., Swar, N.-R.K., Ngoyi, D.M., Rotureau, B., Garside, P., et al. (2019). Resolving the apparent transmission paradox of African sleeping sickness. PLoS Biology *17*, e3000105.

Capewell, P., Cren-Travaillé, C., Marchesi, F., Johnston, P., Clucas, C., Benson, R.A., Gorman, T.-A., Calvo-Alvarez, E., Crouzols, A., Jouvion, G., et al. (2016). The skin is a significant but overlooked anatomical reservoir for vector-borne African trypanosomes. eLife *5*.

Chang, H., Kim, B.J., Kim, Y.S., Suarez, S.S., and Wu, M. (2013). Different migration patterns of sea urchin and mouse sperm revealed by a microfluidic chemotaxis device. PLoS One *8*, e60587.

Cho, H., Jönsson, H., Campbell, K., Melke, P., Williams, J.W., Jedynak, B., Stevens, A.M., Groisman, A., and Levchenko, A. (2007). Self-Organization in High-Density Bacterial Colonies: Efficient Crowd Control. PLoS Biology *5*, e302.

Chung, C.T., Niemela, S.L., and Miller, R.H. (1989). One-step preparation of competent *Escherichia coli*: transformation and storage of bacterial cells in the same solution. Proceedings of the National Academy of Sciences *86*, 2172–2175.

Cross, G.A. (1977). Antigenic variation in trypanosomes. American Journal of Tropical Medicine and Hygiene *26*, 240–244.

Cross, G.A.M., Kim, H.-S., and Wickstead, B. (2014). Capturing the variant surface glycoprotein repertoire (the VSGnome) of *Trypanosoma brucei* Lister 427. Molecular and Biochemical Parasitology *195*, 59–73.

Cubitt, A.B., Heim, R., Adams, S.R., Boyd, A.E., Gross, L.A., and Tsien, R.Y. (1995). Understanding, improving and using green fluorescent proteins. Trends in Biochemical Sciences *20*, 448–455.

Cuvillier, A., Miranda, J.C., Ambit, A., Barral, A., and Merlin, G. (2003). Abortive infection of *Lutzomyia longipalpis* insect vectors by aflagellated LdARL-3A-Q70L overexpressing *Leishmania amazonensis* parasites. Cell Microbiology *5*, 717–728.

Czichos, J., Nonnengaesser, C., and Overath, P. (1986). *Trypanosoma brucei*: cis-aconitate and temperature reduction as triggers of synchronous transformation of bloodstream to procyclic trypomastigotes in vitro. Experimental Parasitology *62*, 283–291.

Danielsson, P.E. (1980). Euclidean Distance Mapping. Computer Graphics and Image Processing *14*, 227–248.

de Andrade Rosa, I., de Souza, W., and Benchimol, M. (2013). High-resolution scanning electron microscopy of the cytoskeleton of *Tritrichomonas foetus*. Journal of Structural Biology *183*, 412–418.

Dean, S. (2008). A functional analysis of a family of proteins implicated in *Trypanosoma brucei* lifecycle progression. PhD thesis, University of Edinburgh.

Dean, S., Marchetti, R., Kirk, K., and Matthews, K.R. (2009). A surface transporter family conveys the trypanosome differentiation signal. Nature *459*, 213–217.

Deitsch, K.W., Lukehart, S.A., and Stringer, J.R. (2009). Common strategies for antigenic variation by bacterial, fungal and protozoan pathogens. Nature Reviews Microbiology *7*, 493–503.

Denissenko, P., Kantsler, V., Smith, D.J., and Kirkman-Brown, J. (2012). Human spermatozoa migration in microchannels reveals boundary-following navigation. Proceedings of the National Academy of Sciences *109*, 8007–8010.

Dobell, C. (1932). Antony Van Leeuwenhoek and His "Little Animals"; Being Some Account of the Father of Protozoology and Bacteriology and His Multifarious Discoveries in These Disciplines. New York: Harcourt, Brace and company.

Domenicali Pfister, D., Burkard, G., Morand, S., Renggli, C.K., Roditi, I., and Vassella, E. (2006). A Mitogen-Activated Protein Kinase Controls Differentiation of Bloodstream Forms of *Trypanosoma brucei*. Eukaryotic Cell *5*, 1126–1135.

Dóró, É., Jacobs, S.H., Hammond, F.R., Schipper, H., Pieters, R.P., Carrington, M., Wiegertjes, G.F., and Forlenza, M. (2019). Visualizing trypanosomes in a vertebrate host reveals novel swimming behaviours, adaptations and attachment mechanisms. eLife *8*.

Dostálová, A., and Volf, P. (2012). *Leishmania* development in and flies: parasite-vector interactions overview. Parasites & Vectors *5*, 276.

Dutton, J.E. (1902). Preliminary note upon a trypanosome occurring in the blood of man. Thompson Yates Lab. Rep *4*, 455–468.

Dwinger, R.H., Rudin, W., Moloo, S.K., and Murray, M. (1988). Development of *Trypanosoma congolense*, *T. vivax* and *T. brucei* in the skin reaction induced in goats by infected *Glossina morsitans centralis*: a light and electron microscopical study. Research in Veterinary Science *44*, 154–163.

Dyer, N.A., Rose, C., Ejeh, N.O., and Acosta-Serrano, A. (2013). Flying tryps: survival and maturation of trypanosomes in tsetse flies. Trends in Parasitology *29*, 188–196.

Elgeti, J., and Gompper, G. (2016). Microswimmers near surfaces. The European Physical Journal Special Topics *225*, 2333–2352.

Elgeti, J., Winkler, R.G., and Gompper, G. (2015). Physics of microswimmers - single particle motion and collective behavior: a review. Reports on Progress in Physics *78*, 056601.

Ellis, D.S., and Evans, D.A. (1977). Passage of *Trypanosoma brucei rhodesiense* through the peritrophic membrane of *Glossina morsitans morsitans*. Nature *267*, 834–835.

Engstler, M., and Boshart, M. (2004). Cold shock and regulation of surface protein trafficking convey sensitization to inducers of stage differentiation in *Trypanosoma brucei*. Genes & Development *18*, 2798–2811.

Engstler, M., Pfohl, T., Herminghaus, S., Boshart, M., Wiegertjes, G., Heddergott, N., and Overath, P. (2007). Hydrodynamic Flow-Mediated Protein Sorting on the Cell Surface of Trypanosomes. Cell *131*, 505–515.

Engstler, M., Thilo, L., Weise, F., Grünfelder, C.G., Schwarz, H., Boshart, M., and Overath, P. (2004). Kinetics of endocytosis and recycling of the GPI-anchored variant surface glycoprotein in *Trypanosoma brucei*. Journal of Cell Science *117*, 1105–1115.

Evans, D.A., and Ellis, D.S. (1978). The penetrative ability of sleeping-sickness trypanosomes. Transaction of the Royal Society of Tropical Medicine and Hygiene *72*, 653–655.

Evans, D.A., and Ellis, D.S. (1983). Recent observations on the behaviour of certain trypanosomes within their insect hosts. Advances in Parasitology *22*, 1–42.

Fenn, K., and Matthews, K.R. (2007). The cell biology of *Trypanosoma brucei* differentiation. Current Opinion in Microbiology *10*, 539–546.

Field, M.C., and Carrington, M. (2009). The trypanosome flagellar pocket. Nature Reviews Microbiology *7*, 775–786.

Forestier, C.-L., Machu, C., Loussert, C., Pescher, P., and Späth, G.F. (2011). Imaging Host Cell-Leishmania Interaction Dynamics Implicates Parasite Motility, Lysosome Recruitment, and Host Cell Wounding in the Infection Process. Cell Host & Microbe *9*, 319–330.

Franco, J.R., Cecchi, G., Priotto, G., Paone, M., Diarra, A., Grout, L., Simarro, P.P., Zhao, W., and Argaw, D. (2018). Monitoring the elimination of human African trypanosomiasis: Update to 2016. PLoS Neglected Tropical Diseases *12*, e0006890–e0006890.

Frank, S.A. (1996). Models of parasite virulence. The Quarterly Review of Biology *71*, 37–78.

Gadelha, C., Wickstead, B., and Gull, K. (2007). Flagellar and ciliary beating in trypanosome motility. Cell Motility and the Cytoskeleton *64*, 629–643.

Gardiner, P.R., and Wilson, A.J. (1987). *Trypanosoma* (Duttonefla) *vivax*. Parasitology Today *3*, 49–52.

Gibson, W., and Bailey, M. (2003). The development of *Trypanosoma brucei* within the tsetse fly midgut observed using green fluorescent trypanosomes. Kinetoplastid Biology and Disease *2*, 1.

Gibson, W., and Peacock, L. (2019). Fluorescent proteins reveal what trypanosomes get up to inside the tsetse fly. Parasites & Vectors *12*, 6.

Glenn, J.D., King, J.G., and Hillyer, J.F. (2010). Structural mechanics of the mosquito heart and its function in bidirectional hemolymph transport. Journal of Experimental Biology *213*, 541–550.

Gray, J. (1955). The movement of sea-urchin spermatozoa. Journal of Experimental Biology *3a*, 775–801.

Gray, J., and Hancock G. (1955). The propulsion of sea-urchin spermatozoa. Journal of Experimental Biology *32*, 802–814.

Grünfelder, C.G., Engstler, M., Weise, F., Schwarz, H., Stierhof, Y.-D., Morgan, G.W., Field, M.C., and Overath, P. (2003). Endocytosis of a glycosylphosphatidylinositol-anchored protein via clathrin-coated vesicles, sorting by default in endosomes, and exocytosis via. Molecular Biology of the Cell *14*, 2029–2040.

Haag, J., O'hUigin, C., and Overath, P. (1998). The molecular phylogeny of trypanosomes: evidence for an early divergence of the Salivaria. Molecular and Biochemical Parasitology *91*, 37–49.

Harmsen, R. (1973). The nature of the establishment barrier for *Trypanosoma brucei* in the gut of *Glossina pallidipes*. Transactions of The Royal Society of Tropical Medicine and Hygiene *67*, 364–373.

Harshey, R.M. (2003). Bacterial motility on a surface: many ways to a common goal. Annual Review of Microbiology *57*, 249–273.

Hartel, A.J.W., Glogger, M., Guigas, G., Jones, N.G., Fenz, S.F., Weiss, M., and Engstler, M. (2015). The molecular size of the extra-membrane domain influences the diffusion of the GPI-anchored VSG on the trypanosome plasma membrane. Scientific Reports *5*, 10394.

Heddergott, N., Krüger, T., Babu, S.B., Wei, A., Stellamanns, E., Uppaluri, S., Pfohl, T., Stark, H., and Engstler, M. (2012). Trypanosome Motion Represents an Adaptation to the Crowded Environment of the Vertebrate Bloodstream. PLoS Pathogens *8*, e1003023.

Heddleston, J.M., and Chew, T.-L. (2016). Light sheet microscopes: Novel imaging toolbox for visualizing life's processes. International Journal of Biochemistry and Cell Biology *80*, 119–123.

Hegedus, D., Erlandson, M., Gillott, C., and Toprak, U. (2009). New Insights into Peritrophic Matrix Synthesis, Architecture, and Function. Annual Review of Entomology *54*, 285–302.

Hemphill, A., Lawson, D., and Seebeck, T. (1991). The cytoskeletal architecture of *Trypanosoma brucei*. The Journal of Parasitology *77*, 603–612.

Herder, S., Votypka, J., Jirku, M., Radrova, J., Janzen, C.J., and Lukes, J. (2007). *Trypanosoma brucei* 29-13 strain is inducible in but not permissive for the tsetse fly vector. Experimental Parasitology *117*, 111–114.

Hirt, R.P. (2013). *Trichomonas vaginalis* virulence factors: an integrative overview. Sexually Transmitted Infections *89*, 439–443.

Hirumi, H., and Hirumi, K. (1989). Continuous Cultivation of Trypanosoma brucei Blood Stream Forms in a Medium Containing a Low Concentration of Serum Protein without Feeder Cell Layers. The Journal of Parasitology *75*, 985.

Hoare, C.A. (1931). The peritrophic membrane of *Glossina* and its bearing upon the life-cycle of *Trypanosoma grayi*. Transactions of The Royal Society of Tropical Medicine and Hygiene *25*, 57–64.

Hoare, C.A., and Wallace, F.G. (1966). Developmental Stages of Trypanosomatid Flagellates: a New Terminology. Nature *212*, 1385–1386.

Hochstetter, A., and Pfohl, T. (2016). Motility, Force Generation, and Energy Consumption of Unicellular Parasites. Trends in Parasitology *32*, 531–541.

Honigberg, B.M. (1990). Host Cell-Trichomonad Interactions and Virulence Assays Using in In Vitro Systems. In Trichomonads Parasitic in Humans, B.M. Honigberg, ed. (New York, NY: Springer New York), pp. 155–212.

Hostettler, L., Grundy, L., Kaser-Pebernard, S., Wicky, C., Schafer, W.R., and Glauser, D.A. (2017). The Bright Fluorescent Protein mNeonGreen Facilitates Protein Expression Analysis *In Vivo*. 3G (Bethesda) *7*, 607–615.

Huang, H.-Y., Wu, T.-L., Huang, H.-R., Li, C.-J., Fu, H.-T., Soong, Y.-K., Lee, M.-Y., and Yao, D.-J. (2014). Isolation of motile spermatozoa with a microfluidic chip having a surface-modified microchannel. Journal of Laboratory Automation *19*, 91–99.

Hulme, S.E., DiLuzio, W.R., Shevkoplyas, S.S., Turner, L., Mayer, M., Berg, H.C., and Whitesides, G.M. (2008). Using ratchets and sorters to fractionate motile cells of *Escherichia coli* by length. Lab on a Chip *8*, 1888.

Hunt, M., Brun, R., and Kohler, P. (1994). Studies on compounds promoting the *in vitro* transformation of *Trypanosoma brucei* from bloodstream to procyclic forms. Parasitology Research *80*, 600–606.

Imhof, S., Knüsel, S., Gunasekera, K., Vu, X.L., and Roditi, I. (2014). Social Motility of African Trypanosomes Is a Property of a Distinct Life-Cycle Stage That Occurs Early in Tsetse Fly Transmission. PLoS Pathogens *10*, e1004493.

Jackson, D.G., Owen, M.J., and Voorheis, H.P. (1985). A new method for the rapid purification of both the membrane-bound and released forms of the variant surface glycoprotein from *Trypanosoma brucei*. Biochemical Journal *230*, 195–202.

Jacobs, S.L., and Lee, N.D. (1964). Determination of citric acid in serum and urine using BR82. Journal of Nuclear Medicine *5*, 297–301.

Jamonneau, V., Bucheton, B., Kabore, J., Ilboudo, H., Camara, O., Courtin, F., Solano, P., Kaba, D., Kambire, R., Lingue, K., et al. (2010). Revisiting the immune trypanolysis test to optimise epidemiological surveillance and control of sleeping sickness in West Africa. PLoS Neglected Tropical Diseases *4*, e917.

Jamonneau, V., Ilboudo, H., Kabore, J., Kaba, D., Koffi, M., Solano, P., Garcia, A., Courtin, D., Laveissiere, C., Lingue, K., et al. (2012). Untreated human infections by *Trypanosoma brucei gambiense* are not 100% fatal. PLoS Neglected Tropical Diseases *6*, e1691.

Jelicks, L.A., Lisanti, M.P., Machado, F.S., Weiss, L.M., Tanowitz, H.B., and Desruisseaux, M.S. (2013). Imaging of small-animal models of infectious diseases. American Journal of Pathology *182*, 296–304.

Josling, G.A., and Llinás, M. (2015). Sexual development in Plasmodium parasites: knowing when it's time to commit. Nature Reviews Microbiology *13*, 573–587.

Kagbadouno, M.S., Camara, M., Rouamba, J., Rayaisse, J.-B., Traore, I.S., Camara, O., Onikoyamou, M.F., Courtin, F., Ravel, S., de Meeus, T., et al. (2012). Epidemiology of sleeping sickness in Boffa (Guinea): where are the trypanosomes? PLoS Neglected Tropical Diseases *6*, e1949.

Kantsler, V., Dunkel, J., Blayney, M., and Goldstein, R.E. (2014). Rheotaxis facilitates upstream navigation of mammalian sperm cells. eLife *3*.

Kennedy, P.G. (2013). Clinical features, diagnosis, and treatment of human African trypanosomiasis (sleeping sickness). The Lancet Neurology *12*, 186–194.

Kleine, F.K. (1909). Weitere wissenschaftliche Beobachtungen über die Entwicklung von Trypanosomen in Glossinen. Dtsch. Medizinische Wochenschrift *35*, 924–925.

Knowlton, S.M., Sadasivam, M., and Tasoglu, S. (2015). Microfluidics for sperm research. Trends in Biotechnology *33*, 221–229.

Knüsel, S., and Roditi, I. (2013). Insights into the regulation of GPEET procyclin during differentiation from early to late procyclic forms of *Trypanosoma brucei*. Molecular and Biochemical Parasitology *191*, 66–74.

Kolev, N.G., Ramey-Butler, K., Cross, G.A.M., Ullu, E., and Tschudi, C. (2012). Developmental Progression to Infectivity in *Trypanosoma brucei* Triggered by an RNA-Binding Protein. Science *338*, 1352–1353.

Krüger, T., and Engstler, M. (2015). Flagellar motility in eukaryotic human parasites. Seminars in Cell & Developmental Biology *46*, 113–127.

Krüger, T., and Engstler, M. (2018). The Fantastic Voyage of the Trypanosome: A Protean Micromachine Perfected during 500 Million Years of Engineering. Micromachines *9*, 63.

Krüger, T., Schuster S., and Engstler M. (2018). Beyond Blood: African Trypanosomes on the Move. Trends in Parasitology *34*, 1056–1067.

Kusdian, G., and Gould, S.B. (2014). The biology of *Trichomonas vaginalis* in the light of urogenital tract infection. Molecular and Biochemical Parasitology *198*, 92–99.

Lacomble, S., Vaughan, S., Gadelha, C., Morphew, M.K., Shaw, M.K., McIntosh, J.R., and Gull, K. (2010). Basal body movements orchestrate membrane organelle division and cell morphogenesis in *Trypanosoma brucei*. Journal of Cell Science *123*, 2884–2891.

Lambrecht, F.L. (1985). Trypanosomes and hominid evolution. Biosience *35*, 640–646.

Langer, R.C., and Vinetz, J.M. (2001). Plasmodium ookinete-secreted chitinase and parasite penetration of the mosquito peritrophic matrix. Trends in Parasitology *17*, 269–272.

Lauga, E., and Powers, T.R. (2009). The hydrodynamics of swimming microorganisms. Reports on Progress in Physics *72*, 096601.

Laxman, S., Riechers, A., Sadilek, M., Schwede, F., and Beavo, J.A. (2006). Hydrolysis products of cAMP analogs cause transformation of *Trypanosoma brucei* from slender to stumpy-like forms. Proceedings of the National Academy of Sciences *103*, 19194–19199.

Le Ray, D., Barry, J.D., Easton, C., and Vickerman, K. (1977). First tsetse fly transmission of the "AnTat" serodeme of *Trypanosoma brucei*. Annales de la Société Belge de Médecine Tropicale *57*, 369–381.

Leeuwenhoek, A. (1685). Wrote letter 45 of 1685-03-30 (ab 84) to members of the royal society. In: Lens on Leeuwenhoek.

Lehane, M.J. (1997). Peritrophic matrix structure and function. Annual Review of Entomology *42*, 525–550.

Lehane, M.J., Allingham, P.G., and Weglicki, P. (1996). Composition of the peritrophic matrix of the tsetse fly, *Glossina morsitans morsitans*. Cell and Tissue Research *283*, 375–384.

Lehane, M.J., and Msangi, A.R. (1991). Lectin and peritrophic membrane development in the gut of *Glossina m.morsitans* and a discussion of their role in protecting the fly against trypanosome infection. Medical and Veterinary Entomology *5*, 495–501.

Lindemann, C.B., and Lesich, K.A. (2016). Functional anatomy of the mammalian sperm flagellum: Mammalian Sperm Mechanics. Cytoskeleton *73*, 652–669.

Livingstone, D. (1857). Missionary Travels and Researches in South Africa. John Murray London, *548*.

Lockery, S.R., Lawton, K.J., Doll, J.C., Faumont, S., Coulthard, S.M., Thiele, T.R., Chronis, N., McCormick, K.E., Goodman, M.B., and Pruitt, B.L. (2008). Artificial Dirt: Microfluidic Substrates for Nematode Neurobiology and Behavior. Journal of Neurophysiology *99*, 3136–3143.

MacGregor, P., and Matthews, K.R. (2012). Identification of the regulatory elements controlling the transmission stage-specific gene expression of PAD1 in *Trypanosoma brucei*. Nucleic Acids Research *40*, 7705–7717.

MacGregor, P., Savill, N.J., Hall, D., and Matthews, K.R. (2011). Transmission Stages Dominate Trypanosome Within-Host Dynamics during Chronic Infections. Cell Host & Microbe *9*, 310–318.

MacGregor, P., Szöőr, B., Savill, N.J., and Matthews, K.R. (2012). Trypanosomal immune evasion, chronicity and transmission: an elegant balancing act. Nature Reviews Microbiology *10*, 431–438.

MacLean, L., Myburgh, E., Rodgers, J., and Price, H.P. (2013). Imaging African trypanosomes. Parasite Immunology *35*, 283–294.

MacLeod, E.T., Maudlin, I., Darby, A.C., and Welburn, S.C. (2007). Antioxidants promote establishment of trypanosome infections in tsetse. Parasitology *134*, 827–831.

Magez, S., Schwegmann, A., Atkinson, R., Claes, F., Drennan, M., De Baetselier, P., and Brombacher, F. (2008). The Role of B-cells and IgM Antibodies in Parasitemia, Anemia, and VSG Switching in *Trypanosoma brucei*-Infected Mice. PLoS Pathogens *4*, e1000122.

Mancini, P., and Patton, C. (1981). Cyclic 3′,5′-adenosine monophosphate levels during the developmental cycle of *Trypanosoma brucei brucei* in the rat. Molecular and Biochemical Parasitology *3*, 19–31.

Maric, D., Epting, C.L., and Engman, D.M. (2010). Composition and sensory function of the trypanosome flagellar membrane. Current Opinion in Microbiology *13*, 466–472.

Maritz, J.M., Land, K.M., Carlton, J.M., and Hirt, R.P. (2014). What is the importance of zoonotic trichomonads for human health? Trends in Parasitology *30*, 333–341.

Matthews, K.R., and Gull, K. (1994). Evidence for an interplay between cell cycle progression and the initiation of differentiation between life cycle forms of African trypanosomes. Journal of Cell Biology *125*, 1147–1156.

Matthews, K.R., Ellis, J.R., and Paterou, A. (2004). Molecular regulation of the life cycle of African trypanosomes. Trends in Parasitology *20*, 40–47.

Matthews, K.R., McCulloch, R., and Morrison, L.J. (2015). The within-host dynamics of African trypanosome infections. Philosophical Transactions of the Royal Society B: Biological Sciences *370*, 20140288.

Matthews, K.R., Sherwin, T., and Gull, K. (1995). Mitochondrial genome repositioning during the differentiation of the African trypanosome between life cycle forms is microtubule mediated. Journal of Cell Science *108 (Pt 6)*, 2231–2239.

Maudlin, I., and Welburn, S.C. (1989). A single trypanosome is sufficient to infect a tsetse fly. Annals of Tropical Medicine and Parasitology *83*, 431–433.

Maudlin, I., Welburn, S.C., and Milligan, P. (1990). Salivary gland infection: a sex-linked recessive character in tsetse? Acta Tropica *48*, 9–15.

Maudlin, I., Welburn, S.C., and Milligan, P.J. (1998). Trypanosome infections and survival in tsetse. Parasitology *116 Suppl*, S23–28.

McCulloch, R., Vassella, E., Burton, P., Boshart, M., and Barry, J.D. (2004). Transformation of monomorphic and pleomorphic Trypanosoma brucei. Methods in Molecular Biology *262*, 53–86.

Mei, Y., Huang, G., Solovev, A.A., Ureña, E.B., Mönch, I., Ding, F., Reindl, T., Fu, R.K.Y., Chu, P.K., and Schmidt, O.G. (2008). Versatile Approach for Integrative and Functionalized Tubes by Strain Engineering of Nanomembranes on Polymers. Advanced Materials *20*, 4085–4090.

Mogk, S., Boßelmann, C.M., Mudogo, C.N., Stein, J., Wolburg, H., and Duszenko, M. (2017). African trypanosomes and brain infection - the unsolved question: Brain infection in African sleeping sickness. Biological Reviews *92*, 1675–1687.

Mogk, S., Meiwes, A., Boßelmann, C.M., Wolburg, H., and Duszenko, M. (2014 a). The lane to the brain: how African trypanosomes invade the CNS. Trends in Parasitology *30*, 470–477.

Mogk, S., Meiwes, A., Shtopel, S., Schraermeyer, U., Lazarus, M., Kubata, B., Wolburg, H., and Duszenko, M. (2014 b). Cyclical Appearance of African Trypanosomes in the Cerebrospinal Fluid: New Insights in How Trypanosomes Enter the CNS. PLoS ONE *9*, e91372.

Moloo, S.K. (1971). An artificial feeding technique for Glossina. Parasitology *63*, 507–512.

Moloo, S.K., Steiger, R.F., and Hecker, H. (1970). Ultrastructure of the peritrophic membrane formation in *Glossina Wiedemann*. Acta Tropica *27*, 378–383.

Morand, S., Renggli, C.K., Roditi, I., and Vassella, E. (2012). MAP kinase kinase 1 (MKK1) is essential for transmission of *Trypanosoma brucei* by *Glossina morsitans*. Molecular and Biochemical Parasitology *186*, 73–76.

Mowatt, M.R., and Clayton, C.E. (1987). Developmental regulation of a novel repetitive protein of *Trypanosoma brucei*. Molecular and Cellular Biology *7*, 2838–2844.

Muthinja, J.M., Ripp, J., Krüger, T., Imle, A., Haraszti, T., Fackler, O.T., Spatz, J.P., Engstler, M., and Frischknecht, F. (2018). Tailored environments to study motile cells and pathogens. Cellular Microbiology *20*, e12820.

Nantulya, V.M., Doyle, J.J. and Jenni, L., (1978). Studies on "*Trypanosoma* (Nannomonas) *congolense*". Part I, On the morphological appearance of the parasite in the mouse. Acta Tropica *35*, 329–337.

Nolan, D.P., Rolin, S., Rodriguez, J.R., Van Den Abbeele, J., and Pays, E. (2000). Slender and stumpy bloodstream forms of Trypanosoma brucei display a differential response to extracellular acidic and proteolytic stress: Differential stress response in *T. brucei*. European Journal of Biochemistry *267*, 18–27.

Oberholzer, M., Lopez, M.A., McLelland, B.T., and Hill, K.L. (2010). Social Motility in African Trypanosomes. PLoS Pathogens *6*, e1000739.

Oberle, M., Balmer, O., Brun, R., and Roditi, I. (2010). Bottlenecks and the Maintenance of Minor Genotypes during the Life Cycle of *Trypanosoma brucei*. PLoS Pathogens *6*, e1001023.

Ogbadoyi, E., Ersfeld, K., Robinson, D., Sherwin, T., and Gull, K. (2000). Architecture of the *Trypanosoma brucei* nucleus during interphase and mitosis. Chromosoma *108*, 501–513.

Ooi, C.-P., Schuster, S., Cren-Travaillé, C., Bertiaux, E., Cosson, A., Goyard, S., Perrot, S., and Rotureau, B. (2016). The Cyclical Development of *Trypanosoma vivax* in the Tsetse Fly Involves an Asymmetric Division. Frontiers in Cellular and Infection Microbiology *6*.

Otieno, L.H., and Darji, N. (1979). The abundance of pathogenic African trypanosomes in the salivary secretions of wild *Glossina pallidipes*. Annals of Tropical Medicine and Parasitology *73*, 583–588.

Overath, P., and Engstler, M. (2004). Endocytosis, membrane recycling and sorting of GPI-anchored proteins: *Trypanosoma brucei* as a model system: The endocytic system of *T. brucei*. Molecular Microbiology *53*, 735–744.

Overath, P., Czichos, J., and Haas, C. (1986). The effect of citrate/ cis-aconitate on oxidative metabolism during transformation of *Trypanosoma brucei*. European Journal of Biochemistry *160*, 175–182.

Overath, P., Czichos, J., Stock, U., and Nonnengaesser, C. (1983). Repression of glycoprotein synthesis and release of surface coat during transformation of *Trypanosoma brucei*. EMBO Journal *2*, 1721–1728.

Patel, N.Y., Youdeowei, A., and Odhiambo, T.R. (1981). The composition of the salivary gland secretion of the tsetse, *Glossina morsitans morsitans* Westwood 1850 (Diptera: Glossinidae). International Journal of Tropical Insect Science *1*, 383–387.

Pays, E., Hanocq-Quertier, J., Hanocq, F., Van Assel, S., Nolan, D., and Rolin, S. (1993). Abrupt RNA changes precede the first cell division during the differentiation of *Trypanosoma brucei* bloodstream forms into procyclic forms *in vitro*. Molecular and Biochemical Parasitology *61*, 107–114.

Pays, E., Vanhollebeke, B., Vanhamme, L., Paturiaux-Hanocq, F., Nolan, D.P., and Pérez-Morga, D. (2006). The trypanolytic factor of human serum. Nature Reviews Microbiology *4*, 477–486.

Peacock, L., Bailey, M., Carrington, M., and Gibson, W. (2014). Meiosis and Haploid Gametes in the Pathogen *Trypanosoma brucei*. Current Biology *24*, 181–186.

Peacock, L., Cook, S., Ferris, V., Bailey, M., and Gibson, W. (2012 a). The life cycle of *Trypanosoma* (Nannomonas) *congolense* in the tsetse fly. Parasites & Vectors *5*, 109.

Peacock, L., Ferris, V., Bailey, M., and Gibson, W. (2006). Multiple effects of the lectin-inhibitory sugars D-glucosamine and N-acetyl-glucosamine on tsetse-trypanosome interactions. Parasitology *132*.

Peacock, L., Ferris, V., Bailey, M., and Gibson, W. (2008). Fly transmission and mating of *Trypanosoma brucei brucei* strain 427. Molecular and Biochemical Parasitology *160*, 100–106.

Peacock, L., Ferris, V., Bailey, M., and Gibson, W. (2012 b). The influence of sex and fly species on the development of trypanosomes in tsetse flies. PLoS Neglected Tropical Diseases *6*, e1515.

Peacock, L., Ferris, V., Sharma, R., Sunter, J., Bailey, M., Carrington, M., and Gibson, W. (2011). Identification of the meiotic life cycle stage of *Trypanosoma brucei* in the tsetse fly. Proceedings of the National Academy of Sciences *108*, 3671–3676.

Plimmer, H. G. and Bradford, J. R. (1899). A preliminary note on the morphology and distribution of the organism found in the tsetse fly disease. Proceedings of the Royal Society B: Biological Sciences *65*, 274-281.

Poole, D.N., and McClelland, R.S. (2013). Global epidemiology of *Trichomonas vaginalis*. Sexually Transmitted Infections *89*, 418–422.

Priest, J.W., and Hajduk, S.L. (1994). Developmental regulation of *Trypanosoma brucei* cytochrome c reductase during bloodstream to procyclic differentiation. Molecular and Biochemical Parasitology *65*, 291–304.

Purcell, E.M. (1977). Life at low Reynolds number. American Journal of Physics *45*, 3.

Qin, D., Xia, Y., and Whitesides, G.M. (2010). Soft lithography for micro- and nanoscale patterning. Nature Protocols *5*, 491–502.

Ralston, K.S., Lerner, A.G., Diener, D.R., and Hill, K.L. (2006). Flagellar Motility Contributes to Cytokinesis in *Trypanosoma brucei* and Is Modulated by an Evolutionarily Conserved Dynein Regulatory System. Eukaryotic Cell *5*, 696–711.

Reuner, B., Vassella, E., Yutzy, B., and Boshart, M. (1997). Cell density triggers slender to stumpy differentiation of *Trypanosoma brucei* bloodstream forms in culture. Molecular and Biochemical Parasitology *90*, 269–280.

Rico, E., Rojas, F., Mony, B.M., Szoor, B., Macgregor, P., and Matthews, K.R. (2013). Bloodstream form pre-adaptation to the tsetse fly in *Trypanosoma brucei*. Frontiers in Cellular and Infection Microbiology *3*, 78.

Riedel, I.H. (2005). A Self-Organized Vortex Array of Hydrodynamically Entrained Sperm Cells. Science *309*, 300–303.

Robertson, M. (1912). Notes on the Polymorphism of *Trypanosoma gambiense* in the Blood and Its Relation to the Exogenous Cycle in *Glossina palpalis*. Proceedings of the Royal Society B: Biological Sciences *85*, 527–539.

Robinson, D.R. (1995). Microtubule polarity and dynamics in the control of organelle positioning, segregation, and cytokinesis in the trypanosome cell cycle. The Journal of Cell Biology *128*, 1163–1172.

Robinson, D.R., and Gull, K. (1991). Basal body movements as a mechanism for mitochondrial genome segregation in the trypanosome cell cycle. Nature *352*, 731–733.

Roditi, I., and Clayton, C. (1999). An unambiguous nomenclature for the major surface glycoproteins of the procyclic form of *Trypanosoma brucei*. Molecular and Biochemical Parasitology *103*, 99–100.

Roditi, I., Carrington, M., and Turner, M. (1987). Expression of a polypeptide containing a dipeptide repeat is confined to the insect stage of *Trypanosoma brucei*. Nature *325*, 272–274.

Roditi, I., Schwarz, H., Pearson, T.W., Beecroft, R.P., Liu, M.K., Richardson, J.P., Buhring, H.J., Pleiss, J., Bulow, R., and Williams, R.O. (1989). Procyclin gene expression and loss of the variant surface glycoprotein during differentiation of *Trypanosoma brucei*. Journal of Cell Biology *108*, 737–746.

Rogers, M.E., Hajmová, M., Joshi, M.B., Sadlova, J., Dwyer, D.M., Volf, P., and Bates, P.A. (2008). Leishmania chitinase facilitates colonization of sand fly vectors and enhances transmission to mice. Cellular Microbiology *10*, 1363–1372.

Rojas, F., Silvester, E., Young, J., Milne, R., Tettey, M., Houston, D.R., Walkinshaw, M.D., Pérez-Pi, I., Auer, M., Denton, H., et al. (2019). Oligopeptide Signaling through TbGPR89 Drives Trypanosome Quorum Sensing. Cell *176*, 306-317.e16.

Rose, C., Dyer, N.A., Casas-Sanchez, A., Beckett, A.J., Solórzano, C., Middlehurst, B., Marcello, M., Lehane, M.J., Prior, I.A., and Acosta-Serrano, Á. (2019). *Trypanosoma brucei* colonises the tsetse gut via an immature peritrophic matrix in the proventriculus. BioRxiv 513689. Posted January 07, 2019. https://www.biorxiv.org/content/10.1101/513689v1

Rothschild (1949). Measurement of sperm activity before artificial insemination. Nature *163*, 358.

Rothschild (1963). Non-random Distribution of Bull Spermatozoa in a Drop of Sperm Suspension. Nature *198*, 1221–1222.

Rotureau, B., and Van Den Abbeele, J. (2013). Through the dark continent: African trypanosome development in the tsetse fly. Frontiers in Cellular and Infection Microbiology *3*.

Rotureau, B., Morales, M.A., Bastin, P., and Späth, G.F. (2009). The flagellum-mitogen-activated protein kinase connection in Trypanosomatids: a key sensory role in parasite signalling and development? Cellular Microbiology *11*, 710–718.

Rotureau, B., Ooi, C.-P., Huet, D., Perrot, S., and Bastin, P. (2014). Forward motility is essential for trypanosome infection in the tsetse fly: Trypanosome motility is essential in tsetse flies. Cellular Microbiology *16*, 425–433.

Rotureau, B., Subota, I., and Bastin, P. (2011). Molecular bases of cytoskeleton plasticity during the Trypanosoma brucei parasite cycle: Plasticity of *Trypanosoma brucei*. Cellular Microbiology *13*, 705–716.

Rotureau, B., Subota, I., Buisson, J., and Bastin, P. (2012). A new asymmetric division contributes to the continuous production of infective trypanosomes in the tsetse fly. Development *139*, 1842–1850.

Savill, N.J., and Seed, J.R. (2004). Mathematical and statistical analysis of the *Trypanosoma brucei* slender to stumpy transition. Parasitology *128*, 53–67.

Schuster, S. (2014). Charakterisierung der Stadien von *T. brucei* in der Tsetsefliege. Master thesis, University of Würzburg.

Schuster, S., Krüger, T., Subota, I., Thusek, S., Rotureau, B., Beilhack, A., and Engstler, M. (2017). Developmental adaptations of trypanosome motility to the tsetse fly host environments unravel a multifaceted *in vivo* microswimmer system. eLife *6*.

Schwarz, U.S. (2015). Physical constraints for pathogen movement. Seminars in Cell & Developmental Biology *46*, 82–90.

Schwede, A., Jones, N., Engstler, M., and Carrington, M. (2011). The VSG C-terminal domain is inaccessible to antibodies on live trypanosomes. Molecular and Biochemical Parasitology *175*, 201–204.

Seed, J.R., and Sechelski, J.B. (1989). Mechanism of long slender (LS) to short stumpy (SS) transformation in the African trypanosomes. The Journal of Protozoology *36*, 572–577.

Seed, J.R., and Wenck, M.A. (2003). Role of the long slender to short stumpy transition in the life cycle of the African trypanosomes. Kinetoplastid Biology and Disease 8.

Shaner, N.C., Campbell, R.E., Steinbach, P.A., Giepmans, B.N.G., Palmer, A.E., and Tsien, R.Y. (2004). Improved monomeric red, orange and yellow fluorescent proteins derived from *Discosoma sp.* red fluorescent protein. Nature Biotechnology *22*, 1567–1572.

Shaner, N.C., Lambert, G.G., Chammas, A., Ni, Y., Cranfill, P.J., Baird, M.A., Sell, B.R., Allen, J.R., Day, R.N., Israelsson, M., et al. (2013). A bright monomeric green fluorescent protein derived from *Branchiostoma lanceolatum*. Nature Methods *10*, 407–409.

Shaner, N.C., Steinbach, P.A., and Tsien, R.Y. (2005). A guide to choosing fluorescent proteins. Nature Methods *2*, 905–909.

Shapiro, O.H., Kramarsky-Winter, E., Gavish, A.R., Stocker, R., and Vardi, A. (2016). A coral-on-a-chip microfluidic platform enabling live-imaging microscopy of reef-building corals. Nature Communications *7*.

Shapiro, S.Z., Naessens, J., Liesegang, B., Moloo, S.K., and Magondu, J. (1984). Analysis by flow cytometry of DNA synthesis during the life cycle of African trypanosomes. Acta Tropica *41*, 313–323.

Sharma, R., Gluenz, E., Peacock, L., Gibson, W., Gull, K., and Carrington, M. (2009). The heart of darkness: growth and form of *Trypanosoma brucei* in the tsetse fly. Trends in Parasitology *25*, 517–524.

Sharma, R., Peacock, L., Gluenz, E., Gull, K., Gibson, W., and Carrington, M. (2008). Asymmetric Cell Division as a Route to Reduction in Cell Length and Change in Cell Morphology in Trypanosomes. Protist *159*, 137–151.

Shaw, S., DeMarco, S.F., Rehmann, R., Wenzler, T., Florini, F., Roditi, I., and Hill, K.L. (2019). Flagellar cAMP signaling controls trypanosome progression through host tissues. Nature Communications *10*.

Sherwin, T., and Gull, K. (1989). The Cell Division Cycle of *Trypanosoma brucei brucei*: Timing of Event Markers and Cytoskeletal Modulations. Philosophical Transactions of the Royal Society B: Biological Sciences *323*, 573–588.

Silvester, E., Ivens, A., and Matthews, K.R. (2018). A gene expression comparison of *Trypanosoma brucei* and *Trypanosoma congolense* in the bloodstream of the mammalian host reveals species-specific adaptations to density-dependent development. PLoS Neglected Tropical Diseases *12*, e0006863.

Silvester, E., Young, J., Ivens, A., and Matthews, K.R. (2017). Interspecies quorum sensing in co-infections can manipulate trypanosome transmission potential. Nature Microbiology *2*, 1471–1479.

Simarro, P.P., Jannin, J., and Cattand, P. (2008). Eliminating Human African Trypanosomiasis: Where Do We Stand and What Comes Next? PLoS Medicine *5*, e55.

Simo, G., Fongho, P., Farikou, O., Ndjeuto-Tchouli, P.I.N., Tchouomene-Labou, J., Njiokou, F., and Asonganyi, T. (2015). Trypanosome infection rates in tsetse flies in the "silent" sleeping sickness focus of Bafia in the Centre Region in Cameroon. Parasites & Vectors *8*, 528.

Smolla, M., Ruchty, M., Nagel, M., and Kleineidam, C.J. (2014). Clearing pigmented insect cuticle to investigate small insects' organs in situ using confocal laser-scanning microscopy (CLSM). Arthropod Structure & Development *43*, 175–181.

Stegner, D., vanEeuwijk, J.M.M., Angay, O., Gorelashvili, M.G., Semeniak, D., Pinnecker, J., Schmithausen, P., Meyer, I., Friedrich, M., Dütting, S., et al. (2017). Thrombopoiesis is spatially regulated by the bone marrow vasculature. Nature Communications *8*.

Steiger, R.F. (1973). On the ultrastructure of *Trypanosoma* (Trypanozoon) *brucei* in the course of its life cycle and some related aspects. Acta Tropica *30*, 64–168.

Steverding, D. (2008). The history of African trypanosomiasis. Parasites and Vectors *1*, 3.

Suarez, S.S. (2016). Mammalian sperm interactions with the female reproductive tract. Cell and Tissue Research *363*, 185–194.

Subota, I., Rotureau, B., Blisnick, T., Ngwabyt, S., Durand-Dubief, M., Engstler, M., and Bastin, P. (2011). ALBA proteins are stage regulated during trypanosome development in the tsetse fly and participate in differentiation. Molecular Biology of the Cell *22*, 4205–4219.

Sunter, J., and Gull, K. (2017). Shape, form, function and *Leishmania* pathogenicity: from textbook descriptions to biological understanding. Open Biology *7*, 170165.

Taylor, A.E.R., and Godfrey, D.G. (1969). A New Organelle of Bloodstream Salivarian Trypanosomes. The Journal of Protozoology *16*, 466–470.

Taylor, J.E., and Rudenko, G. (2006). Switching trypanosome coats: what´s in the wardrobe? Trends in Genetics *22*, 614–620.

Tetley, L., and Vickerman, K. (1985). Differentiation in *Trypanosoma brucei*: host-parasite cell junctions and their persistence during acquisition of the variable antigen coat. Journal of Cell Science *74*, 1–19.

Trindade, S., Rijo-Ferreira, F., Carvalho, T., Pinto-Neves, D., Guegan, F., Aresta-Branco, F., Bento, F., Young, S.A., Pinto, A., Van Den Abbeele, J., et al. (2016). *Trypanosoma brucei* Parasites Occupy and Functionally Adapt to the Adipose Tissue in Mice. Cell Host & Microbe *19*, 837–848.

Tung, C., Hu, L., Fiore, A.G., Ardon, F., Hickman, D.G., Gilbert, R.O., Suarez, S.S., and Wu, M. (2015). Microgrooves and fluid flows provide preferential passageways for sperm over pathogen *Tritrichomonas foetus*. Proceedings of the National Academy of Sciences *112*, 5431–5436.

Turner, C.M., Aslam, N., and Dye, C. (1995). Replication, differentiation, growth and the virulence of *Trypanosoma brucei* infections. Parasitology *111 (Pt 3)*, 289–300.

Turner, C.M.R. (1990). The use of experimental artefacts in African trypanosome research. Parasitology Today *6*, 14–17.

Turner, C.M.R., Barry, J.D., and Vickerman, K. (1988). Loss of variable antigen during transformation of *Trypanosoma brucei rhodesiense* from bloodstream to procyclic forms in the tsetse fly. Parasitology Research *74*, 507–511.

Turner, L., Ryu, W.S., and Berg, H.C. (2000). Real-Time Imaging of Fluorescent Flagellar Filaments. Journal of Bacteriology *182*, 2793–2801.

Tyler, K.M., Higgs, P.G., Matthews, K.R., and Gull, K. (2001). Limitation of *Trypanosoma brucei* parasitaemia results from density-dependent parasite differentiation and parasite killing by the host immune response. Proceedings. Biological Sciences *268*, 2235–2243.

Uppaluri, S., Heddergott, N., Stellamanns, E., Herminghaus, S., Zöttl, A., Stark, H., Engstler, M., and Pfohl, T. (2012). Flow Loading Induces Oscillatory Trajectories in a Bloodstream Parasite. Biophysical Journal *103*, 1162–1169.

Van Den Abbeele, J., Caljon, G., De Ridder, K., De Baetselier, P., and Coosemans, M. (2010). *Trypanosoma brucei* Modifies the Tsetse Salivary Composition, Altering the Fly Feeding Behavior That Favors Parasite Transmission. PLoS Pathogens *6*, e1000926.

Van Den Abbeele, J., Claes, Y., Van Bockstaele, D., Le Ray, D., and Coosemans, M. (1999). *Trypanosoma brucei* spp. development in the tsetse fly: characterization of the post-mesocyclic stages in the foregut and proboscis. Parasitology *118*, 469–478.

Vassella, E., and Boshart, M. (1996). High molecular mass agarose matrix supports growth of bloodstream forms of pleomorphic *Trypanosoma brucei* strains in axenic culture. Molecular and Biochemical Parasitology *82*, 91–105.

Vassella, E., Den Abbeele, J.V., Butikofer, P., Renggli, C.K., Furger, A., Brun, R., and Roditi, I. (2000). A major surface glycoprotein of *Trypanosoma brucei* is expressed transiently during development and can be regulated post-transcriptionally by glycerol or hypoxia. Genes & Development *14*, 615–626.

Vassella, E., Krämer, R., Turner, C.M.R., Wankell, M., Modes, C., Van Den Bogaard, M., and Boshart, M. (2001). Deletion of a novel protein kinase with PX and FYVE-related domains increases the rate of differentiation of *Trypanosoma brucei*: *T. brucei* growth and differentiation. Molecular Microbiology *41*, 33–46.

Vassella, E., Oberle, M., Urwyler, S., Renggli, C.K., Studer, E., Hemphill, A., Fragoso, C., Bütikofer, P., Brun, R., and Roditi, I. (2009). Major Surface Glycoproteins of Insect Forms of *Trypanosoma brucei* Are Not Essential for Cyclical Transmission by Tsetse. PLoS ONE *4*, e4493.

Vassella, E., Reuner, B., Yutzy, B., and Boshart, M. (1997). Differentiation of African trypanosomes is controlled by a density sensing mechanism which signals cell cycle arrest via the cAMP pathway. Journal of Cell Science *110 (Pt 21)*, 2661–2671.

Vickerman, K. (1965). Polymorphism and mitochondrial activity in sleeping sickness trypanosomes. Nature *208*, 762–766.

Vickerman, K. (1969). The Fine Structure of *Trypanosoma congolense* in Its Bloodstream Phase. The Journal of Protozoology *16*, 54–69.

Vickerman, K. (1985). Developmental cycles and biology of pathogenic trypanosomes. British Medical Bulletin *41*, 105–114.

Vickerman, K., and Preston, T.M. (1976). Comparative cell biology of the kinetoplastid flagellates. In Biology of the Kinetoplastida Vol. 2, W.H.R. Lumsden, and D.A. Evans, eds. (London/New York/San Francisco: Academic Press), pp. 35–130.

Vreysen, M.J. (2001). Principles of area-wide integrated tsetse fly control using the sterile insect technique. Médecine tropicale: revue du Corps de santé colonial *61*, 397–411.

Vreysen, M.J., Saleh, K.M., Ali, M.Y., Abdulla, A.M., Zhu, Z.R., Juma, K.G., Dyck, V.A., Msangi, A.R., Mkonyi, P.A., and Feldmann, H.U. (2000). *Glossina austeni* (Diptera: Glossinidae) eradicated on the island of Unguja, Zanzibar, using the sterile insect technique. Journal of Economic Entomology *93*, 123–135.

Walshe, D.P., Lehane, M.J., and Haines, L.R. (2011). Post Eclosion Age Predicts the Prevalence of Midgut Trypanosome Infections in Glossina. PLoS ONE *6*, e26984.

Wang, J., Weiss, B.L., and Aksoy, S. (2013). Tsetse fly microbiota: form and function. Frontiers in Cellular and Infection Microbiology *3*.

Weibel, D.B., DiLuzio, W.R., and Whitesides, G.M. (2007). Microfabrication meets microbiology. Nature Reviews Microbiology *5*, 209–218.

Weingart, J. (2018). Entwicklungsbiologische Analyse der verschiedenen Säugetierstadien von *Trypanosoma brucei brucei* AnTat 1.1. Bachelor thesis, University of Würzburg.

Weiss, B.L., Wang, J., Maltz, M.A., Wu, Y., and Aksoy, S. (2013). Trypanosome Infection Establishment in the Tsetse Fly Gut Is Influenced by Microbiome-Regulated Host Immune Barriers. PLoS Pathogens *9*, e1003318.

Westphal, N. (2014). Charakterisierung von Morphologie und Motilität der *T. brucei brucei* Entwicklungsstadien in der Tsetsefliege *in vivo* und *in vitro*. Bachelor thesis, University of Würzburg.

Wheeler, R.J. (2010). The trypanolytic factor-mechanism, impacts and applications. Trends in Parasitology *26*, 457–464.

Wigglesworth, V.B. (1929). Digestion in the Tsetse-Fly: A Study of Structure and Function. Parasitology *21*, 288–321.

Willett, K.C. (1966). Development of the peritrophic membrane in Glossina (tsetse flies) and its relation to infection with trypanosomes. Experimental Parasitology *18*, 290–295.

Woodward, R., and Gull, K. (1990). Timing of nuclear and kinetoplast DNA replication and early morphological events in the cell cycle of *Trypanosoma brucei*. Journal of Cell Science *95 (Pt 1)*, 49–57.

World Health Organization. (2018). WHO outlines criteria to assess elimination of sleeping sickness. *https://www.who.int/neglected_diseases/news/criteria-eliminate-sleeping-sickness/en/*

Xie, L., Ma, R., Han, C., Su, K., Zhang, Q., Qiu, T., Wang, L., Huang, G., Qiao, J., Wang, J., et al. (2010). Integration of sperm motility and chemotaxis screening with a microchannel-based device. Clinical Chemistry *56*, 1270–1278.

Yawata, Y., Nguyen, J., Stocker, R., and Rusconi, R. (2016). Microfluidic Studies of Biofilm Formation in Dynamic Environments. Journal of Bacteriology *198*, 2589–2595.

Yorke, W., Murgatroyd, F., and Hawking, F. (1933). The Relation of Polymorphic Trypanosomes, Developing in the Gut of Glossina, to the Peritrophic Membrane. Annals of Tropical Medicine and Parasitology *27*, 347–354.

Ziegelbauer, K., Quinten, M., Schwarz, H., Pearson, T.W., and Overath, P. (1990). Synchronous differentiation of *Trypanosoma brucei* from bloodstream to procyclic forms in vitro. European Journal of Biochemistry *192*, 373–378.

Zimmermann, H., Subota, I., Batram, C., Kramer, S., Janzen, C.J., Jones, N.G., and Engstler, M. (2017). A quorum sensing-independent path to stumpy development in *Trypanosoma brucei*. PLoS Pathogens *13*, e1006324.

7 Annex

7.1 List of abbreviations

°C	degrees Celsius
AAT	animal African trypanosomiasis
AMCA	aminomethylcoumarin acetate
aMG	anterior midgut
AnTat	Antwerp Institut Trypanozoon Antigen Typ
avi	audio video interleaved
BABB	benzyl alcohol/benzyl benzoate
bit	binary digit
Blas	blasticidin
bm	blood meal
BSF	bloodstream form
c	cells
cAMP	cyclic adenosine monophosphate
CCTB	Center for Computational and Theoretical Biology
CO_2	carbon dioxide
DAPI	4´,6-diamidino-2-phenylindole
ddH_2O	double-distilled water
DIC	differential interference contrast
DNA	desoxyribonucleic acid
EDTA	ethylenediaminetetraacetic acid
EGFP	enhanced GFP
EP	dipeptide (glu-pro) repeat procyclin
EP1+	EP1 positive
F	flagella
FA	formaldehyde
FACS	fluorescence-activated cell sorting
FAZ	flagellum attachment zone
FCS	fetal calf serum
fps	frames per second
g	gram
g	gravity
GFP	green fluorescent protein
GPEET	pentapeptide (gly-pro-glu-glu-thr) repeat procyclin
GPI	glycosylphosphatidylinositol
h	hour
H_2O	water
H_2O_2	hydrogen peroxide
HAT	human African trypanosomiasis
HEPES	4-(2-hydroxyethyl)-1-piperazineethanesulfonic acid
HMI-9	Hirumi's modified Iscove's medium 9
Hygro	hygromycin

Hz	hertz
K	kinetoplast
l	liter
LB	Luria-Bertani
LSFM	light sheet fluorescence microscopy
M	molarity
MC-HMI-9	methylcellulose-HMI-9
mg	miligram
MG	midgut
min	minute
ml	mililiter
mM	milimolar
mm	milimeter
mp4	moving pictures experts group
mRNA	messenger ribonucleic acid
M-VSG	metacyclic VSG
N	nucleus
NA	numerical aperture
ng	nanogram
NLS	nuclear localization signal
nm	nanometer
PAD	protein associated with differentiation
PAD1-	PAD1 negative
PAD1+	PAD1 positive
PBS	phosphate buffered saline
PC	procyclic trypanosome
PCF	procyclic form
PDMS	polydimethylsiloxane
PFA	paraformaldehyde
PFR	paraflagellar rod
Phleo	phleomycin
Puro	puromycin
PV	proventriculus
rpm	revolutions per minute
s	seconds
SD	standard deviation
SDM-79	semi-defined media 79
SDM-G	SDM79-glycerol
SG	salivary glands
SIF	stumpy induction factor
SL	slender trypanosome
ST	stumpy trypanosome
TAE	TRIS-acetate-EDTA
TDB	trypanosome dilution buffer

tdT	tandem-dimer Tomato
TI	transmission index
TIFF	tagged image file format
TRIS	tris(hydroxymethyl)aminomethane
UTR	untranslated region
v	velocity
v/v	volume per volume
VSG	variant surface glycoprotein
w/v	weight per volume
WGA	wheat germ agglutinin
WHO	World Health Organization
wt	wild type
YFP	yellow fluorescent protein
µg	microgram
µl	microliter
µM	micromolar

7.2 List of figures and tables

List of figures

List of tables

7.3 List of videos

Enclosed to this thesis is a CD containing all movies described in this work, which belong to the corresponding figures in the text.

Video 1 Tsetse fly tissue exhibits a strong autofluorescence signal, which can be recorded by light sheet fluorescence microscopy.

Video 2 The peritrophic matrix inside the tsetse fly midgut shows a high degree of convolution.

Video 3 Trypanosome nuclei can be visualized within the complex folding of the peritrophic matrix on a single cell level at different time points after infection.

Video 4 Multicolor light sheet fluorescence microscopy reveals the distribution pattern of trypanosomes around the bacteriome.

Video 5 Multicolor light sheet fluorescence microscopy reveals the distribution pattern of trypanosomes in the proventriculus.

Video 6 Fluorescent microspheres provide information about flow forces and space constraints inside the fly tissue.

Video 7 Three-dimensional modeling of pleomorphic trypanosomes isolated from the tsetse fly shows a characteristic morphology and corresponding flagellum attachment around the cell body.

Video 8 Procyclic trypanosomes in the posterior midgut.

Video 9 Mesocyclic trypanosomes in the anterior midgut.

Video 10 Proventricular trypanosomes and different epimastigote stages.

Video 11 Trypanosome developmental stages in the tsetse salivary glands.

Video 12 Rapid switching between synchronized and chaotic motion in dense trypanosome accumulations inside the ectoperitrophic space of the midgut.

Video 13 Generation of dynamic cellular waveform models of different trypanosome microswimmer types from the tsetse fly vector.

Video 14 Automated cell tracking of fluorescent trypanosome cell nuclei inside the tsetse fly tissue.

Video 15 Investigation of trypanosome swimming behavior in rolled-up glass microchannels.

Video 16 Slender cells continue to divide inside the tsetse fly and become PAD1 positive after 15 hours.

7.4 Publication list

Parts of this thesis are included in following publications:

*__Schuster S.__, *Subota I., Lisack J., Zimmermann H., Reuter C., Morriswood B., and Engstler M. (2019). A modification to the life cycle of the parasite *Trypanosoma brucei*.

Manuscript is available online on the bioRxiv preprint server for biology. Preprint posted on July 29, 2019 https://www.biorxiv.org/content/10.1101/717975v1

Krüger T., __Schuster S.__, and Engstler M. (2018). Beyond Blood: African Trypanosomes on the Move. Trends in Parasitology *34*, 1056-1067.

__Schuster S.__, Krüger T., Subota I., Thusek S., Rotureau B., Beilhack A., and Engstler M. (2017). Developmental adaptations of trypanosome motility to the tsetse fly host environments unravel a multifaceted *in vivo* microswimmer system. eLife *6*.

Publications that are not part of this thesis:

*Ooi C.P., *__Schuster S.__, Cren-Travaillé C., Bertiaux E., Cosson A., Goyard S., Perrot S., and Rotureau B. (2016). The Cyclical Development of *Trypanosoma vivax* in the Tsetse Fly Involves an Asymmetric Division. Frontiers in Cellular and Infection Microbiology *6*.

*The authors contributed equally to this work.

7.5 Eidesstattliche Erklärung

Eidesstattliche Erklärungen nach §7 Abs. 2 Satz 3, 4, 5 der Promotionsordnung der Fakultät für Biologie

Eidesstattliche Erklärung

Hiermit erkläre ich an Eides statt, die Dissertation: „Analysis of *Trypanosoma brucei* motility and the infection process in the tsetse fly vector", eigenständig, d. h. insbesondere selbständig und ohne Hilfe eines kommerziellen Promotionsberaters, angefertigt und keine anderen, als die von mir angegebenen Quellen und Hilfsmittel verwendet zu haben.

Ich erkläre außerdem, dass die Dissertation weder in gleicher noch in ähnlicher Form bereits in einem anderen Prüfungsverfahren vorgelegen hat.

Weiterhin erkläre ich, dass bei allen Abbildungen und Texten bei denen die Verwertungsrechte (Copyright) nicht bei mir liegen, diese von den Rechtsinhabern eingeholt wurden und die Textstellen bzw. Abbildungen entsprechend den rechtlichen Vorgaben gekennzeichnet sind sowie bei Abbildungen, die dem Internet entnommen wurden, der entsprechende Hypertextlink angegeben wurde.

Würzburg, den

7.6 Danksagung